Phonon Spectra And Thermal Properties Of Some fcc Metals Using Embedded-Atom Potentials

by

Qiuping Bian

A THESIS SUBMITTED IN PARTIAL FULFILMENT OF
THE REQUIREMENTS FOR THE DEGREE OF

MASTER OF SCIENCE

in

The Faculty of Mathematics and Sciences

Department of Physics

BROCK UNIVERSITY

September 2, 2005

In presenting this thesis in partial fulfilment of the requirements for an advanced degree at the Brock University, I agree that the Library shall make it freely available for reference and study. I further agree that permission for extensive copying of this thesis for scholarly purposes may be granted by the head of my department or by his or her representatives. It is understood that copying or publication of this thesis for financial gain shall not be allowed without my written permission.

(Signature) _____

Department of Physics

Brock University
St.Catharines, Canada

Date _____

Abstract

By employing the embedded-atom potentials of Mei *et al.*[1], we have calculated the dynamical matrices and phonon dispersion curves for six fcc metals (Cu,Ag,Au,Ni,Pd and Pt). We have also investigated, within the quasiharmonic approximation, some other thermal properties of these metals which depend on the phonon density of states, such as the temperature dependence of lattice constant, coefficient of linear thermal expansion, isothermal and adiabatic bulk moduli, heat capacities at constant volume and constant pressure, Grüneisen parameter and Debye temperature. The computed results are compared with the experimental findings wherever possible. The comparison shows a generally good agreement between the theoretical values and experimental data for all properties except the discrepancies of phonon frequencies and Debye temperature for Pd, Pt and Au. Further, we modify the parameters of this model for Pd and Pt and obtain the phonon dispersion curves which is in good agreement with experimental data.

Contents

List of Tables

List of Figures

Acknowledgements

I would like to extend my heartfelt thanks to Dr. Bose and Dr. Shukla for their patience in supervising me, for their kindness in helping my life in St. Catharines and for their financial support received from the NSERC grant. I also want to express my sincere gratitude to Dr. Reedyk for her generous donation to Department of Physics Graduate Scholarship and to Ms. Brown for her donation to Ronald Brown Graduate Award. In addition, I wish to acknowledge all professors in the department of physics who taught and helped me before. Finally, a thousand thanks will be given to the department of physics for supplying me with the very pleasant environment of research.

Chapter 1

Introduction

1.1 Embedded Atom Theory

The embedded-atom method (EAM) was first porposed in 1983 by Daw and Baskes[2, 3] as an approach to calculate the energy of a multi-atom system. In this method, the energy of the metal is viewed as the energy to embed an atom into the local electron density provided by the remaining atoms of the system, plus an electrostatic pair interaction potential between the atoms. The ansatz which Daw and Baskes used is

$$E_{tot} = \sum_i F_i(\rho_{h,i}) + \frac{1}{2}\sum_{\substack{i,j \\ (i \neq j)}} \Phi(R_{ij}), \tag{1.1}$$

$$\rho_{h,i} = \sum_{j(j \neq i)} f_j(R_{ij}), \tag{1.2}$$

where E_{tot} is the total internal energy, $\rho_{h,i}$ is the host electron density at atom i due to all other atoms, f_j is the electron density of atom j as a function of distance from its center, R_{ij} is the separation distance between atoms i and j. The function $F_i(\rho_{h,i})$, called the embedding energy, is the energy to embed atom i in an electron density $\rho_{h,i}$. Φ_{ij} is two body central repulsive potential between atoms i and j representing the electrostatic interaction plus the interaction related to Pauli-principle due to the overlap of the charge clouds. The host electron density $\rho_{h,i}$ is assumed to be a linear superposition of contributions from all individual atoms except atom i, which in turn are assumed to be spherically symmetrical.

The embedding energy is assumed to be independent of the gradients of the electron charge density[4].

The EAM is an empirical or semiempirical method. The concrete forms of the embedding functions are determined to describe the bulk equilibrium solid. In particular, they are determined by comparing the simulation results with experimental ones and minimizing the differences to fit to the equilibrium lattice constant, heat of sublimation, elastic constants, vacancy-formation energy, etc[5]. Over the years, many efforts have been made in this area. Daw and Baskes[3] used the form of $F(\rho)$ which was proposed by Puska *et al.* [6] and given by

$$F(\rho) = a\rho - b\rho^{1/2}, \tag{1.3}$$

to calculate the hydrogen embrittlement in metals. In equation (1.3), a and b are the positive constants. Foiles, Baskes, and Daw[7] developed the EAM functions for the fcc metals (Ag, Au, Cu, Ni, Pd and Pt) and their alloys by numerically fitting the functions to the bulk lattice constants, cohesive energy, elastic constants, vacancy-formation energy, and alloy heats of mixing. These EAM functions have been fairly successful in a wide range of applications[8]. Baskes[9] calculated the properties of metastable phases and point defects for silicon by taking the embdedding funtion as

$$F(\rho) = E_o\left[\frac{\rho}{\rho_e}\right]\ln\left[\frac{\rho}{\rho_e}\right], \tag{1.4}$$

where E_o is the sublimation energy, and ρ_e is the density an atom sees at equilibrium in the initial reference structure. Recently Johnson[4, 10], by using an exponentially decaying function instead of the spherically averaged free-atom densities calculated from Hartree-Fock theory, suggested a nearest-neighbor model for fcc metals. In this model, the EAM

potentials are simplified and expressed as the following analytic functions:

$$F(\rho) = -E_c\left[1 - \frac{\alpha}{\beta}\ln\left[\frac{\rho}{\rho_e}\right]\right]\left[\frac{\rho}{\rho_e}\right]^{\alpha/\beta} - \Phi_e\left[\frac{\rho}{\rho_e}\right]^{\gamma/\beta}, \tag{1.5}$$

$$\phi(R) = \phi_e \exp\left[-\gamma\left[\frac{R}{R_{1e}} - 1\right]\right], \tag{1.6}$$

$$f(R) = f_e \exp\left[-\beta\left[\frac{R}{R_{1e}} - 1\right]\right], \tag{1.7}$$

where $\rho_e = 12 f_e$ and $\Phi_e = 6\phi_e$, E_c is the cohesive energy, R_{1e} is the nearest-neighbor distance when the solid is in the static equilibrium state, ϕ_e, β and γ are parameters obtained by fitting. The application of these analytical EAM functions makes the simulations of computer very easy. This model has been applied to study the bulk diffusion in liquid transition metals[11]. However, these EAM functions are valid only for nearest-neighbor interactions. Oh and Johnson[12] have extended this model beyond the nearest-neighbor interactions and first applied the EAM functions to hcp systems. But this extension has caused a problem of a nonanalytic form of the EAM functions when the electron densities in a sample deviate more than $\pm 10\%$ from their equilibrium values. Mei *et al.* [1] has overcome this challenge and developed this nearest-neighbor model into the one in which the embedded-atom potentials for dynamic simulations are analytic and valid for any choice of cutoff distance. To illustrate the application of these embedded-atom potentials, Mei *et al.*[1] has calculated the linear coefficient of thermal expansion at room temperature, lattice constants as a function of temperature and heat capacities per atom at constant pressure for copper by using molecular-dynamics simulations. The model of Mei *et al.*[1] will be investigated in much detail in the next paragraphs.

We plot out Eqs.(1.3), (1.4) and (1.5) with simple parameters in Fig(1.1). All these different embedding functions have been used extensively by various workers in the field.

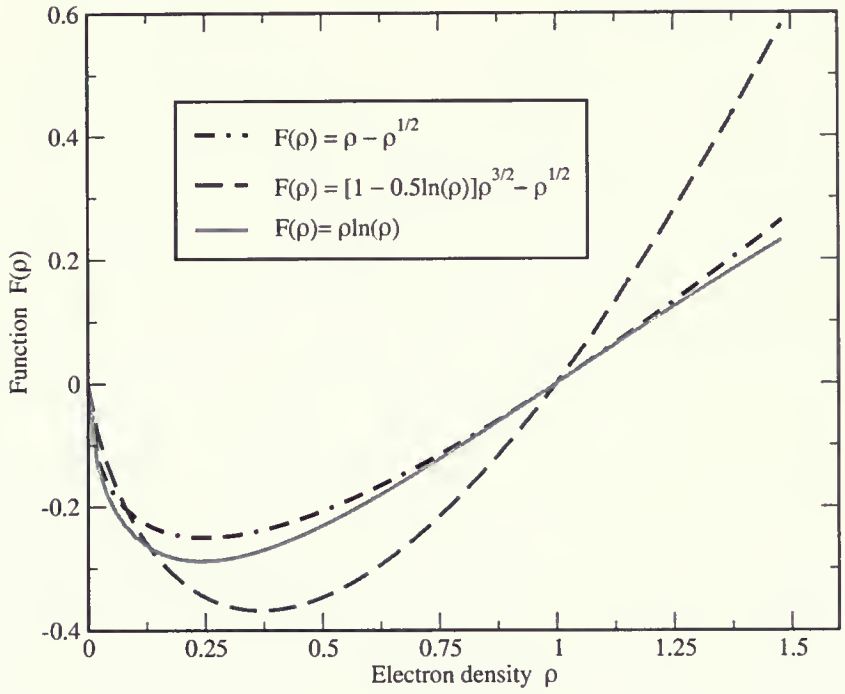

Figure 1.1: Embedding functional $F(\rho)$ against electron density ρ.

The EAM has been widely developed over the past two decades. Finnis and Sinclair[13] proposed a model in which the total energy of an assembly of atoms consists of a binding term proportional to the square-root of the local density and a repulsive pairwise potential term. This model is mathematically equivalent to the EAM. Manninen[14], Jacobsen, Nϕrskov, and Puska[15] also derived the functional form of the energy of the EAM by using density functional theory. Presently the EMB has become a very popular method for computing the energetics of metallic systems for use with various computer simulation techniques, because it overcomes some inherent or practical limitations which often plague the other theories. For example, Band theories[16] are generally limited by basis-set size and the requirement of periodicity[17, 18]. Cluster theories are also limited by the size of clusters or basis sets permitted by computers. The early pair-potential methods, while including corrections due to many body interactions and yielding the total energy directly, require

the use of an accompanying volume-dependent energy to describe the elastic properties of a metal[19]. This volume-dependent term makes it difficult to simulate the surfaces and the extended crystal defects, where the volume of the sample is ambiguous [2]. In addition, *ab initio* methods require large computing resource to study large-scale structures[20]. Because of its computational simplicity and effectiveness, the EAM has been used in study of condensed matter in many areas. Daw and Hatcher [21] successfully applied the EAM to discuss the bulk phonons of some transition metals and Nelson *et al.*[22] calculated surface phonons for copper by using embedded-atom parameters fit to bulk properties. Foiles[5] suggested a set of EAM functions fitted to bulk solid properties to study the structure and pressure of various liquid metals. Daw and Baskes[2] obtained the embedding energy and pair potential for some metals and used them to treat the problem of the defects in metals. Foiles *et al.* [7] determined a set of the EAM functions for some fcc metals and their alloys by fitting to the sublimation energy, equilibrium latttice and elastic constants of the pure metals and the heats of solution of the binary alloys to study the properties of the metals and their alloys. Johnson [23] investigated the phase stability of fcc alloys. Daw and Baskes[2, 3, 20] used the analytical EAM functions to study the properties of impurities for some fcc and bcc materials. The application in other fields, such as fracture, surface structure, surface adsorbate ordering, surface segregation and surface ordered, can be found in Ref.[4, 24–30].

1.2 The EAM Potentials of Mei *et al.*

For a perfect monatomic crystal, Eqs.(1.1) and (1.2) can be simplified to

$$E_{tot} = NE, \tag{1.8}$$

$$E = F(\rho) + 1/2 \sum_{\Lambda} s_{\Lambda} \phi(R_{\Lambda}), \tag{1.9}$$

$$\rho = \sum_{\Lambda} s_{\Lambda} f(R_{\Lambda}), \tag{1.10}$$

where N is the number of atoms in the crystal, E the energy per atom, R_{Λ} the distance of the Λth-neighbor shell with respect to a given atom, and s_{Λ} the number of atoms in that shell.

For a perfect crystal, we have

$$R_{\Lambda} = p_{\Lambda} R_1, \Lambda = 1, 2, ..., \tag{1.11}$$

here the constants p_{Λ} depend on the type of the crystal structure and $p_{\Lambda} = \sqrt{\Lambda}$ for a fcc crystal.

Rose *et al.*[31] has shown that, for most metals, the energy is well approximated by the relation

$$E(R_1) = -E_c[1 + \alpha(R_1/R_{1e} - 1)]\exp[-\alpha(R_1/R_{1e} - 1)], \tag{1.12}$$

with

$$\alpha = (9B_e\Omega_e/E_c)^{1/2}, \tag{1.13}$$

where Ω is the atomic volume and B the bulk modulus. The subscript e indicates the evaluation at equilibrium.

Plotting the electron densities calculated from Hartree-Fock method, Johnson[4] found they are quite well approximated by a single exponential term in the range of distances of interest in EAM calculation:

$$\rho = \rho_e \exp[-\beta(R_1/R_{1e} - 1)], \tag{1.14}$$

where parameters ρ_e and β are determinded from fitting the calculated electron density. Mei *et al.*[1] also did some calculations of the electron density for many metals and proved

$\rho(R_1)$ is really well described by the exponential decay of Eq.(1.14) when R_1 is not far from R_{1e}. Mei *et al.* assumed function $f(R)$ in Eq.(1.10) to have a form

$$f(R) = f_e \sum_{\tau=0}^{\kappa} c_\tau (R_{1e}/R)^\tau, \tag{1.15}$$

where the parameters c_τ are determined by using least-squares fitting to fit the equation

$$\sum_{\Lambda} s_\Lambda f(R_\Lambda) = \rho_e \exp[-\beta(R_1/R_{1e} - 1)], \tag{1.16}$$

or the equivalent equation

$$\sum_{\tau=0}^{\kappa} g_\tau (R_1/R_{1e})^{-\tau} = \exp[-\beta(R_1/R_{1e} - 1)], \tag{1.17}$$

with

$$g_\tau = c_\tau (f_e/\rho_e) \sum_{\Lambda} s_\Lambda p_\Lambda^{-\tau}, \tau = 0, 1, ..., \kappa, \tag{1.18}$$

provided κ is given and $f_e = \rho_e/12.0$. The coefficients c_τ with specifying $\kappa = 5$ for some fcc metals (Ag, Cu, Ni, Pd, Pt and Au) are listed in Table(1.1).

By taking into consideration of Eqs.(1.12) and (1.14), Mei *et al.*[1] took the EAM potentials as the following forms

$$\phi(R) = -\phi_e[1 + \delta(R/R_{1e} - 1)]\exp[-\gamma(R/R_{1e} - 1)], \tag{1.19}$$

$$\begin{aligned} F(\rho) = & - E_c\left[1 - \frac{\alpha}{\beta}\ln\left[\frac{\rho}{\rho_e}\right]\right]\left[\frac{\rho}{\rho_e}\right]^{\alpha/\beta} \\ & + \frac{1}{2}\phi_e \sum_{\Lambda} s_\Lambda \exp[-(p_\Lambda - 1)\gamma] \\ & \times \left[1 + (p_\Lambda - 1)\delta - p_\Lambda \frac{\delta}{\beta}\ln\left[\frac{\rho}{\rho_e}\right]\right] \times \left[\frac{\rho}{\rho_e}\right]^{p_\Lambda \frac{\gamma}{\beta}}, \end{aligned} \tag{1.20}$$

where the parameters γ, δ and ϕ_e are determined by minimizing the difference between the calculated and the experimental values of C_{12}, $G = (C_{11} - C_{12} + 3C_{44})/5$, and the unrelaxed vacancy formation energy E_v^f. β values are taken from Johnson's paper[4]. All

these parameters for those fcc metals are also listed in Table 1.1. The calculated values of the three elastic constants C_{11}, C_{12} and C_{44} are compared with the experimental values to which they were fitted in Table 1.2

Table 1.1: Coefficients c_τ of function $f(R)$ and the model parameters for the six fcc metals. ϕ_e is in units of eV. Other parameters are dimensionless.

	Cu	Ag	Au	Ni	Pd	Pt
c_0	0.14095	0.15326	0.21191	0.19513	0.14775	0.21295
c_1	-1.93222	-2.07431	-2.70735	-2.53828	-2.01097	-2.71705
c_2	9.60043	10.16256	12.39603	11.88049	9.91339	12.42006
c_3	-21.23718	-22.13975	-24.54730	-24.54730	-21.74378	-24.90569
c_4	20.18581	20.69699	21.02527	21.53030	20.47884	20.95506
c_5	-5.81656	-5.85219	-5.04138	-5.55520	-5.84105	-4.99180
β^a	5.85	5.96	6.67	6.41	5.91	6.69
δ	12.06	12.77	8.01	13.12	12.31	7.02
γ	6.82054	7.00515	7.37987	7.54709	6.95925	7.54886
ϕ_e	0.1217	0.0990	0.1443	0.1593	0.1457	0.3065

Submitting the embedded-atom potentials of Eqs.(1.19) and (1.20) into Eq.(1.9), we plot the energy per atom against lattice parameter for copper by taking different shells in the summation and compare with the results calculated from Eq.(1.12) (Rose model). It is very clear from Fig.(1.2) that taking summation up to the third shell will give a very good approximation in the calculation of the energy. Fig(1.3) shows the curves of the embedding potential as a function of lattice parameter with the different summation shells. It is easy to see that all neighbors beyond the sixth shell to a reference atom give very small

Table 1.2: Input and output data for the elastic constants C_{11}, C_{12} and C_{44},which are in units of $10^{11}\mathrm{N/m^2}$

	Cu	Ag	Au	Ni	Pd	Pt
C_{11}	1.70	1.24	1.86	2.465	2.341	3.47[a]
	1.683	1.223	1.839	2.349	2.252	3.203[b]
	1.67	1.29	1.83	2.33	2.18	3.03[c]
C_{12}	1.225	0.934	1.57	1.473	1.76	2.51[a]
	1.223	0.9242	1.571	1.529	1.803	2.630[b]
	1.24	0.91	1.59	1.54	1.84	2.73[c]
C_{14}	0.75	0.461	0.42	1.247	0.712	0.765[a]
	0.766	0.69	0.427	1.305	0.755	0.894[b]
	0.76	0.45	0.45	1.28	0.65	0.68[c]

[a]Input data which are the same as those used by Foiles *et al.*[7],

[b]Results from the model of Mei *et al*,

[c]Results from EAM calculations by Foiles *et al.*[7].

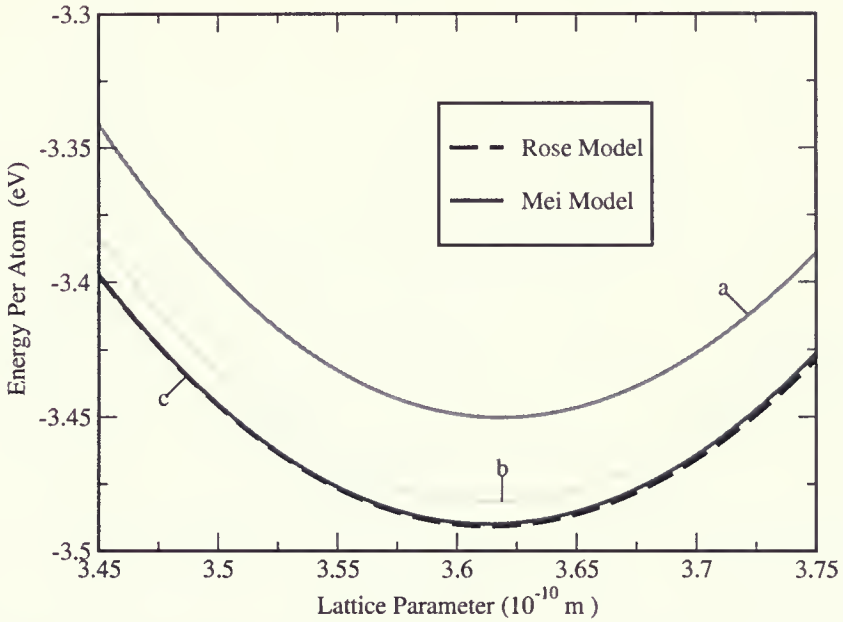

Figure 1.2: The energy per atom as a function of lattice parameter for Cu. *a*:contribution from the first shell. *b*:contribution from the first two shells. *c*:contribution from the first three shells.

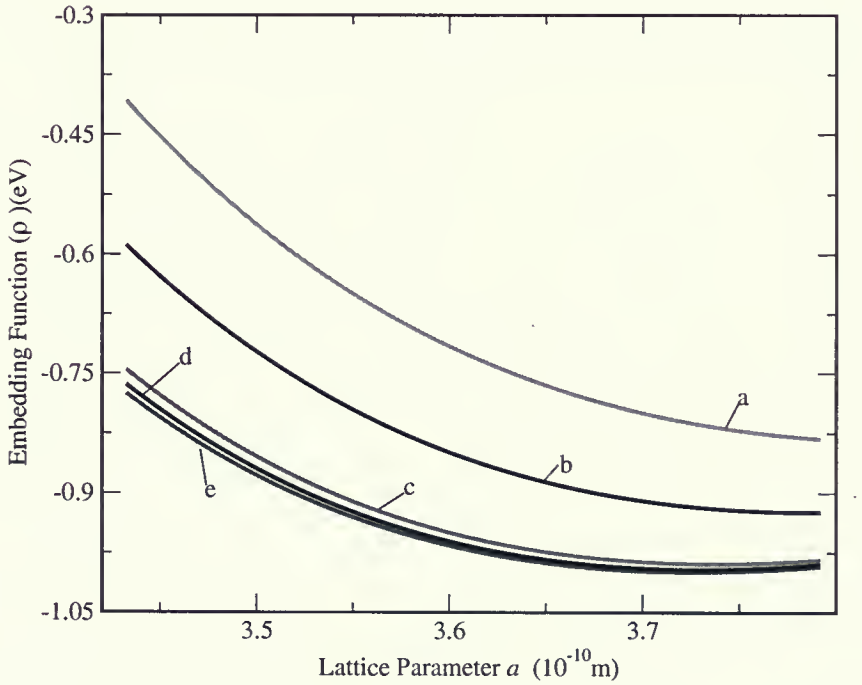

Figure 1.3: Embedding function against lattice parameter for Cu. *a*:contribution from the first shell. *b*:contribution from the first two shell. *c*:contribution from the first three shells. *d*:contribution from the first four shells. *e*:contributioin from the first six shells.

contribution to the embedding potential which can be ignored. So it is reasonable that in later calculations we will consider all summations up to the sixth shell of the neighbors with respect to a given atom.

Mei *et al.*[1] has extended the nearest-neighbor model of Johnson and suggested the analytic forms of the embedded-atom potentials valid for any choice of cutoff distance. Our present work is based on the model of Mei *et al.* . By using these relatively simple analytic EAM potentials, we have calculated the phonon frequencies for six fcc metals (Ag, Cu, Ni, Pd, Pt and Au). To investigate the applicability of this model further, we focus on the other thermodynamic properties of these metals and have computed the zero point free energy at room temperature and temperature dependence of the lattice constant, the coefficient of thermal expansion, the isothermal and adiabatic bulk moduli, Grüneisen parameters, Debye temperature and phonon contributions to the heat capacities at constant volume C_V and at constant pressure C_P. Then we compare the calculated values with the experimental findings and give some conclusions.

Chapter 2

Theory And Calculations

2.1 Phonon Dispersion Curves

2.1.1 Theory of Phonon Vibration

Here we just take into consideration of primitive crystal without losing any generality. For an infinitely extended primitive crystal, if each atom l located instantaneously at positon $\mathbf{R}(l)$ is displaced from its equilibrium position $\mathbf{R}_e(l)$ by $\mathbf{u}(l)$, which means we have

$$\mathbf{R}(l) = \mathbf{R}_e(l) + \mathbf{u}(l), \tag{2.1}$$

and

$$R^i(l) = R^i_e(l) + u_i(l), \tag{2.2}$$

the total kinetic energy of the crystal can be written as

$$T = \sum_{l,i} \frac{1}{2} M_l \dot{u}_i^2(l), \tag{2.3}$$

where M_l is the mass of the atom l and the sum runs over all atoms in crystal. $R^i(l), R^i_e(l)$ and $u_i(l)$ are the i-cartesian components of $\mathbf{R}(l), \mathbf{R}_e(l)$ and $\mathbf{u}(l)$ respectively with $i = x, y, z$.

According to the theory of phonon vibration[32, 33], the total potential energy Φ of the crystal, which is assumed to be a function of the instantaneous positions of all atoms, can be expanded into a Taylor's series in powers of the atomic displacements $\mathbf{u}(l)$ and has the

form

$$\Phi = \Phi_e + \sum_{l,i} \Phi_i(l)u_i(l) + \frac{1}{2}\sum_{\substack{l,m \\ i,j}} \Phi_{ij}(l,m)u_i(l)u_j(m) + \frac{1}{3!}\sum_{\substack{l,m,n \\ i,j,k}} \Phi_{ijk}(l,m,n)u_i(l)u_j(m)u_k(m) + \cdots. \tag{2.4}$$

In this expansion, Φ_e is the potential energy of the static lattice which means all atoms are at rest at their equilibrium positions, while obviously

$$\Phi_i(l) = \left.\frac{\partial \Phi}{\partial u_i(l)}\right|_e, \tag{2.5}$$

$$\Phi_{ij}(l,m) = \left.\frac{\partial^2 \Phi}{\partial u_i(l)\partial u_j(m)}\right|_e, \tag{2.6}$$

$$\Phi_{ijk}(l,m,n) = \left.\frac{\partial^3 \Phi}{\partial u_i(l)\partial u_j(m)\partial u_k(n)}\right|_e, etc. \tag{2.7}$$

where the subscript e means that the derivatives are evaluated with all atoms at the equilirium configuration, and the coefficients $\Phi_i(l), \Phi_{ij}(l,m), \Phi_{ijk}(l,m,n), \cdots$ are known as atomic force constants of the first, second, third,$\cdots$, order, respectivly.

It is clear that a mixed partial derivative is independent of the order in which the differentiations are carried out. The coefficients in the expansion (2.4) are completely symmetrical in the indices, such as

$$\Phi_{ij}(l,m) = \Phi_{ji}(m,l), \tag{2.8}$$

$$\begin{aligned} \Phi_{ijk}(l,m,n) &= \Phi_{jki}(m,n,l) = \Phi_{jik}(m,l,n) = \Phi_{ikj}(l,n,m) \\ &= \Phi_{kji}(n,m,l) = \Phi_{kij}(n,l,m), etc. \end{aligned} \tag{2.9}$$

From the definition fo Eqs.(2.4) and (2.5), we can see the physical interpretation in them. The first order force constant $\Phi_i(l)$ is that it is the negative of the force acting in

the i direction on the atom at $\mathbf{R}(l)$ in the equilibrium configuration. It must vanish because in equilibrium configuration the net force on any atom must be zero, so we have the result

$$\Phi_i(l) = -\mathbf{F}^i(l)|_e = 0. \tag{2.10}$$

Here $\mathbf{F}^i(l)$ denotes the i cartisian component of the force $\mathbf{F}(l)$ acted on atom l. The second order force constant $\Phi_{ij}(l,m)$ is the negative of the force exerted in the i direction on the atom l when the atom m displaced a unit distance in the j direction, all other atoms staying at their equilibrium positions. It can be expressed as

$$\Phi_{ij}(l,m) = -\frac{\partial \mathbf{F}^i(l)}{\partial u_j(m)}\bigg|_e. \tag{2.11}$$

If the lattice as a whole is subjected to an infinitesimal rigid body displacement $\mathbf{v}$, the lattice potential and its derivatives must remain unchanged. This property of the lattice imposes some conditions on the atomic force constants which can be expressed as

$$\sum_l \Phi_i(l) = 0, \tag{2.12}$$

$$\sum_l \Phi_{ij}(l,m) = \sum_m \Phi_{ij}(l,m) = 0, \tag{2.13}$$

$$\sum_l \Phi_{ijk}(l,m,n) = \sum_m \Phi_{ijk}(l,m,n) = \sum_n \Phi_{ijk}(l,m,n) = 0, etc. \tag{2.14}$$

The vibrational hamiltonian for the crystal can be written as

$$H = T + \Phi. \tag{2.15}$$

If we use the harmonic approximation, namely neglect all terms whose orders are higher more than two in Eq(2.4), we can rewrite the vibrational hamiltonian as

$$H = \Phi_e + \frac{1}{2}\sum_{i,l} M_l \dot{u}_i^2(l) + \frac{1}{2}\sum_{\substack{l,m \\ i,j}} \Phi_{ij}(l,m) u_i(l) u_j(m). \tag{2.16}$$

Denoting by $p_i(l)$ the i-cartesian componet of the momentum of the lth atom, we can change Eq.(2.16) into

$$H = \Phi_e + \sum_{i,l} p_i^2(l)/2M_l + \frac{1}{2}\sum_{\substack{l,m \\ i,j}} \Phi_{ij}(l,m)u_i(l)u_j(m). \tag{2.17}$$

From this Hamiltonian, we can immediately obtain the equation of motion of the crystal

$$M_l\ddot{u}_i(l) = -\frac{\partial\Phi}{\partial u_i(l)} = -\sum_{m,j} \Phi_{ij}(l,m)u_j(m). \tag{2.18}$$

The equation of motion Eq(2.18) with different l and i labels forms an infinite set of simultaneous linear differential equations. Their solutions are simplified by the periodicity of the lattice and the restrictions on atomic force constants which follow from the symmetry and structure of a crystal. Therefore we can choose as a solution of this set of coupled equations a function of the form

$$u_i(l) = M_l^{-1/2} e_i(l|\mathbf{K}s)\exp[-\mathbf{i}\omega_s(\mathbf{K})t + \mathbf{i}\mathbf{K}\cdot\mathbf{R}(l)]. \tag{2.19}$$

Here the vector $\mathbf{K}$ in the exponent is called wave vector, and its magnitude is equal to 2π times the reciprocal of the wavelength of an elastic wave propagation through the medium, and its direction is the direction of propagation of the wave. The coefficient $e_i(l|\mathbf{K}s)$ satisfies the equation

$$\omega_s^2(\mathbf{K})e_i(l|\mathbf{K}s) = \sum_{m,j} D_{ij}(l,m|\mathbf{K})e_j(m|\mathbf{K}s), \tag{2.20}$$

where

$$D_{ij}(l,m|\mathbf{K}) = (M_lM_m)^{-1/2}\sum_m \Phi_{ij}(l,m)\exp[-i\mathbf{K}\cdot(\mathbf{R}(l) - \mathbf{R}(m))]. \tag{2.21}$$

Usually, the matrix $D_{ij}(l,m|\mathbf{K})$ is called dynamical matrix of the crystal. It is a hermitian matrix and has the properties

$$D_{ij}(l,m|\mathbf{K}) = D_{ji}^*(m,l|\mathbf{K}) \tag{2.22}$$

$$D_{ij}(l,m|-\mathbf{K}) = D^*_{ij}(l,m|\mathbf{K}). \tag{2.23}$$

The condition that the set of Eq.(2.20) have a nontrivial solution is that the determinant of coefficients vanish

$$|D_{ij}(l,m|\mathbf{K}) - \omega_s^2(\mathbf{K})\delta_{ij}\delta_{lm}| = 0. \tag{2.24}$$

Eq.(2.24) is a 3×3 matrix equation. For each given vector $\mathbf{K}$, the allowed values of the frequency ω have three branches denoted by $\omega_s(\mathbf{K}), s = 1,2,3$, and their square are the eigenvalues of dynamical matrix. Furthermore, Eq.(2.20) defines the eigenvectors $e_i(l|\mathbf{K}s)$ only to within an arbitrarily chosen constant, so they are assumed to satisfy the orthonormality and closure conditions:

$$\sum_i e_i^*(l|\mathbf{K}s)e_i(l|\mathbf{K}s') = \delta_{ss'}, \tag{2.25}$$

$$\sum_s e_i^*(l|\mathbf{K}s)e_j(m|\mathbf{K}s) = \delta_{ij}\delta_{lm}. \tag{2.26}$$

It is clear that $\mathbf{R}(l)$ and $\mathbf{u}(l)$ are related linarly, so the derivative with respect to $\mathbf{u}(l)$ makes no difference from the derivative with respect to $\mathbf{R}(l)$. In following sections, we more often use the expression $\partial/\partial\mathbf{R}(l)$ instead of $\partial/\partial\mathbf{u}(l)$.

2.1.2 Phonon Frequencies

The application of the theory of phonon vibration to the model of Mei *et al*[1] is straightforward. Keeping the notations used in section (2.1.1), we substitue Eq.(1.15) into Eq.(1.10), and write the electron density at the position of atom l as

$$\rho_l = f_e \sum_m \sum_{\tau=0}^{\tau=5} c_\tau (R_{1e}/R_{lm})^\tau, \tag{2.27}$$

where R_{lm} is the distance between atom l and atom m which can be written as

$$R_{lm} = |\mathbf{R}(l) - \mathbf{R}(m)|, \tag{2.28}$$

the sum m runs over the all neighbors of the reference atom l.

Considering Eqs.(1.19) and (1.20), the embedded atom potentials of Mei *et al.*, we can obtain the total energy of the crystal

$$\begin{aligned} E_{tot} &= \sum_l \left\{ F_l(\rho_l) + 1/2 \sum_{m(\neq l)} \Phi(R_{lm}) \right\} \\ &= \sum_l F_l(\rho_l) + 1/2 \sum_{\substack{l,m \\ l\neq m}} \Phi(R_{lm}) \\ &= -E_c \sum_l \left[1 - \frac{\alpha}{\beta} \ln\left[\frac{\rho_l}{\rho_e}\right] \right] \left[\frac{\rho_l}{\rho_e}\right]^{\alpha/\beta} \\ &\quad + \frac{1}{2}\phi_e \sum_{\substack{l,m \\ l\neq m}} \exp[-(p_{lm}-1)\gamma] \times \left[1 + (p_{lm}-1)\delta - p_{lm}\frac{\delta}{\beta}\ln\left[\frac{\rho_l}{\rho_e}\right] \right] \left[\frac{\rho_l}{\rho_e}\right]^{p_{lm}\frac{\gamma}{\beta}} \\ &\quad - \frac{1}{2}\phi_e \sum_{\substack{l,m \\ l\neq m}} \left[1 + \delta(R_{lm}/R_{1e} - 1)\right] \exp[-\gamma(R_{lm}/R_{1e} - 1)], \end{aligned} \tag{2.29}$$

with p_{lm} having the form

$$p_{lm} = R_{lm}/R_{1e}, \tag{2.30}$$

here the first summation l runs over all atoms in the crystal, and the second one m runs over all neighbors of a given atom l.

Using the expression of the total energy Eq.(2.29), we can calculate the net force excerting on the atom l which is of the form(see details in Appendix A.1)

$$\mathbf{F}(l) = -\nabla_l E_{tot} = -\sum_{m(\neq l)} [F_l'(\rho_l) f_m'(R_{lm}) + F_m'(\rho_m) f_l'(R_{lm}) + \phi_{lm}'(R_{lm})] \frac{\mathbf{R}_{lm}}{R_{lm}}, \tag{2.31}$$

here ∇_l means to do derivative with respect to the three components of the position vector $\mathbf{R}(l)$ of atom l, namely

$$\nabla_l = \frac{\partial}{\partial R^x(l)}\mathbf{x_0} + \frac{\partial}{\partial R^y(l)}\mathbf{y_0} + \frac{\partial}{\partial R^z(l)}\mathbf{z_0}, \tag{2.32}$$

$\mathbf{x_0}, \mathbf{y_0}$ and $\mathbf{z_0}$ are the unit vectors in the directions of x, y and z respectively. The prime in the function of Eq.(2.31) donetes the derivative of the function with respect to its argument,

$\mathbf{R}_{lm}/R_{lm}$ is a unit vector which points from atom l to atom m, it has the form

$$\frac{\mathbf{R}_{lm}}{R_{lm}} = \frac{\mathbf{R}(l) - \mathbf{R}(m)}{R_{lm}}. \tag{2.33}$$

with the three components

$$\frac{R^i_{lm}}{R_{lm}} = \frac{R^i(l) - R^i(m)}{R_{lm}}. \tag{2.34}$$

The second force constant can be obtained in the same straightforward way as it was deduced in Ref.[13, 22]

$$\mathbf{\Phi}_{ij}(l,m) = \frac{\partial^2 E_{tot}}{\partial R^i(l)\partial R^j(m)} = -\frac{\partial \mathbf{F}^i(l)}{\partial R^j(m)}. \tag{2.35}$$

The result for $l \neq m$ is (see details in Appendix A.2)

$$\begin{aligned}
\mathbf{\Phi}_{ij}(l,m) &= -F_l'(\rho_l)f_m''(R_{lm})\frac{R^j_{lm}R^i_{lm}}{R^2_{lm}} - F_m'(\rho_m)f_l''(R_{lm})\frac{R^j_{lm}R^i_{lm}}{R^2_{lm}} - \Phi''(R_{lm})\frac{R^j_{lm}R^i_{lm}}{R^2_{lm}} \\
&\quad -[F_l'(\rho_l)f_m'(R_{lm}) + F_m'(\rho_m)f_l'(R_{lm}) + \Phi'(R_{lm})]\left\{\frac{\delta_{ij}}{R_{lm}} - \frac{R^i_{lm}R^j_{lm}}{R^3_{lm}}\right\} \\
&\quad + \sum_{n(\neq l,m)} F_n''(\rho_n)f_l'(R_{ln})f_m'(R_{mn})\frac{R^j_{mn}}{R_{mn}}\frac{R^i_{ln}}{R_{ln}}.
\end{aligned} \tag{2.36}$$

Using Eq.(2.13), we can obtain the second force constant for $l = m$.

$$\mathbf{\Phi}_{ij}(l,l) = -\sum_{m(\neq l)} \mathbf{\Phi}_{ij}(l,m). \tag{2.37}$$

Noticing Eq.(2.37), we can rewrite Eq.(2.21) as

$$\begin{aligned}
D_{ij}(l,m|\mathbf{K}) &= (M_l M_m)^{-1/2}\sum_m \mathbf{\Phi}_{ij}(l,m)\exp[-i\mathbf{K}\cdot(\mathbf{R}(l) - \mathbf{R}(m))] \\
&= (M_l M_m)^{-1/2}\left\{\mathbf{\Phi}_{ij}(l,l) + \sum_{m(\neq l)} \mathbf{\Phi}_{ij}(l,m)\exp[-i\mathbf{K}\cdot(\mathbf{R}(l) - \mathbf{R}(m))]\right\} \\
&= (M_l M_m)^{-1/2}\sum_{m(\neq l)} \mathbf{\Phi}_{ij}(l,m)\left\{\exp[-i\mathbf{K}\cdot(\mathbf{R}(l) - \mathbf{R}(m))] - 1\right\}.
\end{aligned} \tag{2.38}$$

Combining Eq.(2.36) with the following equations(see appendix A.3 in details),

$$F'(\rho_l) = \frac{\partial F(\rho_l)}{\partial \rho_l} = \frac{E_c}{\rho_e}\frac{\alpha^2}{\beta^2}\ln\left[\frac{\rho_l}{\rho_e}\right]\left[\frac{\rho_l}{\rho_e}\right]^{\alpha/\beta-1} + \frac{1}{2}\frac{\phi_e}{\rho_e}\sum_{t(\neq l)}\exp[-(p_{lt}-1)\gamma] \times\left\{-p_{lt}\frac{\delta}{\beta}+p_{lt}\frac{\gamma}{\beta}\left[1+(p_{lt}-1)\delta-p_{lt}\frac{\delta}{\beta}\ln\left[\frac{\rho_l}{\rho_e}\right]\right]\right\}\left[\frac{\rho_l}{\rho_e}\right]^{p_{lt}\frac{\gamma}{\beta}-1} \quad (2.39)$$

$$F''(\rho_l) = \frac{\partial F'(\rho_l)}{\partial \rho_l} = \frac{E_c}{\rho_e^2}\frac{\alpha^2}{\beta^2}\left[1+(\frac{\alpha}{\beta}-1)\ln\left[\frac{\rho_l}{\rho_e}\right]\right]\left[\frac{\rho_l}{\rho_e}\right]^{\frac{\alpha}{\beta}-2} + \frac{1}{2}\frac{\phi_e}{\rho_e^2}\sum_{t(\neq l)}\exp[-(p_{lt}-1)\gamma]\times\left\{-p_{lt}^2\frac{\delta\gamma}{\beta^2} + (p_{lt}\frac{\gamma}{\beta}-1)\left[-p_{lt}\frac{\delta}{\beta}+p_{lt}\frac{\gamma}{\beta}\left[1+(p_{lt}-1)\delta-p_{lt}\frac{\delta}{\beta}\ln\left[\frac{\rho_l}{\rho_e}\right]\right]\right]\right\}\left[\frac{\rho_l}{\rho_e}\right]^{p_{lt}\frac{\gamma}{\beta}-2} \quad (2.40)$$

$$\Phi'(R_{lm}) = -\frac{\phi_e}{R_{1e}}\left\{\delta-\gamma\left[1+\delta(\frac{R_{lm}}{R_{1e}}-1)\right]\right\}\exp[-\gamma(\frac{R_{lm}}{R_{1e}}-1)], \quad (2.41)$$

$$\Phi''(R_{lm}) = \frac{\phi_e\gamma}{R_{1e}^2}\left\{2\delta-\gamma\left[1+\delta(\frac{R_{lm}}{R_{1e}}-1)\right]\right\}\exp[-\gamma(\frac{R_{lm}}{R_{1e}}-1)], \quad (2.42)$$

$$f'(R_{lm}) = -\frac{f_e}{R_{1e}}\left[c_1(\frac{R_{1e}}{R_{lm}})^2+2c_2(\frac{R_{1e}}{R_{lm}})^3 + 3c_3(\frac{R_{1e}}{R_{lm}})^4+4c_4(\frac{R_{1e}}{R_{lm}})^5+5c_6(\frac{R_{1e}}{R_{lm}})^6\right], \quad (2.43)$$

$$f''(R_{lm}) = \frac{f_e}{R_{1e}^2}\left[2c_1(\frac{R_{1e}}{R_{lm}})^3+6c_2(\frac{R_{1e}}{R_{lm}})^4 + 12c_3(\frac{R_{1e}}{R_{lm}})^5+20c_4(\frac{R_{1e}}{R_{lm}})^6+30c_6(\frac{R_{1e}}{R_{lm}})^7\right], \quad (2.44)$$

and then substituting it in Eq.(2.38), we can get the dynamical matrix for this model. Furthermore, by solving Eq.(2.20), we can obtain the phonon frequencies.

In practice, the above procedure for the solution of the eigenvalues of Eq.(2.24) is intricate. In order to evaluate the dynamical matrix, we take 201 mesh points in each

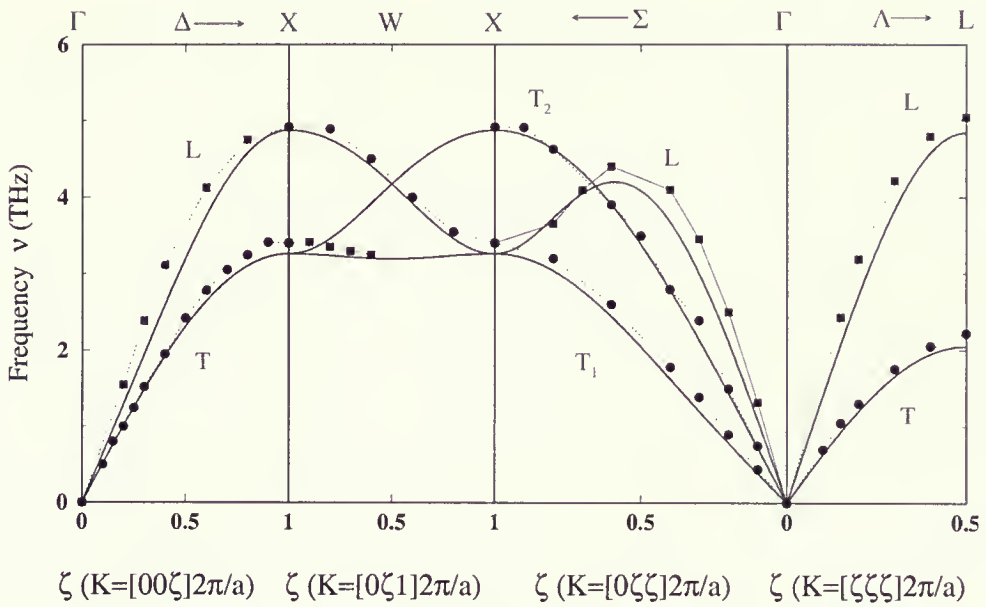

Figure 2.1: Phonon dispersion curves for Ag. The solid lines are the calculated phonon dispersion curves at the lattice parameter corresponding to static equilibrium. The square and round points are the experimental data from[34] at room temperature. L and T represent transverse modes and longitudinal modes respectively.

cartesian direction of the wave vectors **K** in the Brillouin Zone. For each **K** value, we compute the dynamical matrix, and digonalize it to get the eigenvalues. The square root of these eigenvalues will give the phonon frequencies(the program is available on contacting with the author).

We have plotted the phonon dispersion curves along four symmetry directions of **K** for these fcc matels (Fig.2.1 - Fig. 2.6).

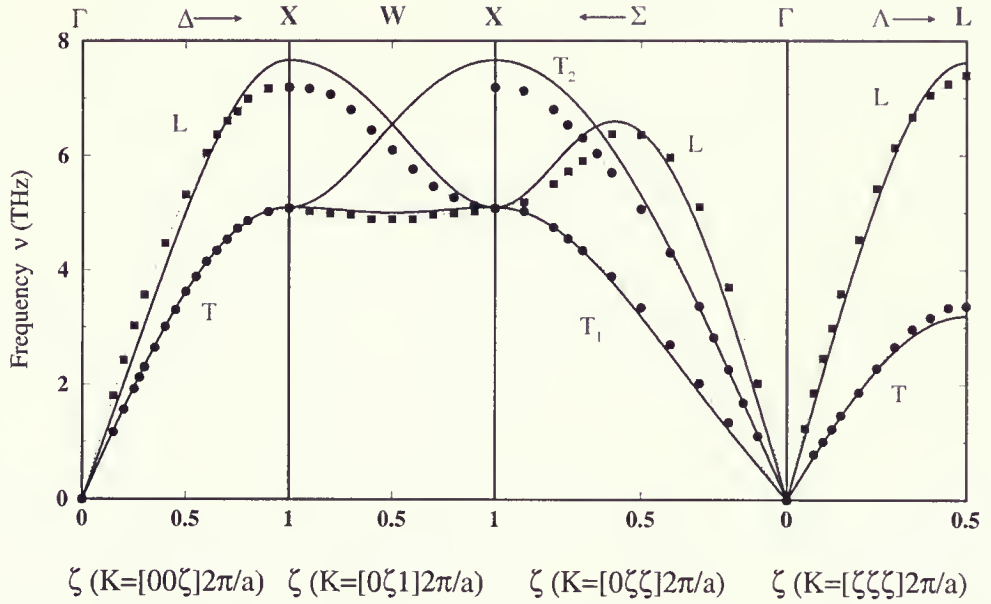

Figure 2.2: Phonon dispersion curves for Cu. The solid lines are the calculated phonon dispersion curves at the lattice parameter corresponding to static equilibrium. The square and round points are the experimental data from [35] at 296K. L and T represent transverse modes and longitudinal modes respectively.

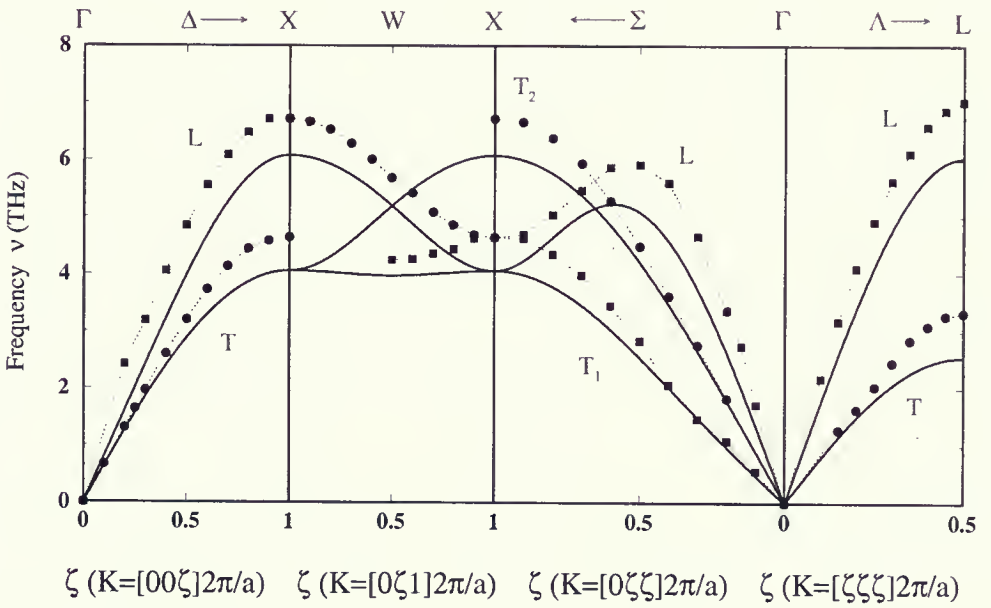

Figure 2.3: Phonon dispersion curves for Pd. The solid lines are the calculated phonon dispersion curves at the lattice parameter corresponding to static equilibrium. The square and round points are the experimental data from [36] at 120K. L and T represent transverse modes and longitudinal modes respectively.

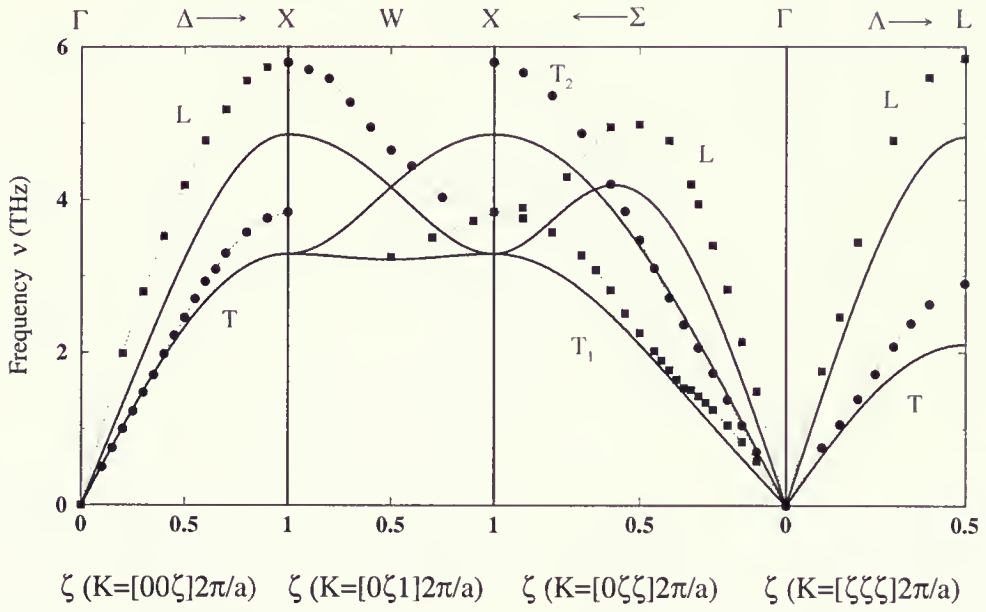

Figure 2.4: Phonon dispersion curves for Pt. The solid lines are the calculated phonon dispersion curves at the lattice parameter corresponding to static equilibrium. The square and round points are the experimental data from [37] at 90K. L and T represent transverse modes and longitudinal modes respectively.

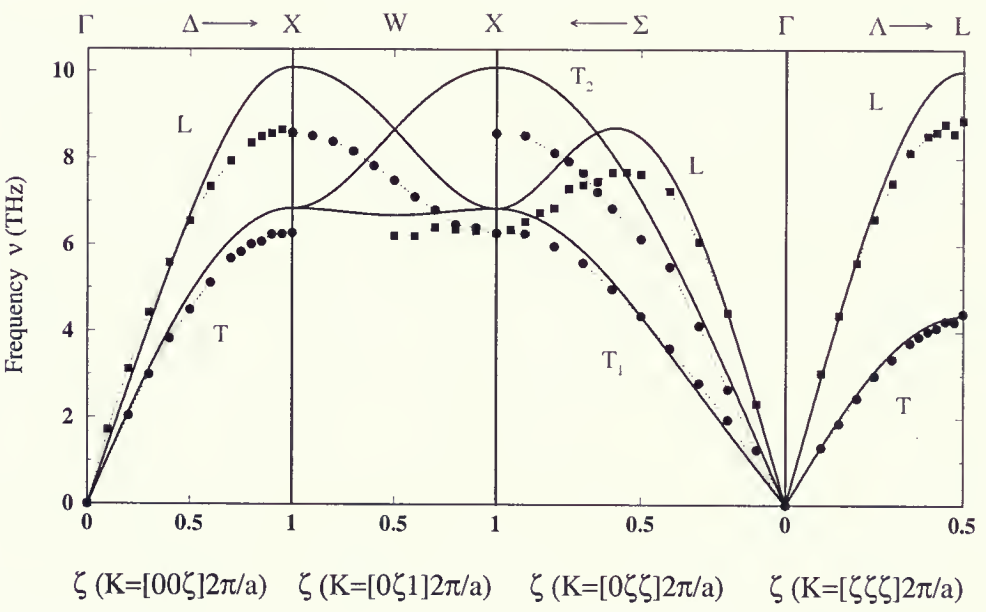

Figure 2.5: Phonon dispersion curves for Ni. the solid lines are the calculated phonon dispersion curves at the lattice parameter corresponding to static equilibrium. The square and round points are the experimental data from [38] at 296K. L and T represent transverse modes and longitudinal modes respectively.

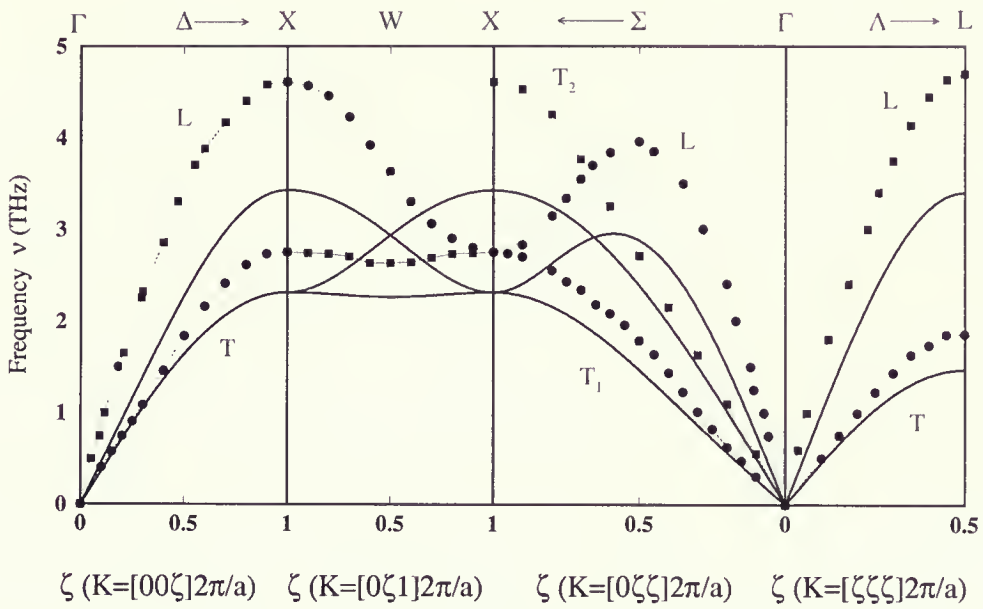

Figure 2.6: Phonon dispersion curves for Au. The solid lines are the calculated phonon dispersion curves at the lattice parameter corresponding to static equilibrium. the square and round points are the experimental data from [39] at 296K. L and T represent transverse modes and longitudinal modes respectively.

2.2 Thermodynamical Properties

2.2.1 Zero-Point Energy

By introducing phonon creation operator $b^+_{\mathbf{K}s}$ and destruction operator $b_{\mathbf{K}s}$ which satisfy the commutation relations

$$[b^+_{\mathbf{K}s}, b^+_{\mathbf{K}'s'}] = [b_{\mathbf{K}s}, b_{\mathbf{K}'s'}] = 0, \tag{2.45}$$

$$[b_{\mathbf{K}s}, b^+_{\mathbf{K}'s'}] = \Delta(\mathbf{K} - \mathbf{K}')\delta_{ss'}, \tag{2.46}$$

with

$$\Delta(\mathbf{K}) = \frac{1}{N}\sum_l e^{i\mathbf{K}\cdot\mathbf{R}(l)}. \tag{2.47}$$

and using the expansions of $u_i(l)$ and $p_i(l)$ in the terms of plane waves

$$u_i(l) = \left(\frac{\hbar}{2NM_l}\right)^{\frac{1}{2}} \sum_{\mathbf{K}s} \omega_s^{-1/2}(\mathbf{K}) e_i(l|\mathbf{K}s) e^{i\mathbf{K}\cdot\mathbf{R}(l)} (b_{\mathbf{K}s} + b^+_{-\mathbf{K}s}), \tag{2.48}$$

$$p_i(l) = \frac{1}{\mathbf{i}}\left(\frac{\hbar M_l}{2N}\right)^{\frac{1}{2}} \sum_{\mathbf{K}s} \omega_s^{1/2}(\mathbf{K}) e_i(l|\mathbf{K}s) e^{\mathbf{i}\mathbf{K}\cdot\mathbf{R}(l)} (b_{\mathbf{K}s} - b^+_{-\mathbf{K}s}), \tag{2.49}$$

and the inverses to these expansions

$$b_{\mathbf{K}s} = (2N\hbar)^{-1/2} \sum_{li} e_i^*(l|\mathbf{K}s) e^{-\mathbf{i}\mathbf{K}\cdot\mathbf{R}(l)} \left\{ [M_l\omega_s(\mathbf{K})]^{1/2} u_i(l) + \mathbf{i}[M_l\omega_s(\mathbf{K})]^{-1/2} p_i(l) \right\}, \tag{2.50}$$

$$b^+_{\mathbf{K}s} = (2N\hbar)^{-1/2} \sum_{li} e_i(l|\mathbf{K}s) e^{\mathbf{i}\mathbf{K}\cdot\mathbf{R}(l)} \left\{ [M_l\omega_s(\mathbf{K})]^{1/2} u_i(l) - \mathbf{i}[M_l\omega_s(\mathbf{K})]^{-1/2} p_i(l) \right\}, \tag{2.51}$$

where $\hbar$ is Planck's constant, N is the number of primitive unit cells in a parallelepiped all of which fill of crystal space without gaps and overlap, both $\mathbf{K}$ and $\mathbf{K}'$ are restricted to lie inside the first Brillouin zone, we can obtain the Hamiltonian in the forms of these new operators

$$H = \sum_{\mathbf{K}s} \hbar\omega_s(\mathbf{K})[b^+_{\mathbf{K}s} b_{\mathbf{K}s} + 1/2]. \tag{2.52}$$

The ground state $|0>$ is defined by

$$b_{\mathbf{K}s}|0> = 0, \text{ for all } (\mathbf{K}s). \tag{2.53}$$

Therefore, the eigensolutions of the Hamiltonian (2.52) read

$$\begin{aligned} &|n_{s_1}(\mathbf{K}_1), \cdots, n_{s_3}(\mathbf{K}_1), \cdots, n_{s_1}(\mathbf{K}_N), \cdots, n_{s_3}(\mathbf{K}_N)> \\ &= \left\{ \prod_{\mathbf{K}}^{N} \prod_{s=1}^{3} (n_{\mathbf{K}s})! \right\}^{-1/2} \prod_{\mathbf{K}}^{N} \prod_{s=1}^{3} (b^+_{\mathbf{K}s})^{n_{\mathbf{K}s}} |0>, \end{aligned} \tag{2.54}$$

$$E(\{n_{\mathbf{K}s}\}) = \sum_{\mathbf{K}}^{N} \sum_{s=1}^{3} \hbar\omega_s(\mathbf{K})[n_{\mathbf{K}s} + \frac{1}{2}], \tag{2.55}$$

where

$$n_{\mathbf{K}s} = 0, 1, 2, \cdots \tag{2.56}$$

denotes the number of phonons of frequency $\omega_s(\mathbf{K})$ present in the state (2.54).

Table 2.1: Zero-Point Energy in Rydberg per atom at 300 K.

Elements	Zero-Point Energy			
	Present	Ref.[40]	Ref.[41]	Ref.[42]
Cu	0.00220	0.00220	0.00226	0.00231
Ag	0.00140	0.00147	0.00147	0.00158
Ni	0.00295	0.00270	0.00275	0.00279
Pt	0.00141	0.00167	0.00167	0.00184
Pd	0.00175	0.00200	0.00198	0.00218
Au	0.00098	0.00140	0.00134	0.00146

For the ground state, the energy is

$$E_0 = \sum_{\mathbf{K}s} \frac{1}{2}\hbar\omega_s(\mathbf{K}). \tag{2.57}$$

This is called the zero-point energy of the crystal[33].

We use the lattice parameter at room temperature to calculate the phonon freqencies on a $20 \times 20 \times 20$ **K**-point mesh in the Brillouin Zone, and then do summation over these frequencies to obtain the zero-point energy per atom. Table (2.1) gives the results and its comparison with other theorectical findings. To the best of our knowledge, experimental data for this property is not available yet.

2.2.2 Linear Thermal Expansion

The thermodynamic functions of crystal in the harmonic approximation can be obtained from the partition function

$$Z = Tr\{e^{-\beta H}\}, \tag{2.58}$$

where H is Hamiltonian in the harmonic approximation, $\beta = 1/k_BT$, k_B is Boltzmann's constant, and T is the absolute temperature. It is convenient to evaluate the trace in Eq.(2.58) in the space in which H is diagonal. Therefore, if taking the forms of Eq.(2.52) and Eq.(2.54) and submitting in Eq.(2.58), we can find

$$\begin{aligned} Z &= \sum_{n_{\mathbf{K}_1 s_1}=0}^{\infty} \cdots \sum_{n_{\mathbf{K}_N s_3}=0}^{\infty} \exp\Big\{ -\beta \sum_{\mathbf{K}s} \hbar\omega_s(\mathbf{K})[n_{\mathbf{K}s} + \frac{1}{2}] \Big\} \\ &= \prod_{\mathbf{K}s} \frac{\exp[-\frac{1}{2}\beta\hbar\omega_s(\mathbf{K})]}{1-\exp[-\beta\hbar\omega_s(\mathbf{K})]}. \end{aligned} \tag{2.59}$$

The Helmholtz free energy which comes from the contribution of phonon vibration is given by

$$F_{vib} = -k_BT\ln Z = k_B \sum_{\mathbf{K}s} \ln\{2sinh\frac{\hbar\omega_s(\mathbf{K})}{2k_BT}\}. \tag{2.60}$$

The entropy S , the internal energy E and the specific heat at constant volume C_V of the crystal become

$$S = -\left(\frac{\partial F}{\partial T}\right) = k_B \sum_{\mathbf{K}s} \left\{ \frac{\hbar\omega_s(\mathbf{K})}{2k_BT} coth\frac{\hbar\omega_s(\mathbf{K})}{2k_BT} - \ln\big(2sinh\frac{\hbar\omega_s(\mathbf{K})}{2k_BT}\big) \right\} \tag{2.61}$$

$$E = F + TS = \sum_{\mathbf{K}s} \frac{1}{2}\hbar\omega_s(\mathbf{K}) coth\frac{\hbar\omega_s(\mathbf{K})}{2k_BT} \tag{2.62}$$

$$\begin{aligned} C_V &= \left(\frac{\partial E}{\partial T}\right)_V \\ &= \sum_{\mathbf{K},s} C_V(\mathbf{K}s) \\ &= k_B \sum_{\mathbf{K}s} \left\{ \frac{\hbar\omega_s(\mathbf{K})}{2k_BT} \right\}^2 \frac{1}{sinh^2[\hbar\omega_s(\mathbf{K})/2k_BT]}. \end{aligned} \tag{2.63}$$

In the quasiharmonic approximation, the total Helmholtz free energy of crystal at temperature T and volume V or lattice constant a is [43]

$$F(a,T) = E_{tot}(a) + F_{vib}(a,T) = E_{tot}(a) + k_B \sum_{\mathbf{K}s} \ln\{2sinh\frac{\hbar\omega_s(\mathbf{K},a)}{2k_BT}\} \tag{2.64}$$

where E_{tot} is static total energy at a given volume V or lattice constant a which is defined by Eq.(1.1). We use $\omega_s(\mathbf{K},a)$ instead of $\omega_s(\mathbf{K})$ in Eq.(2.64) to specify that frequency is also a function of lattice parameter a.

At a given temperature T and zero pressure, the equilibrium geometry is determined by the minmum of the Helmhotz free energy[43], that is

$$(\frac{\partial F(a,T)}{\partial a})_T = \frac{\partial E(a)}{\partial a} + (\frac{\partial F_{vib}(a,T)}{\partial a})_T = 0. \tag{2.65}$$

In application of Eq.(2.65), we use the free energy per atom instead of the free energy of the crystal by evaluating F_{vib} on a $20 \times 20 \times 20$ $\mathbf{K}$-points mesh in the Brillouin Zone and plus the static energy per atom which is defined in Eq.(1.9). First, we set up an array for the lattice parameter a, and then we change the temperature T value at a step equal to $2K$ from $0K$ to $1400K$ to calculate the free energy per atom at different lattice parameter. The equilibrium lattice constant $a_e(T)$ at the given temperature T is the one corresponding to the minimun of the free energy per atom at that temperature. In Fig.(2.7), we plot the lattice parameter against temperature.

Using the results obtained for the lattice constant as a function of temperature, we can determine the linear thermal expansion[43]

$$\epsilon(T) = \frac{a_e(T) - a_e(T_c)}{a_e(T_c)}, \tag{2.66}$$

where we have chosen lattice constant $a_e(T_c)$ at $T_c = 293K$ to be the reference length as [44] did. Figs.(2.8-2.13) give the calculated results and experimental data.

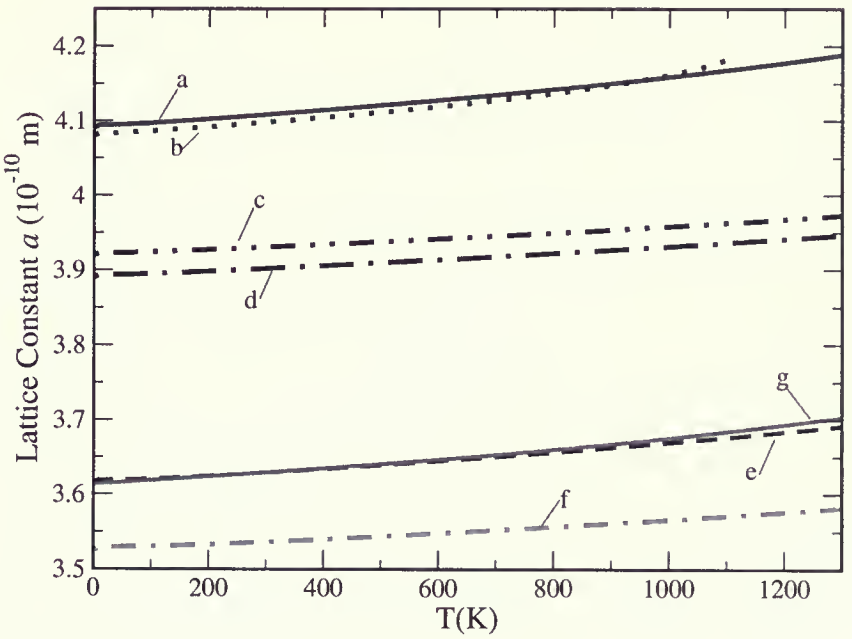

Figure 2.7: Lattice Constant Against Temperature for the fcc Metals. Line a is for Ag, b is for Au, c is for Pt, d is for Pd, e is for Cu, and f is for Ni. line g is the results of the MD simulation from Ref.[1] for Cu.

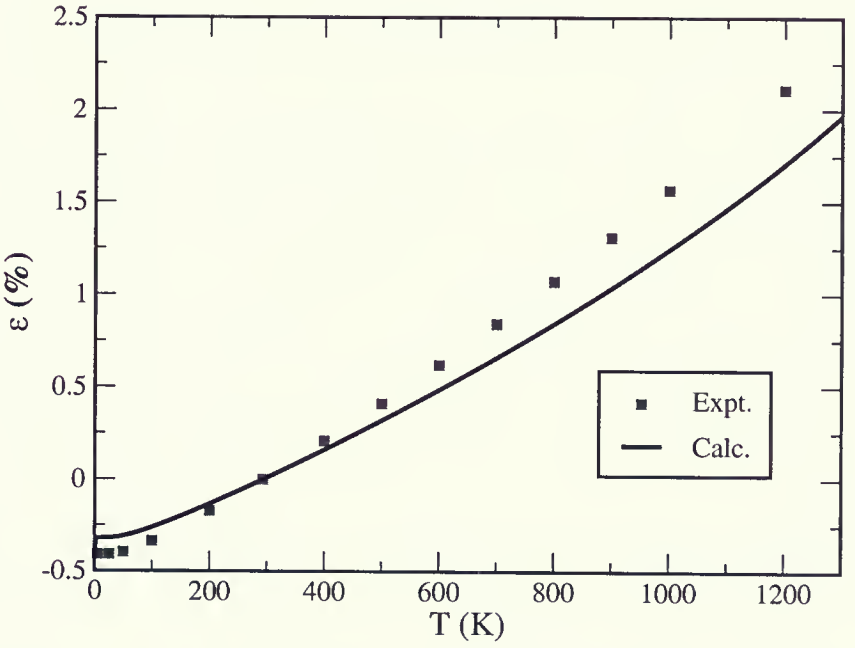

Figure 2.8: Temperature dependence of linear thermal expansion $\epsilon(T)$ for Ag. the solid line is the calculated values, and the square points are the experimental values from Ref.[45]

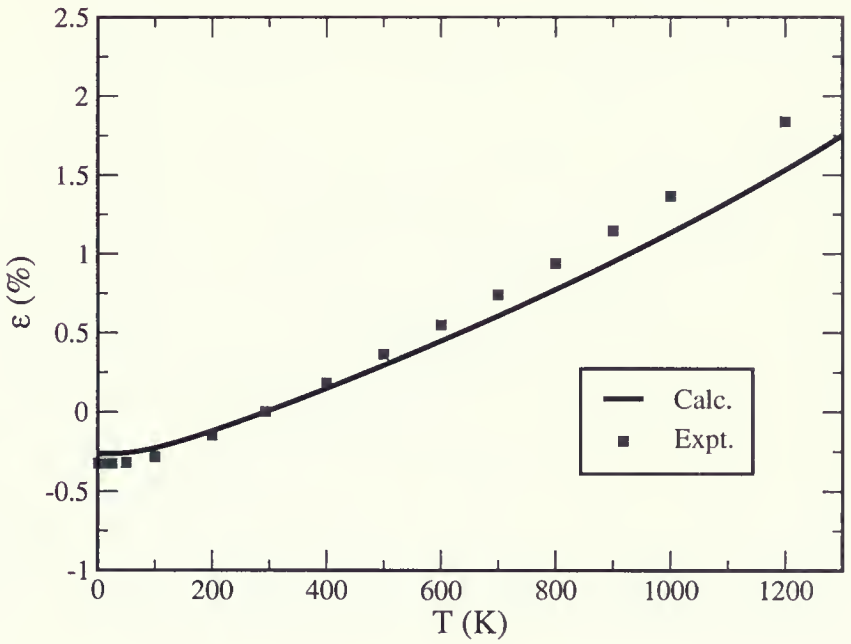

Figure 2.9: Temperature dependence of linear thermal expansion $\epsilon(T)$ for Cu. the solid line is the calculated values, and the square points are the experimental values from Ref.[45]

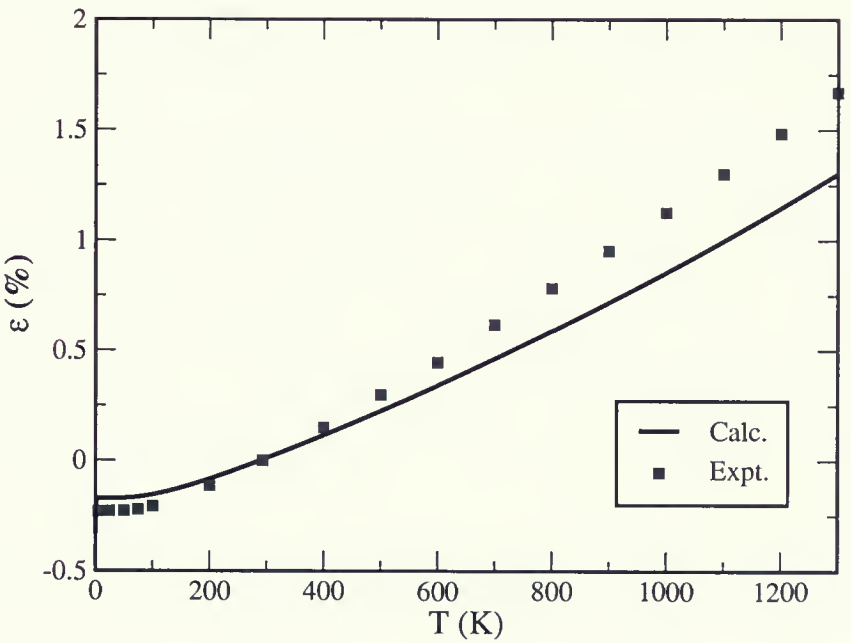

Figure 2.10: Temperature dependence of linear thermal expansion $\epsilon(T)$ for Ni. the solid line is the calculated values, and the square points are the experimental values from Ref.[45]

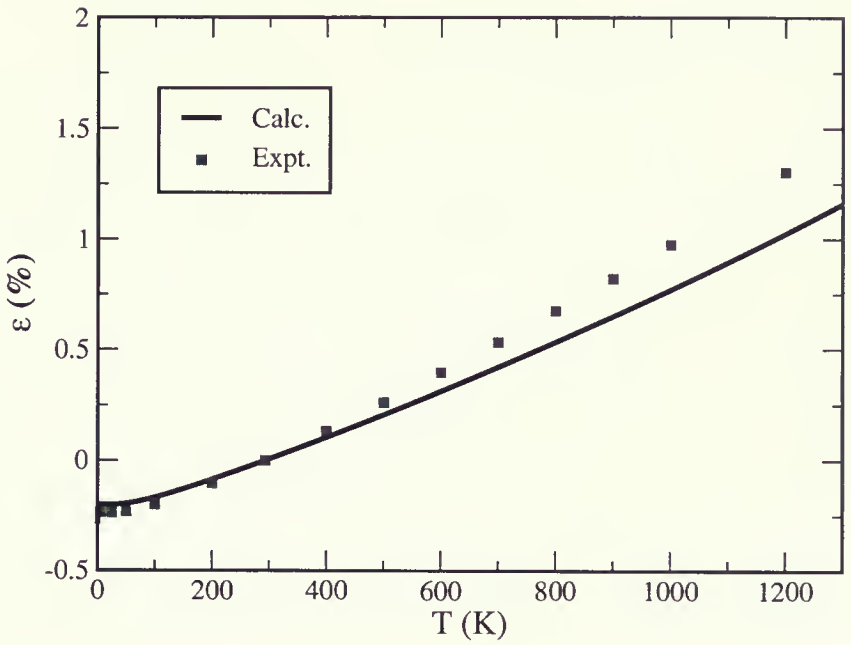

Figure 2.11: Temperature dependence of linear thermal expansion $\epsilon(T)$ for Pd. the solid line is the calculated values, and the square points are the experimental values from Ref.[45]

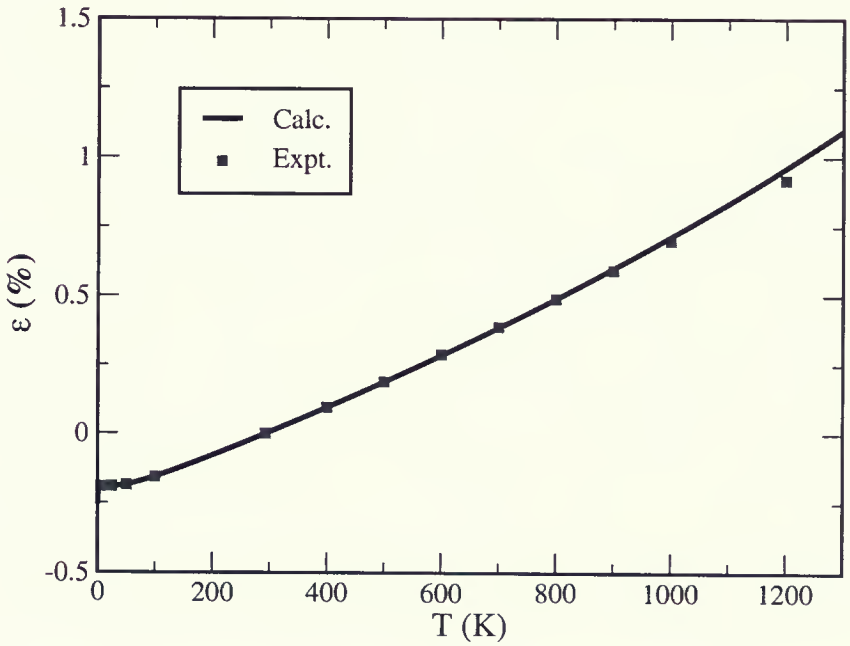

Figure 2.12: Temperature dependence of linear thermal expansion $\epsilon(T)$ for Pt. the solid line is the calculated values, and the square points are the experimental values from Ref.[45]

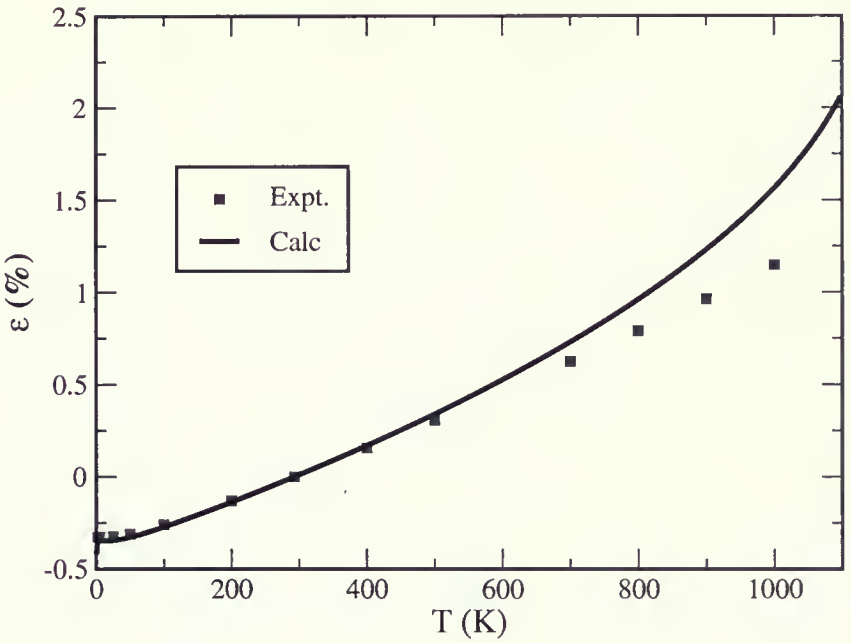

Figure 2.13: Temperature dependence of linear thermal expansion $\epsilon(T)$ for Au. the solid line is the calculated values, and the square points are the experimental values from Ref.[45]

The definition of the coefficient of linear thermal expansion [44] is

$$\alpha(T) = \frac{1}{a_e(T)}\left(\frac{da_e(T)}{dT}\right)_p. \tag{2.67}$$

In experimental case, Eq.(2.67) is replaced by the following the equation[43]

$$\alpha(T) = \frac{1}{a_e(T_c)}\left(\frac{da_e(T)}{dT}\right)_p, \tag{2.68}$$

where T_c is a reference temperature and in the present case we take $T_c = 293$. Using Eq.(2.68), we calculate the coefficients of linear expansion $\alpha(T)$ for these six metals and plot them in Figs.(2.14 - 2.19) with experimental values.

2.2.3 Isothermal Bulk Modulus

For a system at a given temperature T and volume V, the equation of state of the system is obtained from Eq.(2.62) and Eq.(2.64) by equating the pressure P to minus the volume

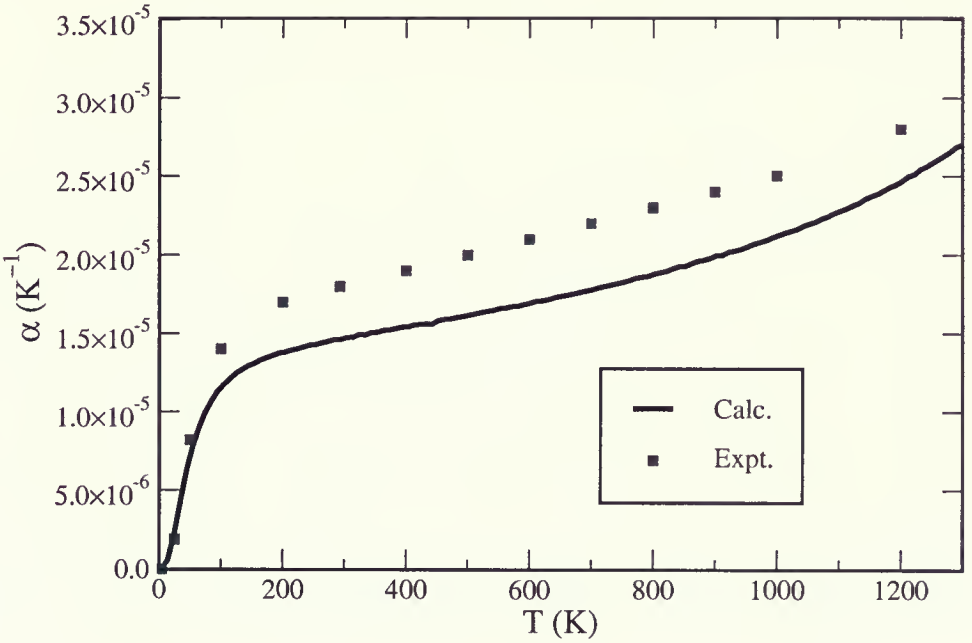

Figure 2.14: Coefficient of linear thermal expansion $\alpha(T)$ as a function of temperature for Ag. the solid line is the calculated values, and the square points are the experimental values from Ref.[45].

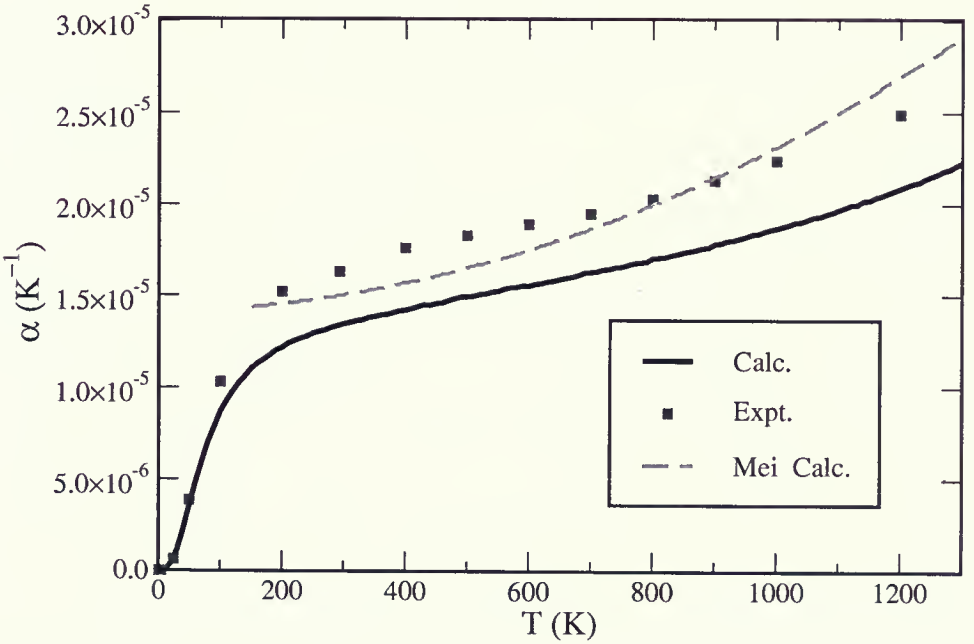

Figure 2.15: Coefficient of linear thermal expansion $\alpha(T)$ as a function of temperature for Cu. the solid line is the calculated values, the square points are the experimental values from Ref.[45], and the dash line is the results of the MD simulation from Ref.[1].

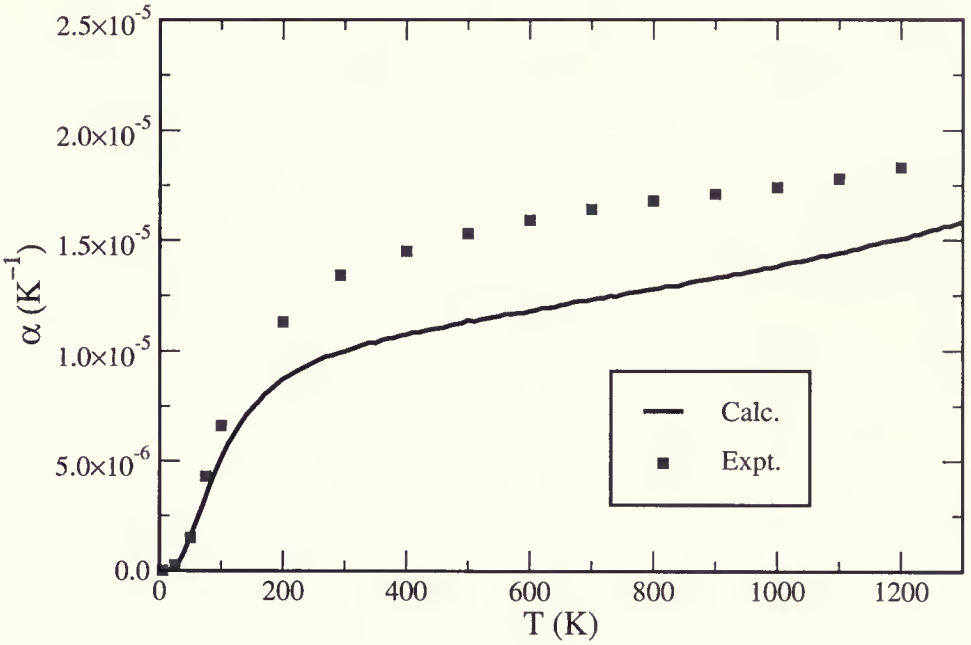

Figure 2.16: Coefficient of linear thermal expansion $\alpha(T)$ as a function of temperature for Ni. the solid line is the calculated values, and the square points are the experimental values from Ref.[45].

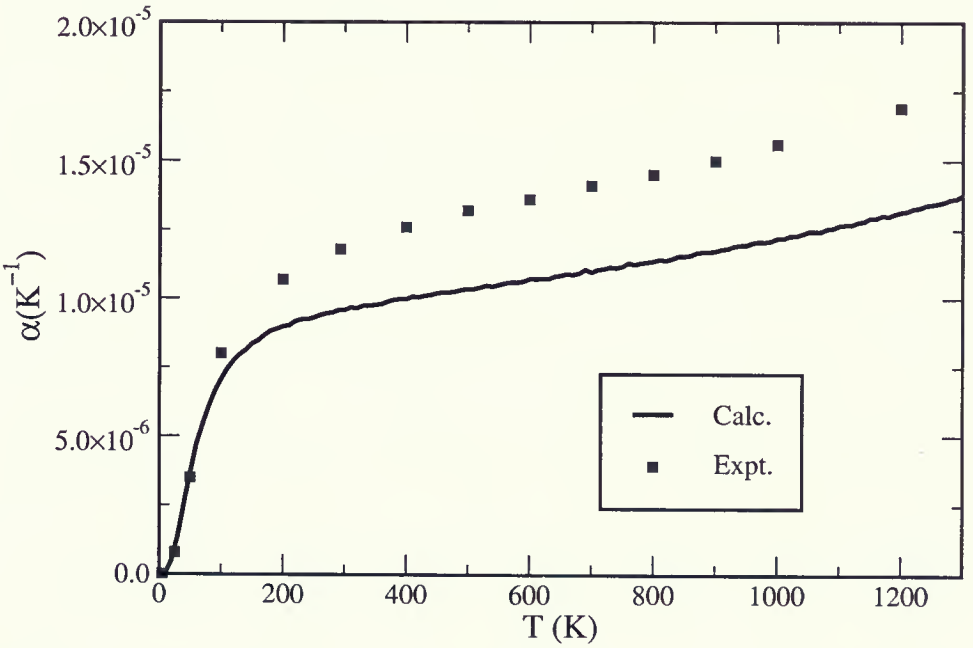

Figure 2.17: Coefficient of linear thermal expansion $\alpha(T)$ as a function of temperature for Pd. the solid line is the calculated values, and the square points are the experimental values from Ref.[45]

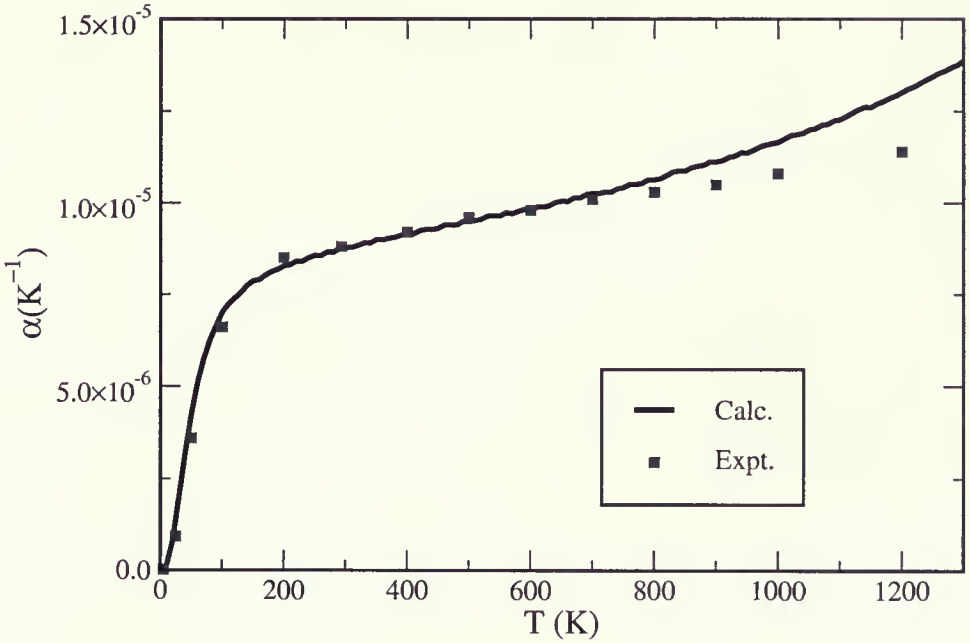

Figure 2.18: Coefficient of linear thermal expansion $\alpha(T)$ as a function of temperature for Pt. the solid line is the calculated values, and the square points are the experimental values from Ref.[45]

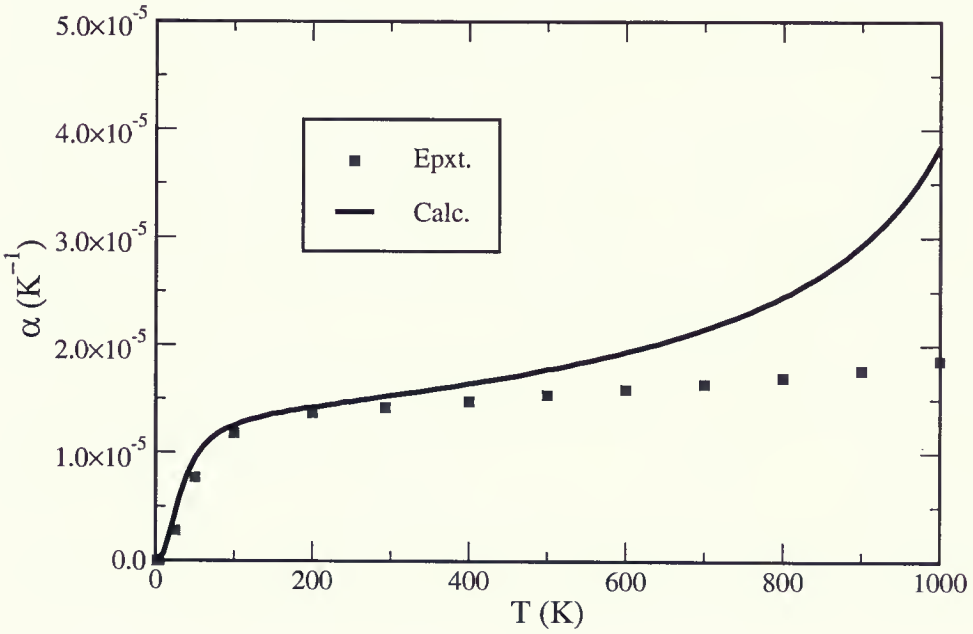

Figure 2.19: Coefficient of linear thermal expansion $\alpha(T)$ as a function of temperature for Au. the solid line is the calculated values, and the square points are the experimental values from Ref.[45]

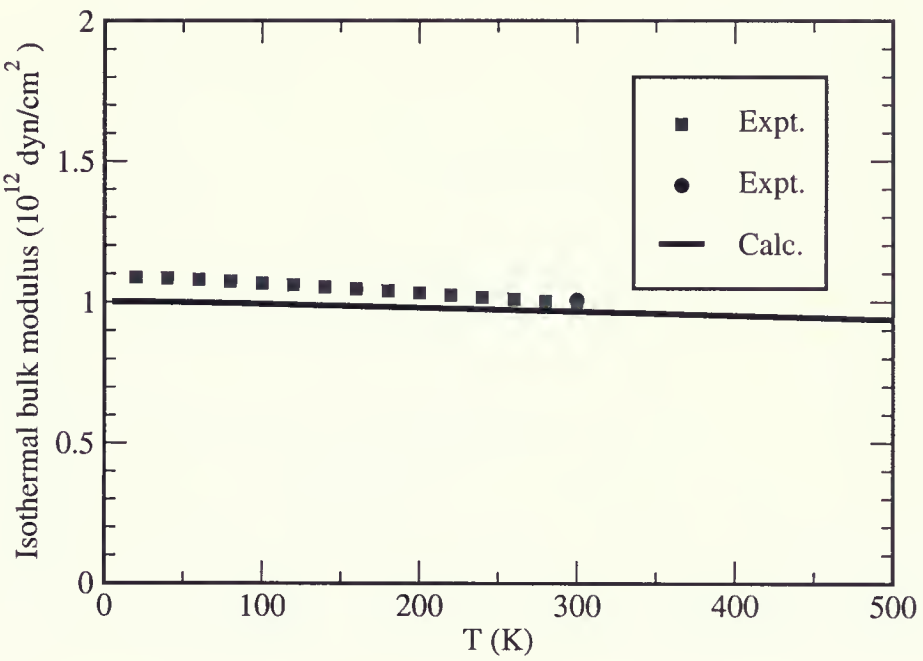

Figure 2.20: Isothermal bulk modulus $B(T)$ as a function of temperature for Ag. the solid line is the calculated values, the square points are the experimental values from Ref.[47] and the round point is the experimental value from[48].

derivative of the free energy [46]:

$$P = -(\frac{\partial F}{\partial V})_T. \tag{2.69}$$

The temperature dependence of the isothermal bulk modulus is defined by[46]

$$B(T) = -V(\frac{\partial P}{\partial V})_T \tag{2.70}$$

or

$$\begin{aligned} B(T) &= V(\frac{\partial^2 F}{\partial V^2})_T \\ &= V(\frac{\partial^2 E}{\partial V^2}) + V(\frac{\partial^2 F_{vib}(a,T)}{\partial V^2})_T. \end{aligned} \tag{2.71}$$

We use the numerical method to evaluate the Eq.(2.71) and plot the results with experimental data in Figs.(2.20 - 2.25).

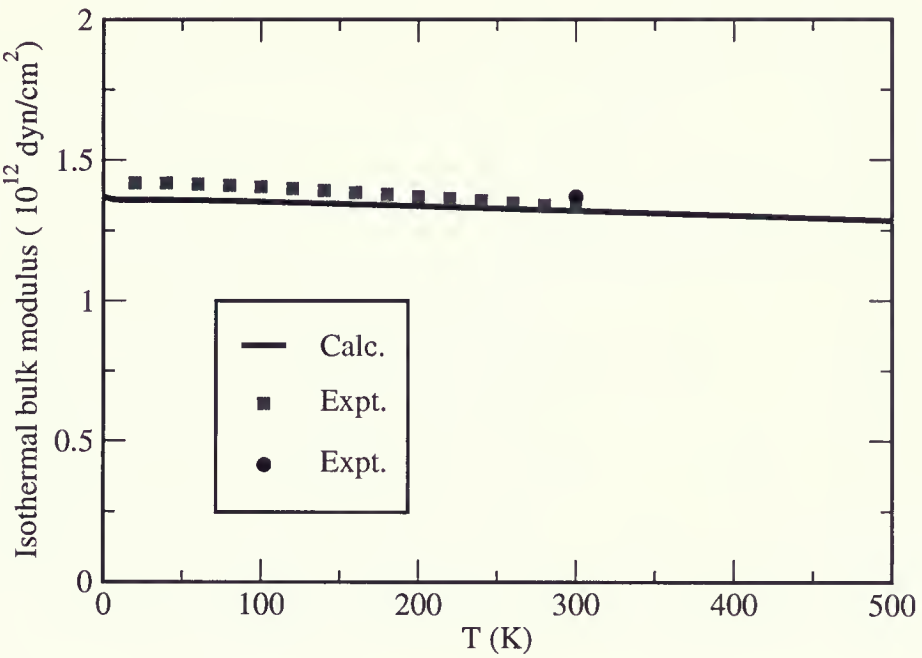

Figure 2.21: Isothermal bulk modulus $B(T)$ as a function of temperature for Cu. the solid line is the calculated values, the square points are the experimental values from Ref.[47]and the round point is the experimental value from[48].

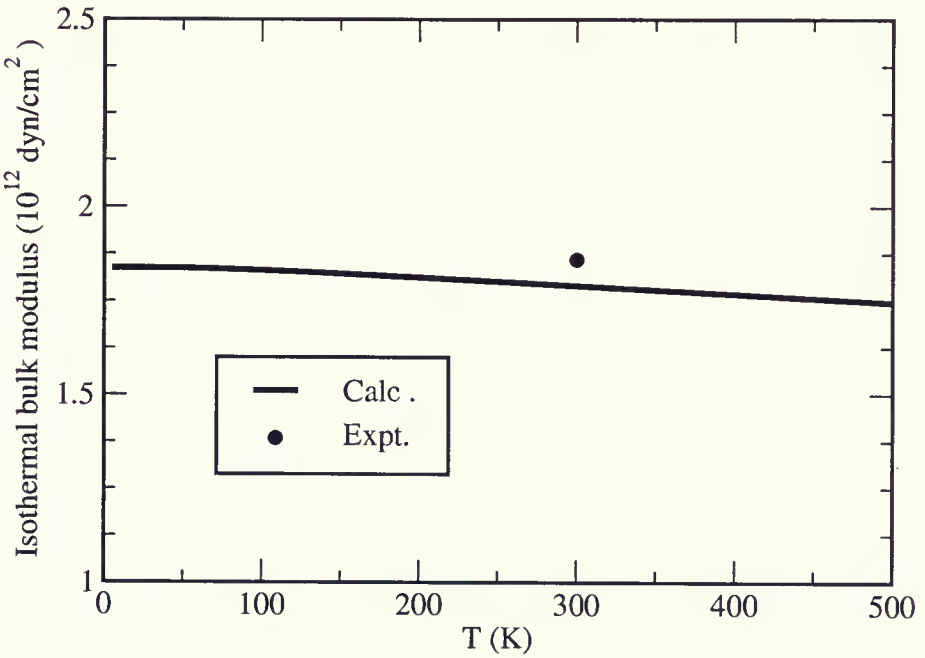

Figure 2.22: Isothermal bulk modulus $B(T)$ as a function of temperature for Ni. the solid line is the calculated values, and the round point is the experimental value from Ref.[48].

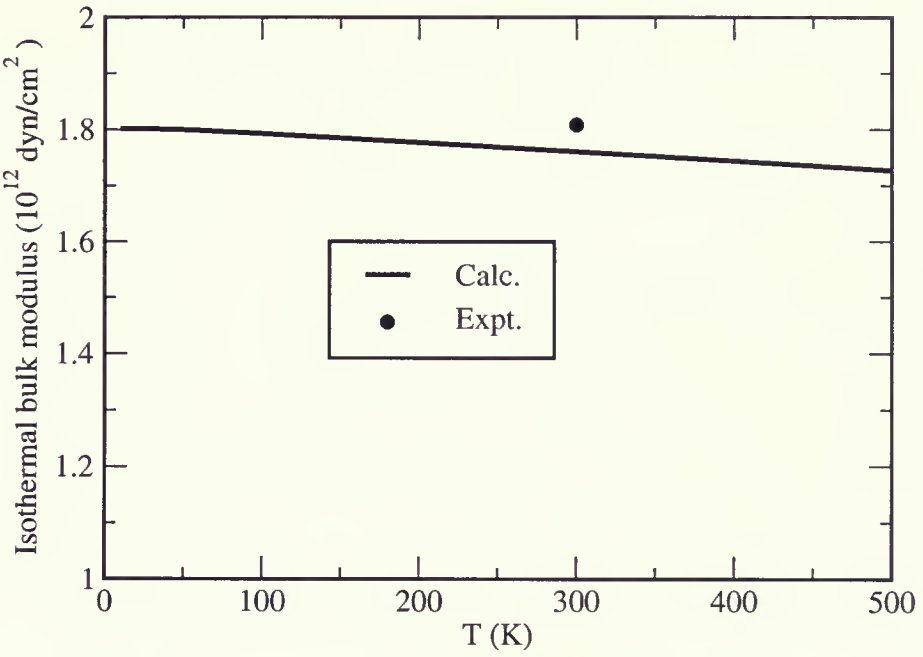

Figure 2.23: Isothermal bulk modulus $B(T)$ as a function of temperature for Pd. the solid line is the calculated values, and the round point is the experimental value from Ref.[48].

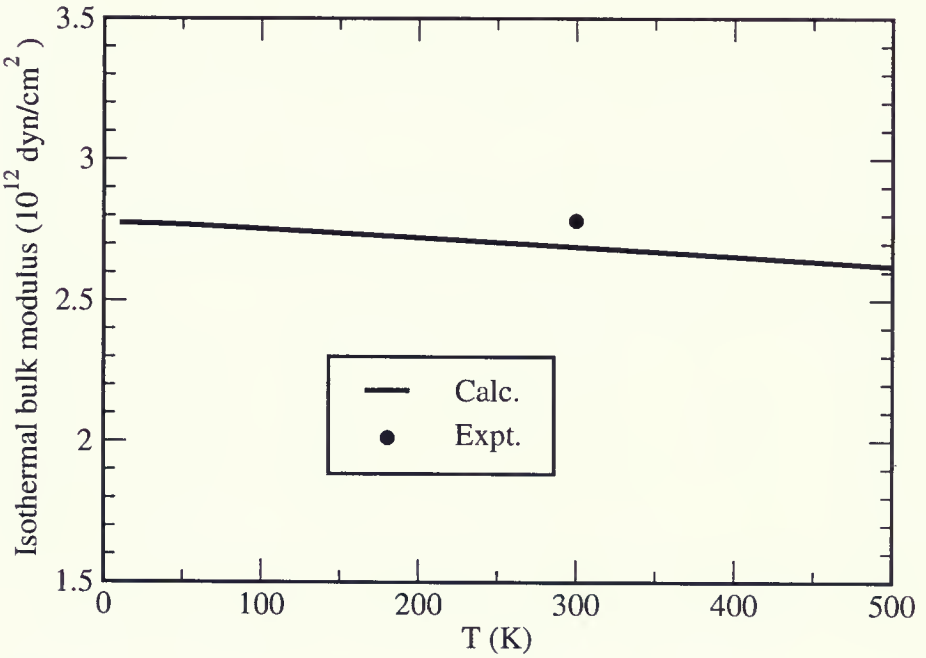

Figure 2.24: Isothermal bulk modulus $B(T)$ as a function of temperature for Pt. the solid line is the calculated values, and the round point is the experimental value from Ref.[48].

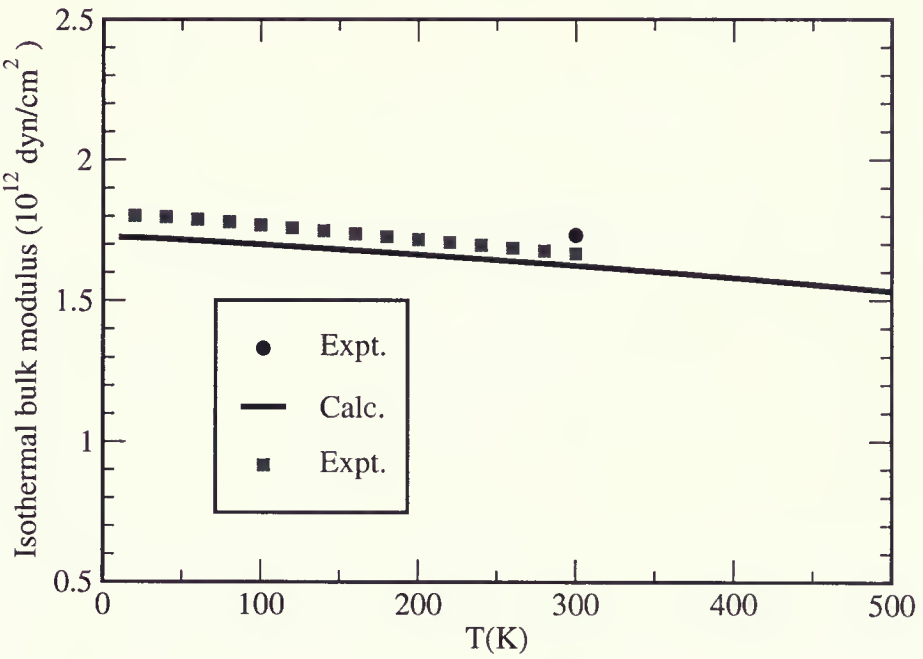

Figure 2.25: Isothermal bulk modulus $B(T)$ as a function of temperature for Au. the solid line is the calculated values, the square points are the experimental values from Ref.[47] and the round point is experimental value from Ref.[48].

2.2.4 Heat Capacity C_V and C_P

The specific heat at constant volume comes from two contributions: one is from the phonons and determined by Eq.(2.63), the other is from electrons. We denote the two parts as $C_V^{ph}(T)$ and $C_V^{el}(T)$ respectively. The total specific heat at constant volume is

$$C_V(T) = C_V^{ph}(T) + C_V^{el}(T). \tag{2.72}$$

The relation between C_V and C_P is[49]

$$C_P(T) - C_V(T) = -T(\frac{\partial V}{\partial T})_P^2(\frac{\partial P}{\partial V})_T. \tag{2.73}$$

Using the definition of the volume thermal expansion coefficient[49]

$$\alpha_V(T) = \frac{1}{V}(\frac{\partial V}{\partial T})_P \tag{2.74}$$

and submitting Eq.(2.69) into Eq.(2.73), we can obtain

$$C_P(T) - C_V(T) = \alpha_V^2(T)B(T)VT. \tag{2.75}$$

It is clear that the linear thermal expansion coefficient and the volume thermal expansion coefficient are related by the following equation

$$\alpha_V(T) = 3\alpha(T). \tag{2.76}$$

Noticing the volume of each atom in fcc structure is $V = a_e^3(T)/4$, we rewrite Eq.(2.75) as

$$C_P(T) - C_V(T) = \frac{9}{4}\alpha^2(T)B(T)a_e^3(T)T \tag{2.77}$$

or

$$C_P(T) = C_V^{ph}(T) + C_V^{el}(T) + \frac{9}{4}\alpha^2(T)B(T)a_e^3(T)T. \tag{2.78}$$

We use Eq.(2.63) to calculate the first term $C_V^{ph}(T)$ in Eq.(2.78) at different temperature by evaluating it on a $20 \times 20 \times 20$ **K**-point mesh in the Brillouin Zone, and then we apply the STUTGART TB-LMTO-ASA program to compute the electronical contribution to heat capacity $C_V^{el}(T)$. We take the results $\alpha(T), B(T)$ and $a_e(T)$ from the above to calculate the third term in Eq.(2.78) and plus three terms together to obtain the temperature dependant $C_P(T)$. Figs.(2.26 - 2.31) show the temperature dependence of heat capacity at constant volume C_V^{ph}, at constant pressure C_P and electronical contribution C_V^{el} with the experimental data.

2.2.5 Grüneisen Parameter

Submitting Eq.(2.64) into Eq.(2.69), we can write the equation of state as

$$\begin{aligned} P &= \frac{dE_{tot}(a)}{dV} + \left(\frac{\partial F_{vib}(a,T)}{\partial V}\right)_T \\ &= \frac{dE_{tot}(a)}{dV} + \frac{1}{V}\sum_{\mathbf{K},s}\gamma_s(\mathbf{K})\epsilon(\omega_s(\mathbf{K})), \end{aligned} \tag{2.79}$$

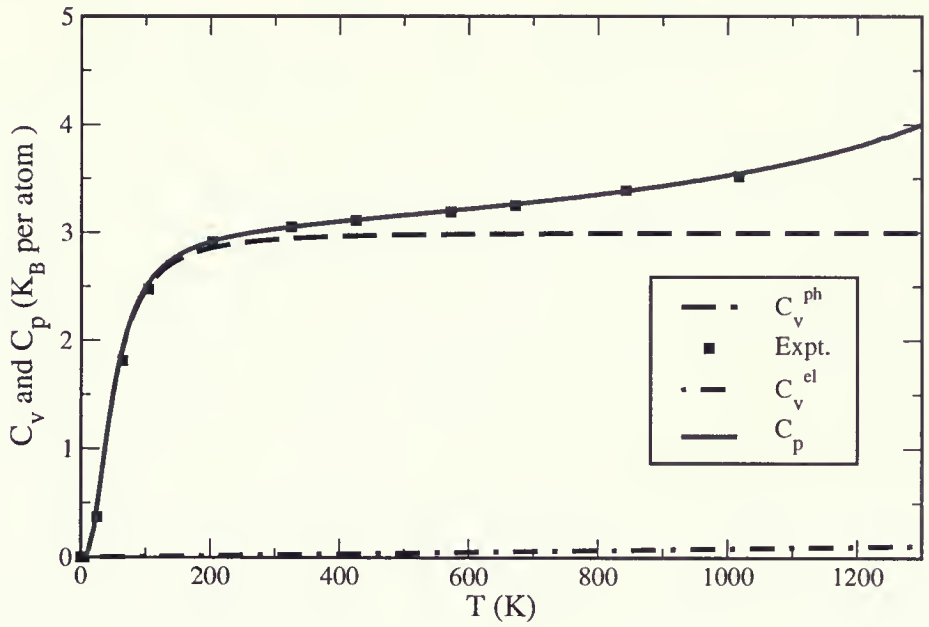

Figure 2.26: Calculated temperature dependence of heat capacity of Ag at constant volume C_V^{ph}, at constant pressure C_P and electronical contribution C_V^{ph}. The square points are the experimental data of heat capacitiy at constant pressure from Ref.[50].

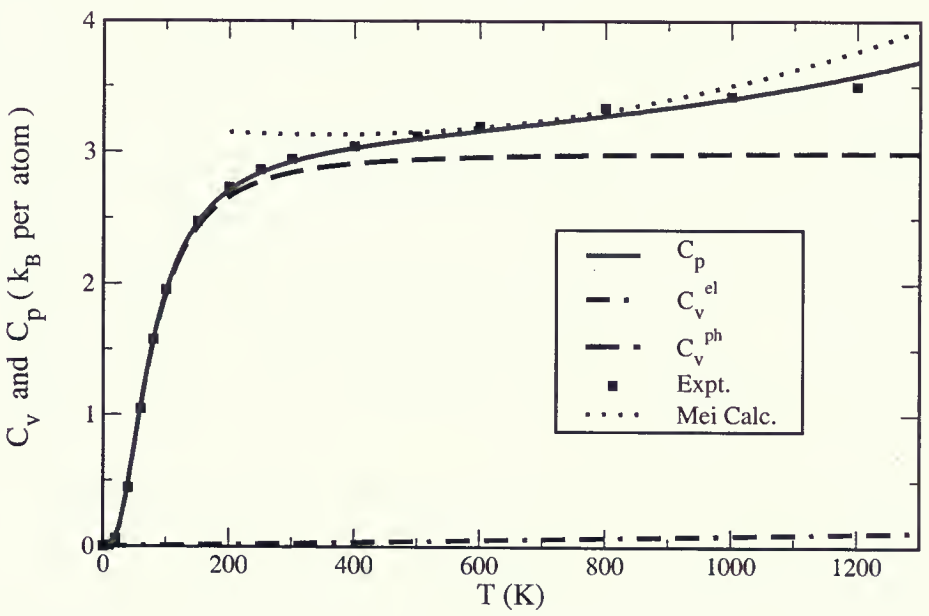

Figure 2.27: Calculated temperature dependence of heat capacity of Cu at constant volume C_V^{ph}, at constant pressure C_P and electronical contribution C_V^{ph}. The square points are the experimental data heat capacitiy at constant pressure from Ref.[50]. The point line is the results from Ref.[1].

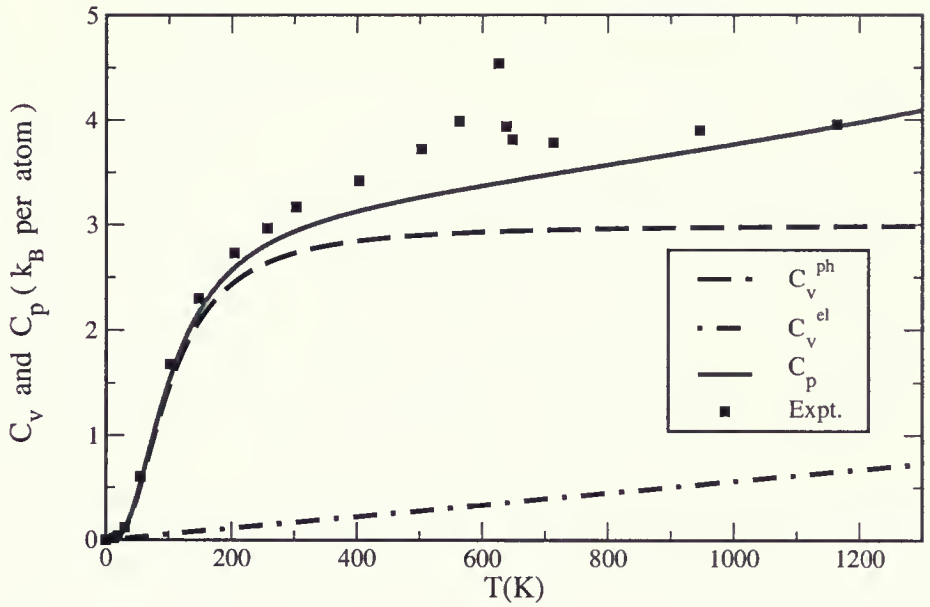

Figure 2.28: Calculated temperature dependence of heat capacity of Ni at constant volume C_V^{ph}, at constant pressure C_P and electronical contribution C_V^{ph}. The square points are the experimental data heat capacitiy at constant pressure from Ref.[50].

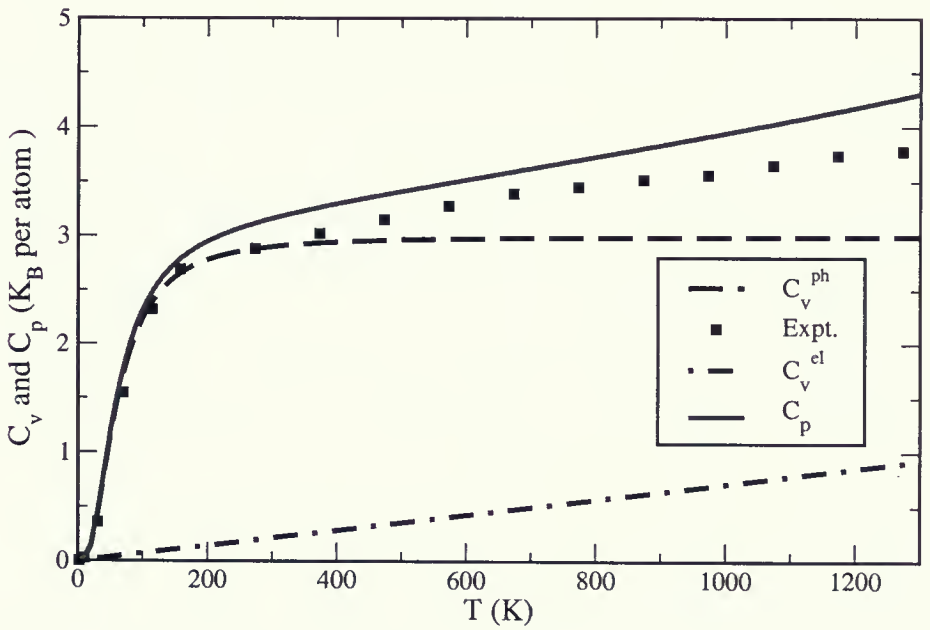

Figure 2.29: Calculated temperature dependence of heat capacity of Pd at constant volume C_V^{ph}, at constant pressure C_P and electronical contribution C_V^{ph}. The square points are the experimental data heat capacitiy at constant pressure from Ref.[50].

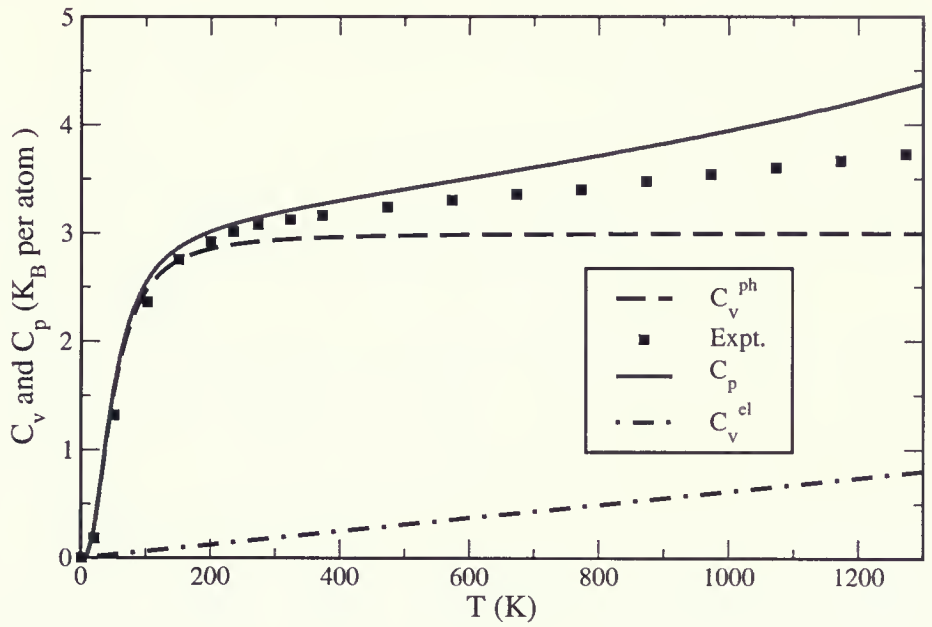

Figure 2.30: Calculated temperature dependence of heat capacity of Pt at constant volume C_V^{ph}, at constant pressure C_p and electronical contribution C_V^{ph}. The square points are the experimental data heat capacitiy at constant pressure from Ref.[50].

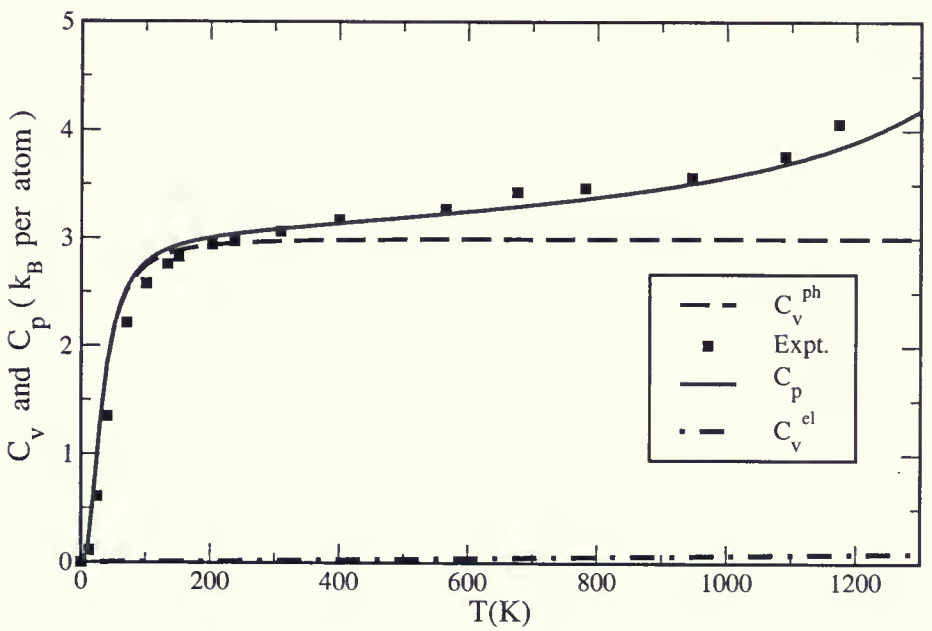

Figure 2.31: Calculated temperature dependence of heat capacity of Au at constant volume C_V^{ph}, at constant pressure C_P and electronical contribution C_V^{ph}. The square points are the experimental data heat capacitiy at constant pressure from Ref.[50].

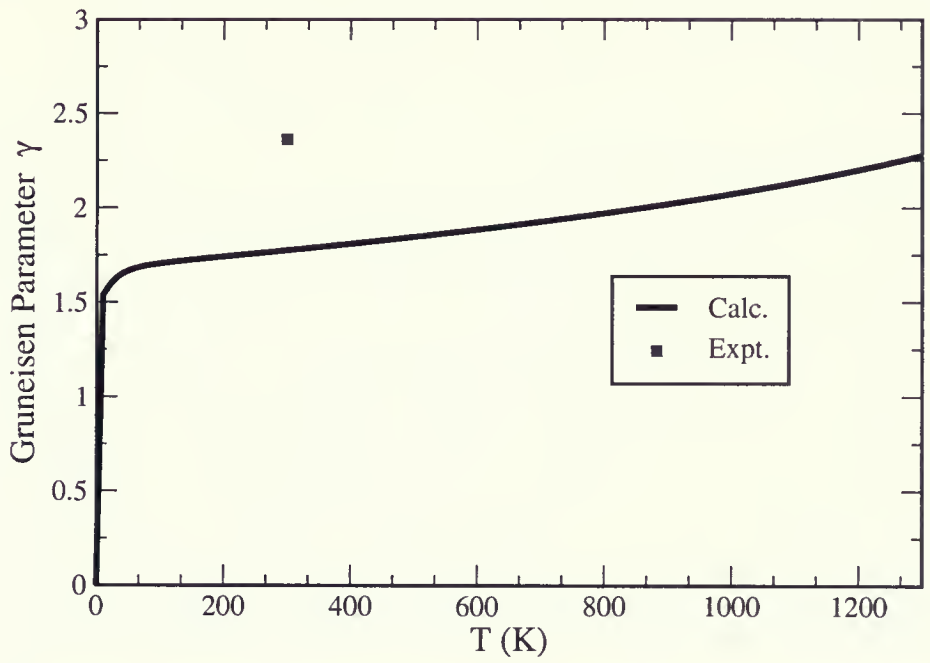

Figure 2.32: Overall Grüneisen Parameter γ as a function of temperature for Ag. The solid line is the calculated values and the square point is the experimental values taken from Ref.[44].

where

$$\gamma_s(\mathbf{K}) = -\frac{\mathbf{V}}{\omega_s(\mathbf{K})}\frac{\partial\omega_s(\mathbf{K})}{\partial\mathbf{V}} \tag{2.80}$$

is called the mode Grüneisen parameter corresponding to the $(\mathbf{K}, s)$ phonon mode, and

$$\epsilon(\omega_s(\mathbf{K})) = \hbar\omega_s(\mathbf{K})\left[\frac{1}{2} + \frac{1}{\exp(\hbar\omega_s(\mathbf{K})/k_BT) - 1}\right] \tag{2.81}$$

is the mean vibrational energy of the $(\mathbf{K}, s)$ phonon mode. The overall Grüneisen parameter $\gamma(T)$ is defined by averaging over the individual Grüneisen parameters $\gamma_s(\mathbf{K})$ of all the modes with a weight of $C_V(\mathbf{K}s)$ from each mode$(\mathbf{K}s)$, i.e.,

$$\gamma(T) = \frac{\sum_{\mathbf{K}s}\gamma_s(\mathbf{K})C_V(\mathbf{K}s)}{\sum_{\mathbf{K}s}C_V(\mathbf{K}s)}. \tag{2.82}$$

We numerically calculate the mode Grüneisen parameter $\gamma_s(\mathbf{K})$ and use Eq.(2.63) to calculate the weight $C_V(\mathbf{K}s)$. Submitting these results in Eq.(2.82), we obtain the temper-

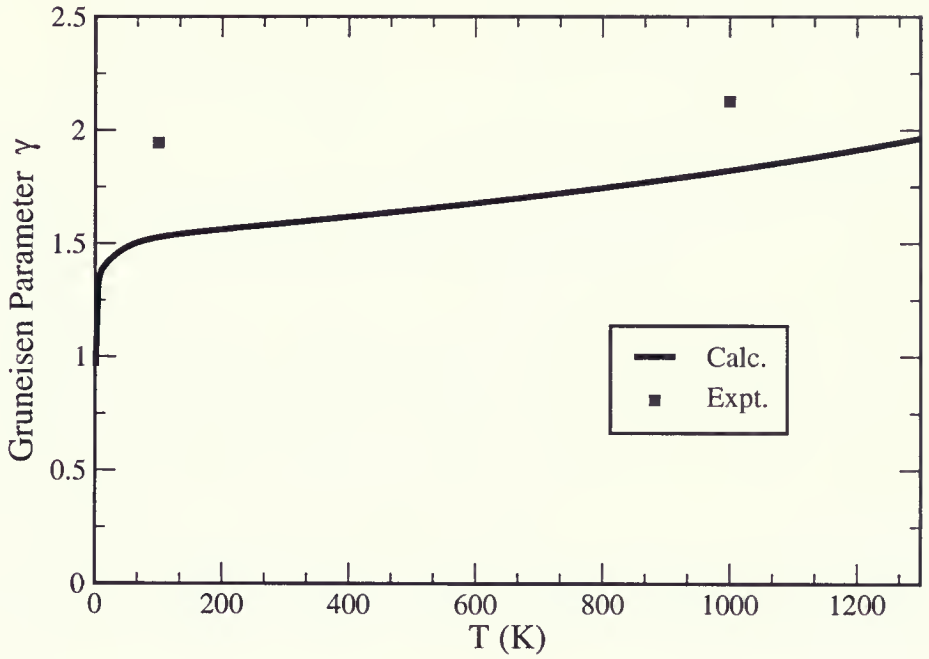

Figure 2.33: Overall Grüneisen Parameter γ as a function of temperature for Cu. The solid line is the calculated values and the square points are the experimental values taken from Ref.[44].

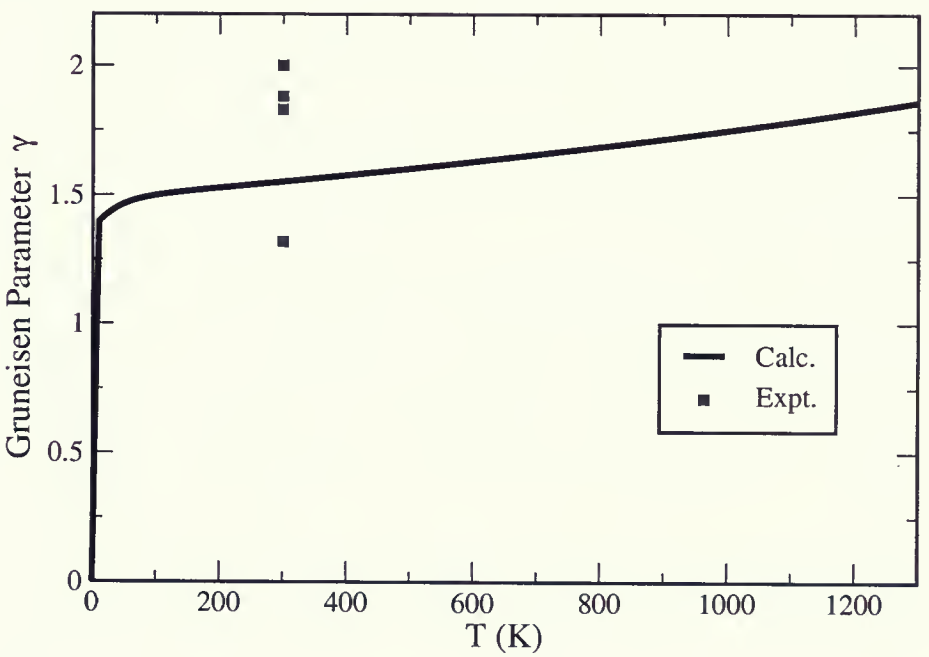

Figure 2.34: Overall Grüneisen Parameter γ as a function of temperature for Ni. The solid line is the calculated values and the square points are the experimental values taken from Ref.[51].

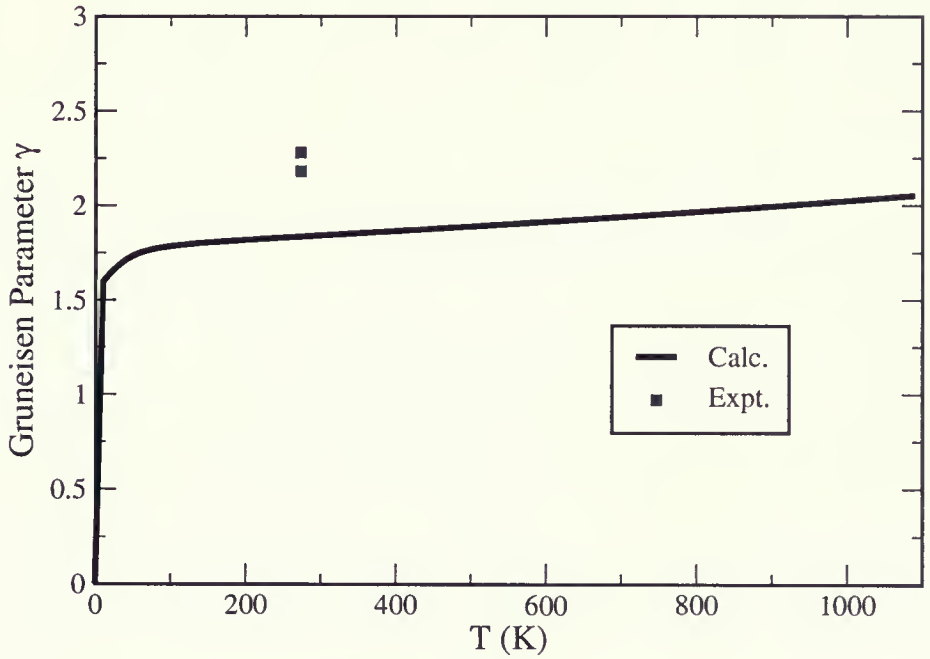

Figure 2.35: Overall Grüneisen Parameter γ as a function of temperature for Pd. The solid line is the calculated values and the square points are the experimental values taken from Ref.[51].

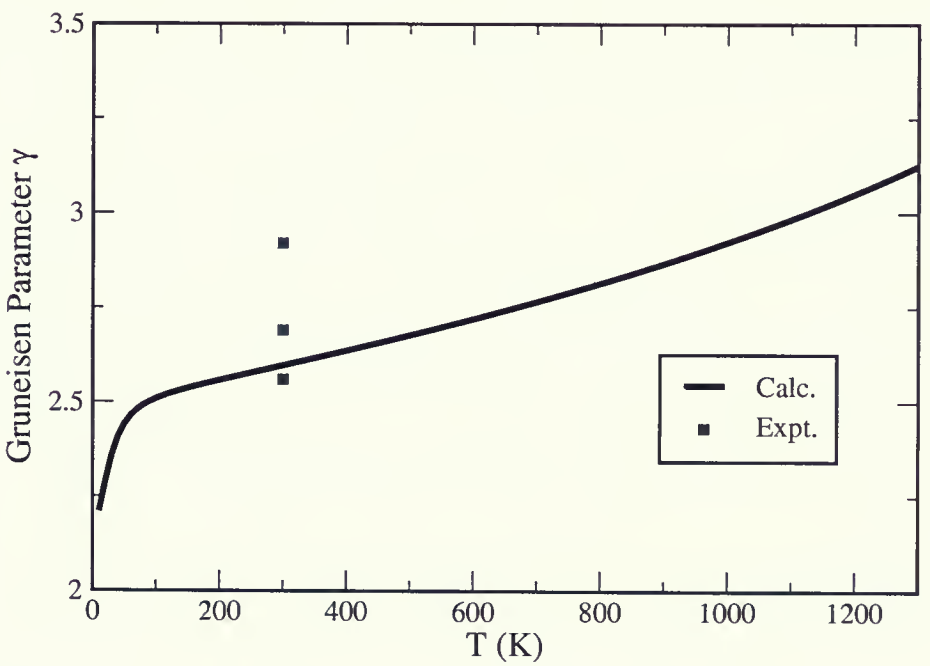

Figure 2.36: Overall Grüneisen Parameter γ as a function of temperature for Pt. The solid line is the calculated values and the square points are the experimental values taken from Ref.[51].

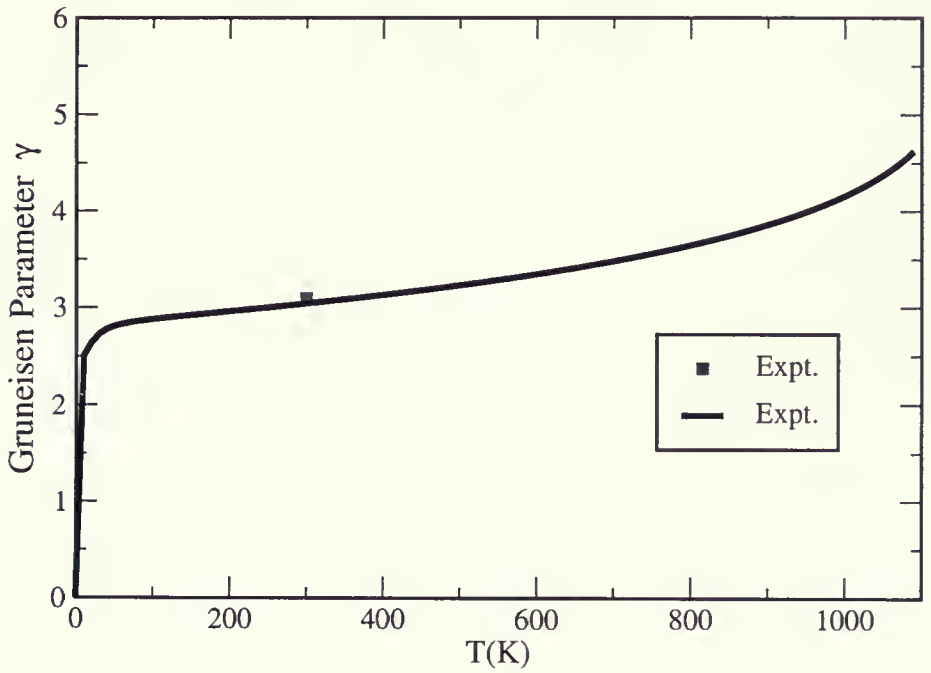

Figure 2.37: Overall Grüneisen Parameter γ as a function of temperature for Au. The solid line is the calculated values and the square point is the experimental values taken from Ref.[51].

ature dependent Grüneisen parameter $\gamma(T)$. Figs(2.32 - 2.37) show the calculated results for the variation of the overall Grüneisen parameter $\gamma(T)$ as a function of temperature.

2.2.6 Debye Temperature

From the theory of solid state physics[52], we know that heat capacity per atom can be written as

$$C_V(T) = 9k_B(\frac{T}{\Theta_D})^3 \int_0^{X_D} \frac{X^4 \exp(X)}{[\exp(X)-1]^2} dX, \tag{2.83}$$

where

$$X \equiv \hbar\omega/k_B T \tag{2.84}$$

and

$$X_D \equiv \Theta_D/T, \tag{2.85}$$

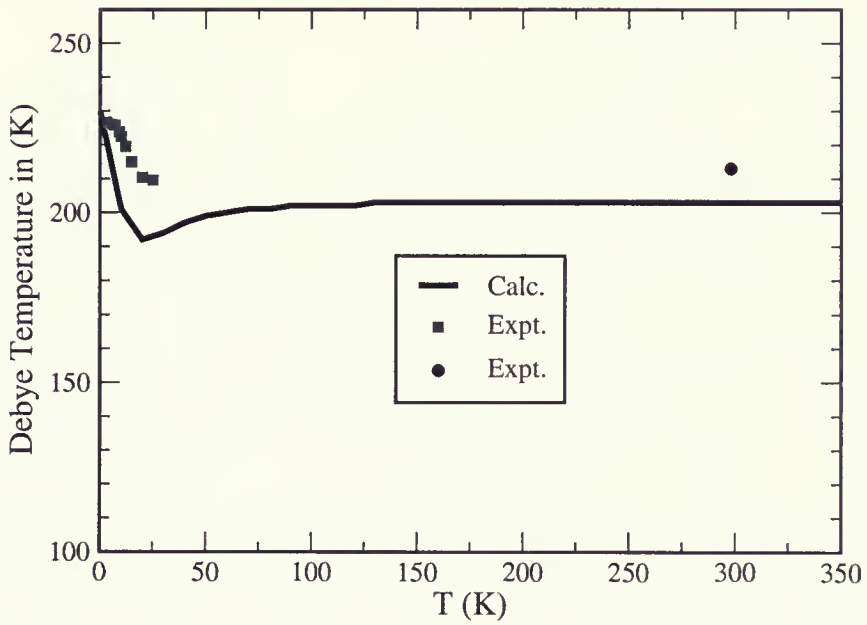

Figure 2.38: Debye temperature Θ_D as a function of temperature T for Ag. The solid line is the calculated results, the square points are the experimental values from Ref. [53], the round point is the experimental value at the temperature $T = 298K$ from Ref.[54].

Θ_D is called Debye temperature. From the results of temperature dependent $C_V(T)$ calculated in the above subsection, we can obtain the temperature dependent Debye temperature $\theta_D(T)$ by numerically evaluating the integral in the right side of Eq.(2.83) and matching it with $C_V(T)$ in the left side. The results are plotted in Figs.(2.38 - 2.43)

2.2.7 Adiabatic Bulk Modulus

The adiabatic compressibility $k_S(T)$ is[47]

$$k_S(T) = -\frac{1}{V}(\frac{\partial V}{\partial P})_S. \tag{2.86}$$

The adiabatic bulk modulus $B_S(T)$ is the inverse of the adiabatic compressibility:

$$B_S(T) = \frac{1}{k_S(T)} = -V(\frac{\partial P}{\partial V})_S. \tag{2.87}$$

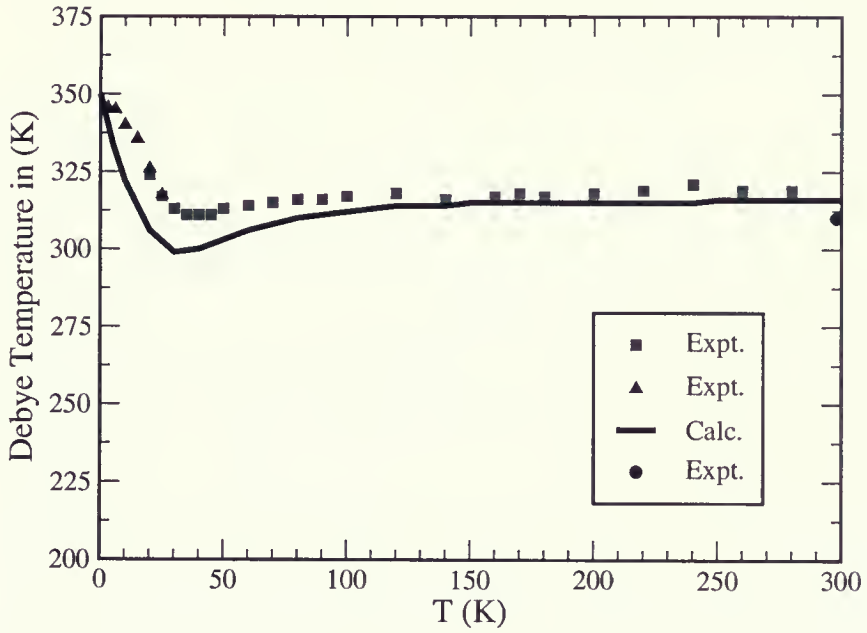

Figure 2.39: Debye temperature Θ_D as a function of temperature T for Cu. The solid line is the calculated results, the up triangle points are the experimental values from Ref. [53], the round point is the experimental values at the temperature $T = 298K$ from Ref.[54], the square points are experimental values from [55].

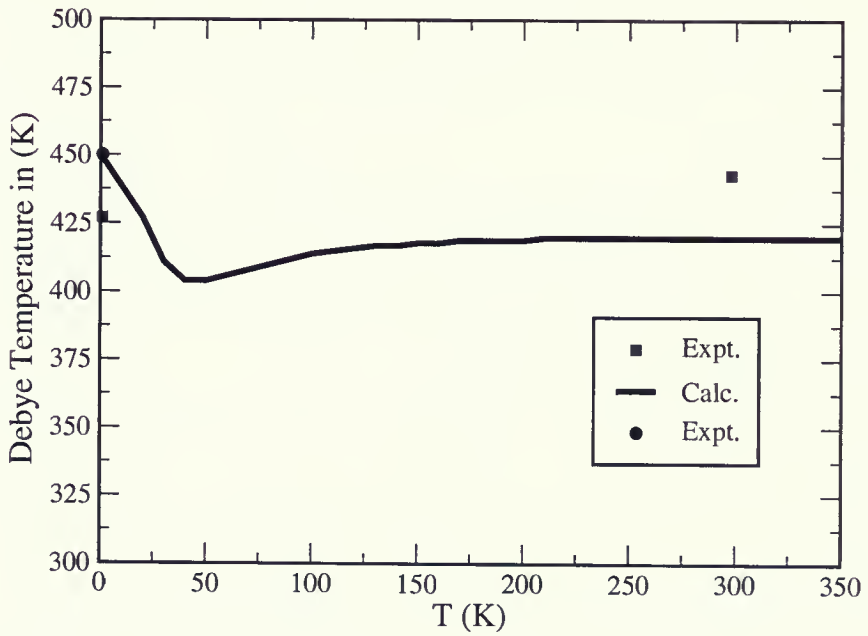

Figure 2.40: Debye temperature Θ_D as a function of temperature T for Ni. The solid line is the calculated results, the round point is the experimental values at very low temperature from Ref. [48], the square points are the experimental values at $T = 0K$ and $T = 298K$ from Ref.[54].

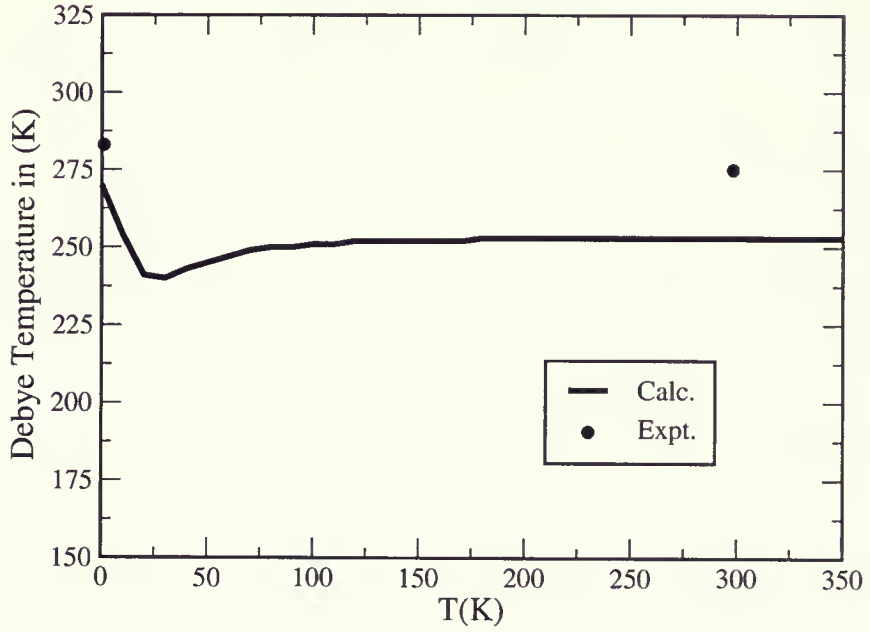

Figure 2.41: Debye temperature Θ_D as a function of temperature T for Pd. The solid line is the calculated results, the round points are the experimental values at the temperature $T = 298K$ and $T = 0K$ respectively from Ref.[54].

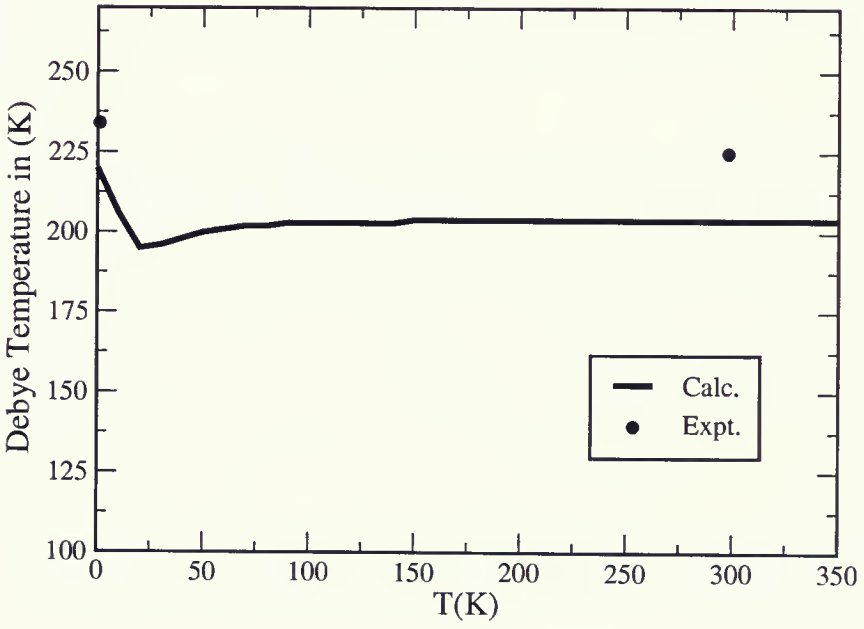

Figure 2.42: Debye temperature Θ_D as a function of temperature T for Pt. The solid line is the calculated results, the round points are the experimental values at the temperature $T = 298K$ and $T = 0K$ respectively from Ref.[54].

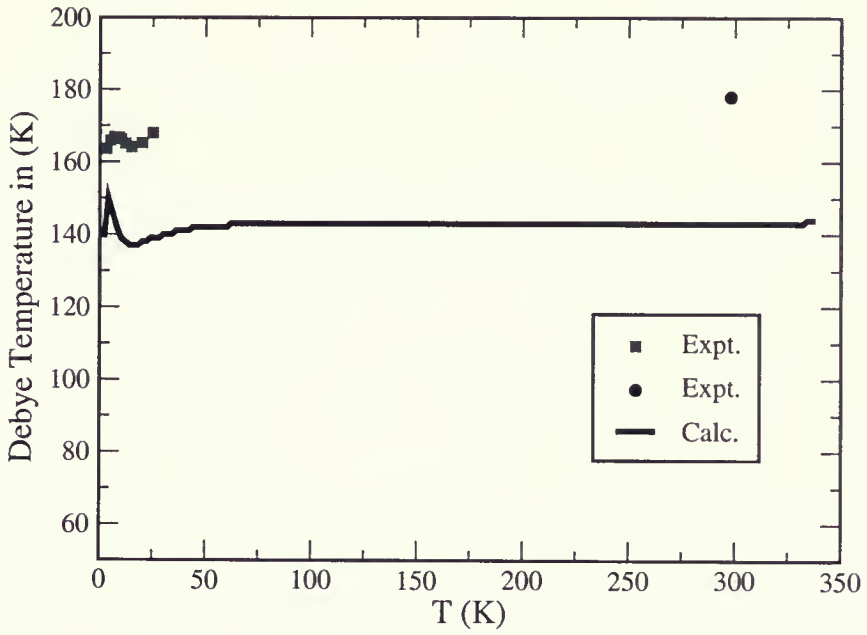

Figure 2.43: Debye temperature Θ_D as a function of temperature T for Au. The solid line is the calculated results, the square points are the experimental values from Ref. [53], the round points (a and b) are the experimental values at the temperature $T = 298K$ from Ref.[54].

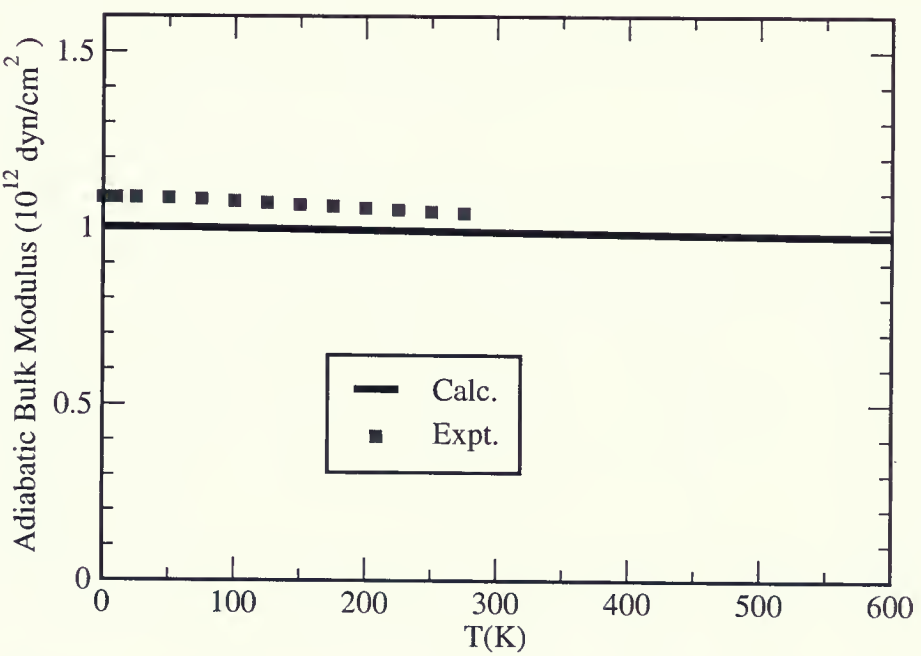

Figure 2.44: Adiabatic bulk modulus $B(T)$ as a function of temperature for Ag. The solid lines are the calculated values and the square points are the experimental values from Ref.[56].

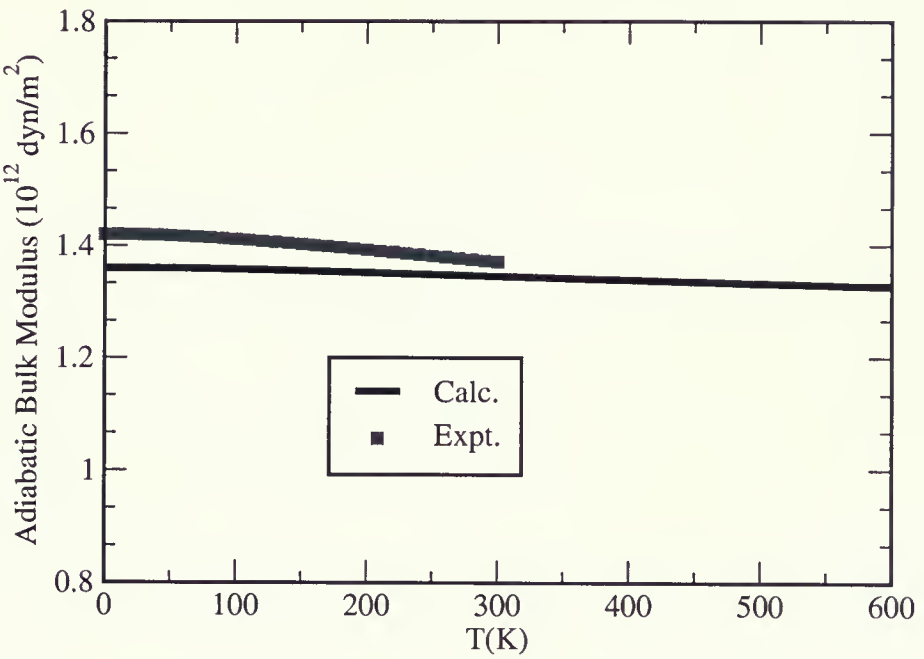

Figure 2.45: Adiabatic bulk modulus $B(T)$ as a function of temperature for Cu. The solid lines are the calculated values and the square points are the experimental values from Ref.[57].

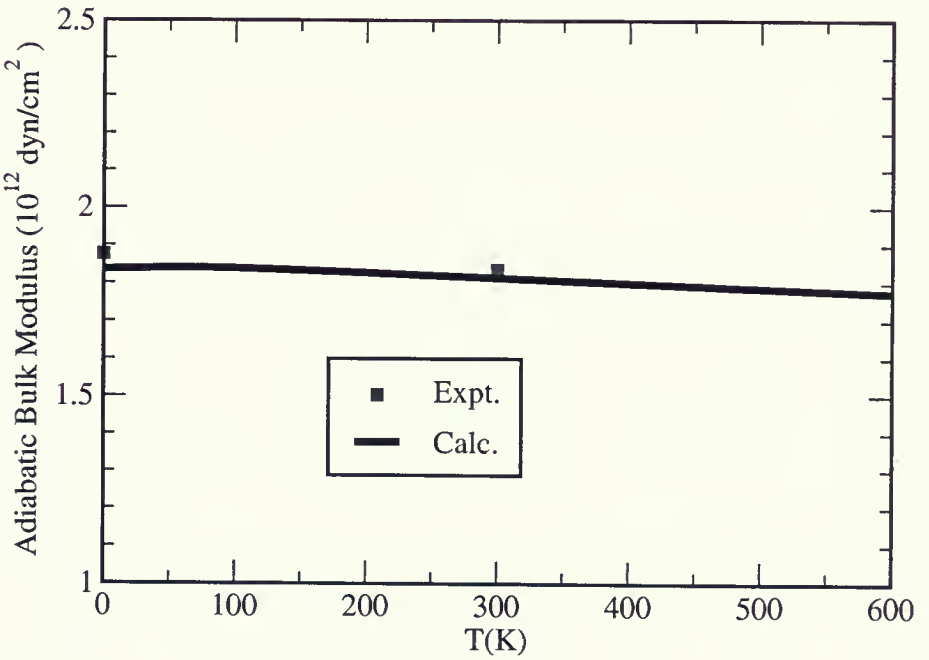

Figure 2.46: Adiabatic bulk modulus $B(T)$ as a function of temperature for Ni. The solid lines are the calculated values and square points are the experimental values from Ref.[48].

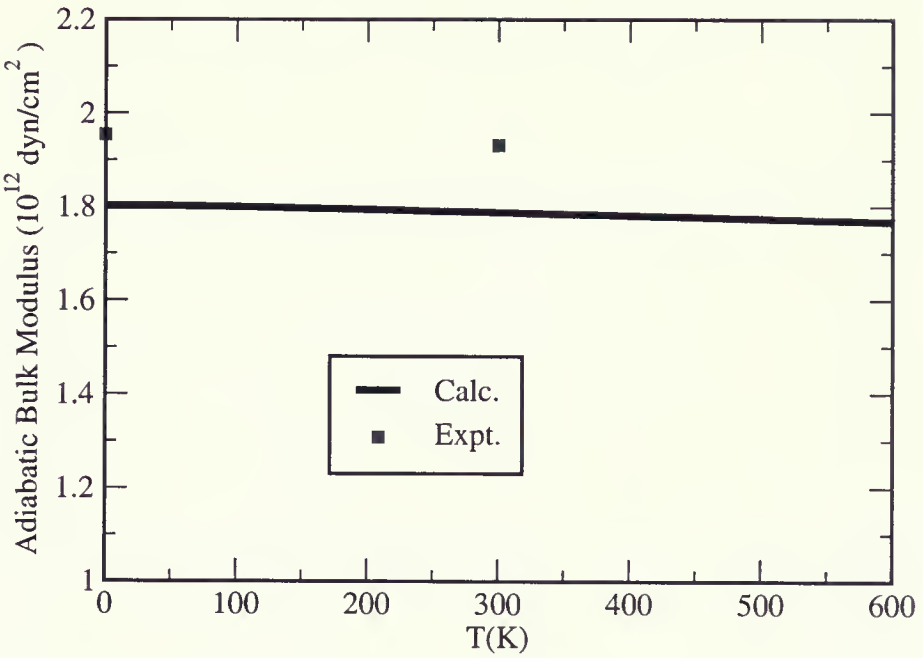

Figure 2.47: Adiabatic bulk modulus $B(T)$ as a function of temperature for Pd. The solid lines are the calculated values and the square points are the experimental values from Ref.[48].

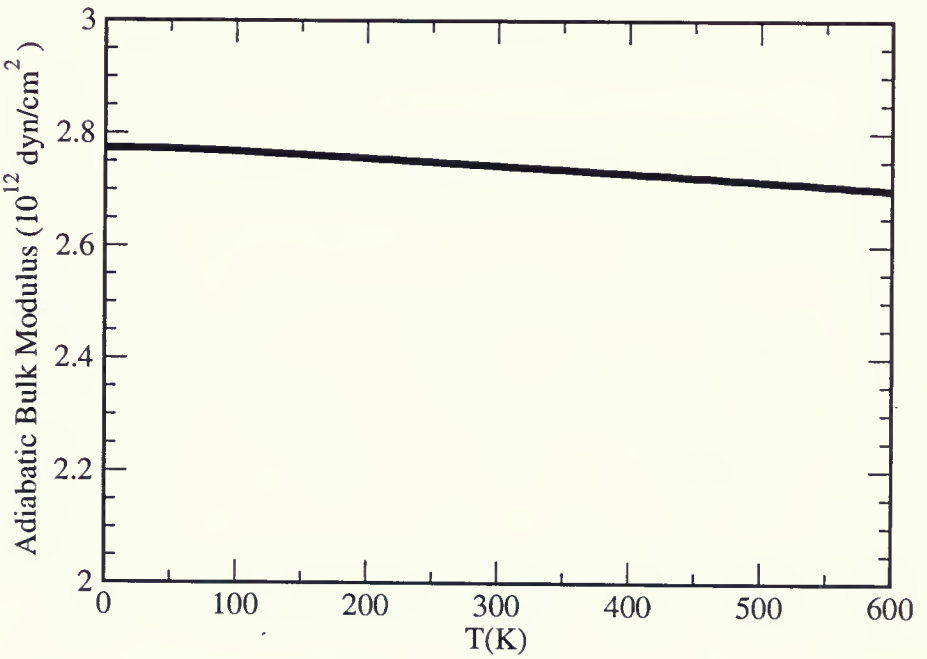

Figure 2.48: Adiabatic bulk modulus $B(T)$ as a function of temperature for Pt.

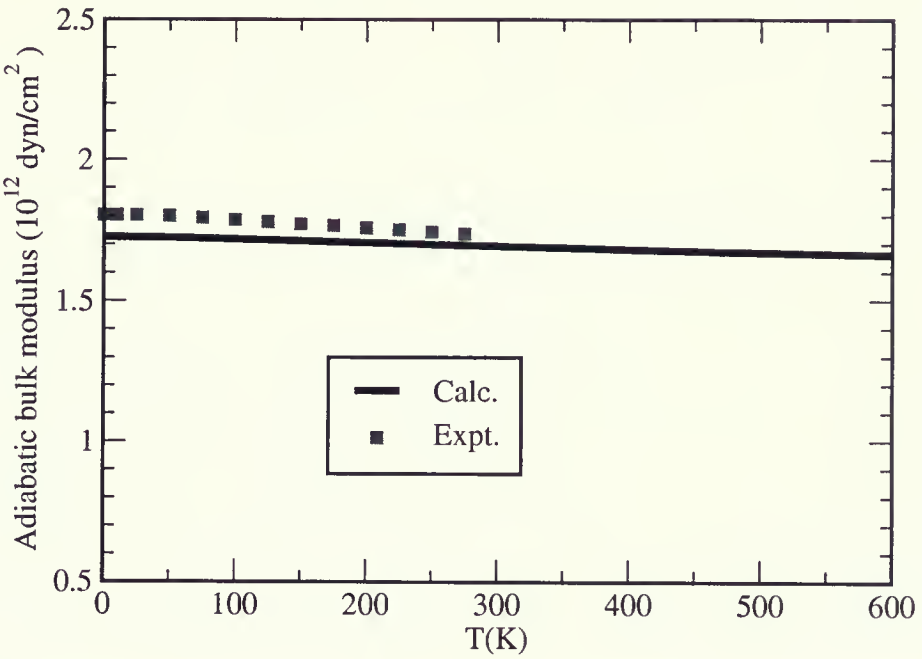

Figure 2.49: Adiabatic bulk modulus $B(T)$ as a function of temperature for Au. The solid lines are the calculated values and the square points are the experimental values from Ref.[56].

The isothermal compressibility $k(T)$ is [47]

$$k(T) = -\frac{1}{V}(\frac{\partial V}{\partial P})_T, \tag{2.88}$$

and obviously it is the inverse of the isothermal bulk modulus:

$$k(T) = \frac{1}{B(T)}. \tag{2.89}$$

From the definitions, it is easy to show[47]

$$k(T) - k_S(T) = \frac{TV\alpha_V^2(T)}{C_P}. \tag{2.90}$$

Combining this equation with Eq.(2.75) leads to the result

$$C_P(k(T) - k_S(T)) = k(T)(C_P - C_V), \tag{2.91}$$

or

$$B_S(T) = \frac{C_P}{C_V}B(T) \tag{2.92}$$

We calculate the adiabatic bulk modulus for the fcc metals and plot them as the functions of temperature in Figs.(2.44 - 2.49).

Chapter 3

Discussions and Conclusions

We apply the analytic embedding functions of Mei *et al.*[1] to calculate the phonon dispersion curves and some other dynamical properties of fcc metals. From Figs.(2.1 - 2.6), it is clear that the calculated phonon dispersion curves for Cu and Ag agree quite well with experimental data. The relative error, which is defined as the absolute difference between the theoretical value and experimental value divided by the experimental value, when wave vector **K** is at Γ, $X$and L points, is not more than 5.0% for Ag and 7.0% for Cu. Xie[46] used density functional theory(DFT) and density functional perturbation theroy(DFPT) to perform first-principles calculation of thermal properties for Ag. Narasimhan[43] has used local density approximation(LDA) and generalized gradient approximations(GGA) to carry out *ab initio* calculation of the thermal properties for Cu. From the phonon dispersion curves in these works, it appears that their results are no better than the present results. Daw[21] used different embedded atom potentials[2] to calculate phonon dispersion curves for Ni and Pd. For Ni, present results are close to the ones in Ref.[21], which agree with experimental values very well at small wave vector **K**. However, for Pd, present longitudinal mode results are worse than those in Ref.[21] at small wave vector **K** in comparion with experimental values. The parameters in the embedding functions of Mei *et al.*[1] are obtained from fitting the total energy of the crystal and elastic constants to the experimeantal values, not from fitting the force constants as has been done by Miller[36]. The approach of Mei *et al.*[1], thus, is more fundamental than that of Miller, even though it is

not a completely first-principles method.

In an attempt to improve the computed results of phonon frequencies, we made small changes in parameters in the model of Mei *et al.*[1] for Pd and Pt, which are listed in the following table (3.1). Using these modified parameters we computed the phonon frequencies again. The interesting thing is that, with the modified parameters, the calculated phonon dispersion curves agree with experimental values very well (see Fig.3.1 and Fig.3.2). However, we apply the same formula[2] as used by Mei to calculate the elastic constants C_{11}, C_{12} and C_{44} and find that the calculated results have large deviation from the ones obtained in Ref.[1] and Ref.[5]. We list the results in table (3.2). This interesting result suggests that there is room for imrovement in the parameters. This can be the subject of future research. For example, how are the parameters improved in this model to make the theoretically calculated values get closer and closer to the experimental values for all other dynamical properties.

We have studied the temperature dependent thermodynamical properties. First, we obtain the variation of lattice constants with temperature(see Fig.2.7). It is easy to see that present calculation based on the theory of lattice dynamics is very close to the results obtained by Mei *et al.* from the molecular dynamics simulation. To check the results, we calculate the linear thermal expansions. From the Figs.(2.8 - 2.13), we can say that the model of Mei *et al.*[1] works very well. T.Çağin[58] also use molecular dynamics(MD) to study the thermal and mechanical properties of some fcc transition metals. As a comparison, we list the linear thermal expansion results in table 3.3. Obviously, the results calculated from the model of Mei *et al.*[1] are much better than Ref.[58].

For the coefficient of linear thermal expansion, it is clear to see in Figs.(2.14 - 2.19) that the values calculated from the model of Mei *et al.*[1] give a good prediction for each metal, especailly at low temperatures, although they are slightly underestimated for Cu, Ag, Pd

Table 3.1: Modified Parameters In Mei's Model

	Pd	Pd (Mod.)	Pt	Pt (Mod.)
c_0	0.14775	0.14775	0.21295	0.21295
c_1	-2.01097	-2.01097	-2.71705	-2.71705
c_2	9.91339	9.91339	12.42006	12.62006
c_3	-21.74378	-21.74378	-24.90569	-24.90569
c_4	20.07884	20.77884	20.95506	20.95506
c_5	-5.84105	-5.84105	-4.99180	-4.99180
β^a	5.91	5.91	6.69	6.69
δ	12.31	12.31	7.02	7.02
γ	6.95925	6.95925	7.54886	7.54886
ϕ_e	0.1457	0.1457	0.3065	0.3065

Table 3.2: The elastic constants C_{11}, C_{12} and C_{44} calculated from the modified paramters,which are in units of $10^{11}\mathrm{N/m^2}$

	Pd	Pd (Mod)	Pt	Pt (Mod.)
C_{11}	2.341^a		3.470	
	2.252^b	3.037	3.203	4.725
	2.180^c		3.03	
C_{12}	1.760^a		2.51	
	1.803^b	2.128	2.630	3.250
	1.840^c		2.73	
C_{14}	0.712^a		0.765	
	0.755^b	1.057	0.894	1.553
	0.650^c		0.680	

a,b and c are the same as in table1.2

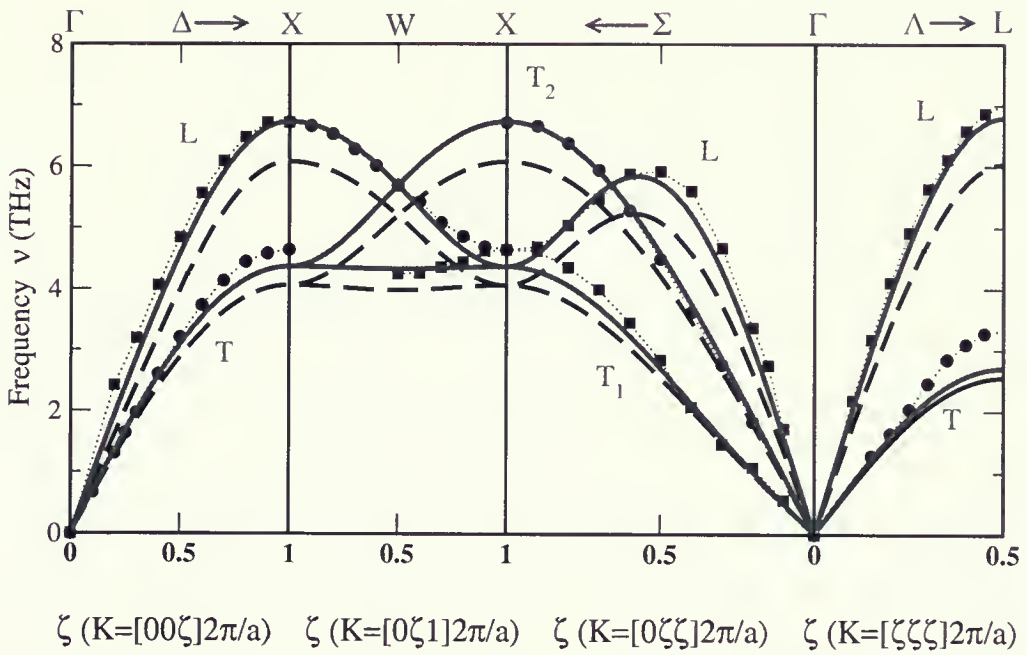

Figure 3.1: Phonon dispersion curves for Pd. the dash lines are the calculated values from Mei's parameter, the solid lines are the calculated results from the modified parameters, and the round and squre points are the experimental data.

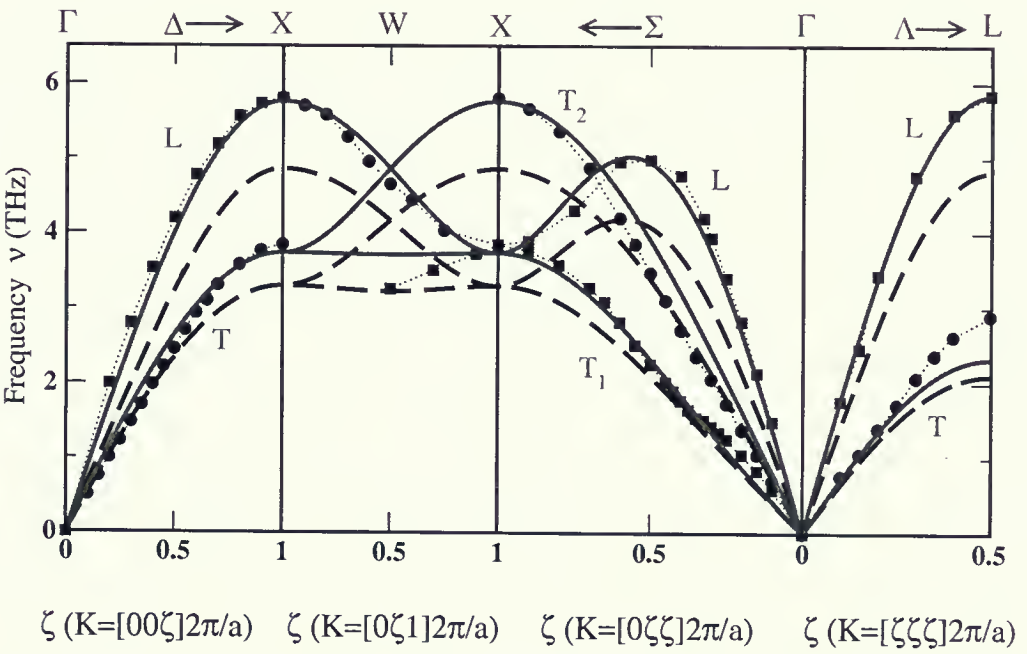

Figure 3.2: Phonon dispersion curves for Pt. The dash lines are the calculated values from Mei's parameter, the solid lines are the calculated results from the modified parameters, and the round and squre points are the experimental data.

Table 3.3: The Linear Thermal Expansion of Ni, Cu, Ag, and Au as a Function of Temperature

Elements	T(K)	500	750	1000
Ni	This work	0.23	0.53	0.86
	Ref.[58]	0.44	1.04	1.72
	Experiment	0.29	0.69	1.13
Cu	This work	0.29	0.69	1.13
	Ref.[58]	0.58	1.40	2.42
	Experiment	0.34	0.82	1.36
Ag	This work	0.32	0.75	1.24
	Ref.[58]	0.44	1.04	1.72
	Experiment	0.43	0.99	1.61
Au	This work	0.34	0.84	1.56
	Ref.[58]	0.58	1.44	2.60
	Experiment	0.31	0.70	1.14

Table 3.4: Comparison of Grüneisen parameter γ with experimental and other theoretical values.

Elements	Experimental Values Ref.[59]	Present	Other Theor.Value
Ag	2.44, 2.46, 2.29	1.77	2.14 (Ref.[60])
	2.36 ± 0.12, 0.32,		1.26 (Ref.[61])
Cu	1.97, 2.0 ± 0.08	1.59	1.19 (Ref.[61])
	1.88 ± 0.08, 2.93		1.73 (Ref.[60])
Ni	2.0, 1.83,2.0 ± 0.19	1.55	1.32 (Ref.[62])
	1.88 ± 0.08, 1.28		1.62 (Ref.[63])
Pd	2.47, 2.28 ± 0.1	1.84	2.18 (Ref.[62])
	2.84, 2.18		2.03 (Ref.[62])
Pt	2.69, 2.92	2.60	1.32 (Ref.[62])
	2.56 ± 0.12, 1.81,		1.62 (Ref.[62])
Au	3.09, 3.04 ± 0.04	3.04	2.47 (Ref.[60])
	1.84, 2.22		1.31 (Ref.[61])

and Ni, and overestimated for Au and Pt at very high temperatures. MacDonald *et al.* in Ref.[44] also calculated the coefficient of linear thermal expansion using a kind of the volume dependent free energy. However, their results are not satisfatory: there are deviations from the experimental values both ant high and low temperature regions. For Cu, we also plot the results from Ref.[1] as a comparison (see Fig.2.15). At room temperature, Mei *et al.* gave a value of $1.5 \times 10^{-6} K^{-1}$ better than present value of $1.35 \times 10^{-6} K^{-1}$, while at lower temperature the MD simulation fails.

The lattice contributions to the isothermal and adiabatic bulk moduli are shown in Figs.(2.20 - 2.25) and in Figs.(2.44 - 2.49). For all cases our calculations give a remarkably successful prediction, as they agree with experimental data very well.

Heat capacity is an important thermal property of solids. The calculated C_P and C_V are displayed in Figs.(2.26 - 2.31). As we can see that the calculated curves for C_P are all in very good agreement with experimental data, except for Ni. Curie temperature of Nickel is $627K$. Below this temperature Nickel is ferromagnetic. Above this temperature, Nickel becomes paramagnetic. However, the embedded atom method, as used by Mei et al, does not have the necessary degrees of freedom (i.e., treating spin up and spin down eletrons separately) required to describe the magnetic state. The heat capacity C_V^{ph} for all cases approches the value of $3k_B$ per atom at very high temperatures, the classical harmonic limit. In Fig.2.27, we also give the results of C_P for copper calculated by Mei *et al.*[1]. Their results agree quite well with experimental values in a range from $500K$ to $1000K$, but at low temperatures there is a big discrepancy with experimental data.

Another important thermodynamic quantity is Grüneisen parameter. The overall Grüneisen parameter is the average of mode Grüneisen parameter relative to the volume derivative of frequency with the weight of the heat capacity at each mode. Due to the shortage of direct way to measure, there is a large variation with experimental results as shown in table 3.4.

Compared to the indirect measured values of this quantity, the agreement between theory and experiment is poor for Cu and Ag.

Debye temperature as a function of temperature is calculated and plotted in Figs.(2.38 - 2.43). Obviously, the calculated Debye temperature for Cu and Ag is in excellent agreement with experimental values. In fact, it is easy for us to predict this result by noticing the very good agreement between the calculated values and experimental ones in phonon dispersion curves. For Pd, Pt and Ni, the Debye temperature are slightly underestimated, but for Au, the Debye temperature is underestimated too much, close to 20 percent.

We have applied the analytical embedded atom potentials of Mei *et al.*[1] to investigate the dynamical properties of some fcc metals. Under the harmonic aprroximation, we have calculated the phonon frequencies, lattice parameter as a function of temperature, zero-point energy of phonon vibration at room temperature. We have also calculated the temperature dependence of linear thermal expansion, coefficient of linear thermal expansion, isothermal bulk modulus, adiabatic bulk modulus, heat capacity at constant volume and at constant pressure, Grüneisen parameter and Debye temperature. After comparing the theoretically calculated values with experimental data, we have found that our calculations give good predictions for most of the dynamical properties of all these metals. Therefore, this model should be useful and might be one of good choices in the investigation of pure crystal properties.

Appendix A

Proofs of some Equations

A.1 The proof of Eq.(2.31)

We can write the derivative of E_{tot} with respect to the position vector of atom l in i-cartecian component as

$$\begin{aligned}\frac{\partial E_{tot}}{\partial R_i(l)} &= \frac{\partial}{\partial R_i(l)}\left[\sum_n F_n(\rho_n) + 1/2 \sum_{\substack{n,m \\ n\neq m}} \Phi(R_{nm})\right] \\ &= \sum_n \frac{\partial}{\partial R_i(l)} F_n(\rho_n) + 1/2 \sum_{\substack{n,m \\ n\neq m}} \frac{\partial}{\partial R_i(l)} \Phi(R_{nm}). \end{aligned} \tag{A.1}$$

Recalling the following equations,

$$R_{nm} = \sqrt{(R_i(n) - R_i(m))^2 + (R_j(n) - R_j(m))^2 + (R_k(n) - R_k(m))^2}, \tag{A.2}$$

and

$$\frac{\partial R_{nm}}{\partial R_i(l)} = \frac{R_i(n) - R_i(m)}{R_{nm}} (\delta_{ln} - \delta_{lm}), \tag{A.3}$$

we can write the first term in Eq.(A.1) as

$$\begin{aligned}\sum_n \frac{\partial}{\partial R_i(l)} F_n(\rho_n) &= \sum_n F_n'(\rho_n) \frac{\partial}{\partial R_i(l)} \rho_n \\ &= \sum_n F_n'(\rho_n) \frac{\partial}{\partial R_i(l)} \left(\sum_{m(\neq n)} f(R_{nm}) \right) \\ &= \sum_n F_n'(\rho_n) \sum_{m(\neq n)} f_m'(R_{nm}) \frac{R_i(n) - R_i(m)}{R_{nm}} (\delta_{nl} - \delta_{ml}). \end{aligned} \tag{A.4}$$

Simplifing it, we have

$$\begin{aligned}\sum_n \frac{\partial}{\partial R_i(l)} F_n(\rho_n) &= \sum_{m(\neq l)} F_l'(\rho_l) f_m'(R_{lm}) \frac{R_i(l) - R_i(m)}{R_{lm}} \\ &\quad - \sum_{n(\neq l)} F_n'(\rho_n) f_l'(R_{nl}) \frac{R_i(n) - R_i(l)}{R_{nl}} \\ &= \sum_{n(\neq l)} [F_l'(\rho_l) f_n'(R_{ln}) + F_n'(\rho_n) f_l'(R_{ln})] \frac{R_i(l) - R_i(n)}{R_{ln}}. \end{aligned} \tag{A.5}$$

The second term as

$$\begin{aligned}1/2 \sum_{\substack{n,m \\ n\neq m}} \frac{\partial}{\partial R_i(l)} \Phi(R_{nm}) &= 1/2 \sum_{\substack{n,m \\ n\neq m}} \Phi'(R_{nm}) \frac{R_i(n) - R_i(m)}{R_{nm}} (\delta_{nl} - \delta_{ml}) \\ &= 1/2 \sum_{m(\neq l)} \Phi'(R_{lm}) \frac{R_i(l) - R_i(m)}{R_{lm}} \\ &\quad -1/2 \sum_{n(\neq l)} \Phi'(R_{nl}) \frac{R_i(n) - R_i(l)}{R_{nl}} \\ &= \sum_{n(\neq l)} \Phi'(R_{ln}) \frac{R_i(l) - R_i(n)}{R_{ln}}. \end{aligned} \tag{A.6}$$

Substituting Eqs.(A.5) and (A.6) in Eq.(A.1), we can obtain

$$\frac{\partial E_{tot}}{\partial R_i(l)} = \sum_{n(\neq l)} [F_l'(\rho_l) f_n'(R_{ln}) + F_n'(\rho_n) f_l'(R_{ln}) + \Phi'(R_{ln})] \frac{R_i(l) - R_i(n)}{R_{ln}}. \tag{A.7}$$

In the same way, we can write the derivative of E_{tot} with respect to the position vector of atom l in j and k-cartesian component respectively as

$$\frac{\partial E_{tot}}{\partial R_j(l)} = \sum_{n(\neq l)} [F_l'(\rho_l) f_n'(R_{ln}) + F_n'(\rho_n) f_l'(R_{ln}) + \Phi'(R_{ln})] \frac{R_j(l) - R_j(n)}{R_{ln}} \tag{A.8}$$

and

$$\frac{\partial E_{tot}}{\partial R_k(l)} = \sum_{n(\neq l)} [F_l'(\rho_l) f_n'(R_{ln}) + F_n'(\rho_n) f_l'(R_{ln}) + \Phi'(R_{ln})] \frac{R_k(l) - R_k(n)}{R_{ln}}. \tag{A.9}$$

Combining Eqs.(A.7, (A.8 and (A.9) together, we have

$$\begin{aligned}
\mathbf{F}(l) = & - \nabla_l E_{tot} = -\left\{ \frac{\partial E_{tot}}{\partial R_i(l)} i + \frac{\partial E_{tot}}{\partial R_j(l)} j + \frac{\partial E_{tot}}{\partial R_k(l)} k \right\} \\
= & - \sum_{n(\neq l)} [F_l'(\rho_l) f_n'(R_{ln}) + F_n'(\rho_n) f_l'(R_{ln}) + \Phi'(R_{ln})] \frac{R_i(l) - R_i(n)}{R_{ln}} i \\
& - \sum_{n(\neq l)} [F_l'(\rho_l) f_n'(R_{ln}) + F_n'(\rho_n) f_l'(R_{ln}) + \Phi'(R_{ln})] \frac{R_j(l) - R_j(n)}{R_{ln}} j \\
& - \sum_{n(\neq l)} [F_l'(\rho_l) f_n'(R_{ln}) + F_n'(\rho_n) f_l'(R_{ln}) + \Phi'(R_{ln})] \frac{R_k(l) - R_k(n)}{R_{ln}} k \\
= & - \sum_{n(\neq l)} [F_l'(\rho_l) f_n'(R_{ln}) + F_n'(\rho_n) f_l'(R_{ln}) + \Phi'(R_{ln})] \frac{\mathbf{R}(l) - \mathbf{R}(n)}{R_{ln}}. \qquad \text{(A.10)}
\end{aligned}$$

This is exactly the Eq.(2.31).

A.2 The proof of Eq.(2.36)

To verify Eq.(2.36), we substitute Eq.(2.29) into Eq.(2.11) and then we get

$$\begin{aligned}
& \Phi_{ij}(l,m) = \frac{\partial^2 E_{tot}}{\partial R_i(l) \partial R_j(m)} = -\frac{\partial F_i(l)}{\partial R_j(m)} \\
= & \frac{\partial}{\partial R_j(m)} \left\{ \sum_{n(\neq l)} [F_l'(\rho_l) f_n'(R_{ln}) + F_n'(\rho_n) f_l'(R_{ln}) + \Phi'(R_{ln})] \frac{R_i(l) - R_i(n)}{R_{ln}} \right\} \\
= & \sum_{n(\neq l)} \left\{ \frac{\partial}{\partial R_j(m)} [F_l'(\rho_l) f_n'(R_{ln}) + F_n'(\rho_n) f_l'(R_{ln}) + \Phi'(R_{ln})] \right\} \frac{R_i(l) - R_i(n)}{R_{ln}} \\
+ & \sum_{n(\neq l)} [F_l'(\rho_l) f_n'(R_{ln}) + F_n'(\rho_n) f_l'(R_{ln}) + \Phi'(R_{ln})] \frac{\partial}{\partial R_j(m)} \left\{ \frac{R_i(l) - R_i(n)}{R_{ln}} \right\} \\
= & \sum_{n(\neq l)} [F_l''(\rho_l) \frac{\partial \rho_l}{\partial R_j(m)} f_n'(R_{ln}) + F_l'(\rho_l) f_n''(R_{ln}) \frac{\partial R_{ln}}{\partial R_j(m)}] \frac{R_i(l) - R_i(n)}{R_{ln}} \\
+ & \sum_{n(\neq l)} [F_n''(\rho_n) \frac{\partial \rho_n}{\partial R_j(m)} f_l'(R_{ln}) + F_n'(\rho_n) f_l''(R_{ln}) \frac{\partial R_{ln}}{\partial R_j(m)}] \frac{R_i(l) - R_i(n)}{R_{ln}} \\
+ & \sum_{n(\neq l)} \Phi''(R_{ln}) \frac{\partial R_{ln}}{\partial R_j(m)} \frac{R_i(l) - R_i(n)}{R_{ln}} \\
+ & \sum_{n(\neq l)} [F_l'(\rho_l) f_n'(R_{ln}) + F_n'(\rho_n) f_l'(R_{ln}) + \Phi'(R_{ln})] \frac{\partial}{\partial R_j(m)} \left\{ \frac{R_i(l) - R_i(n)}{R_{ln}} \right\}. \qquad \text{(A.11)}
\end{aligned}$$

As did in Appendix A.1, we can write

$$\frac{\partial \rho_l}{\partial R_j(m)} = \sum_{q(\neq l)} f'_q(R_{lq}) \frac{R_j(l) - R_j(q)}{R_{lq}} (\delta_{lm} - \delta_{qm}), \tag{A.12}$$

$$\frac{\partial \rho_n}{\partial R_j(m)} = \sum_{q(\neq n)} f'_q(R_{nq}) \frac{R_j(n) - R_j(q)}{R_{nq}} (\delta_{nm} - \delta_{qm}). \tag{A.13}$$

If noticing the following equations,

$$\begin{aligned} \frac{\partial R_{ln}}{\partial R_j(m)} &= \frac{\partial}{\partial R_j(m)} \sqrt{(R_i(l) - R_i(n))^2 + (R_j(l) - R_j(n))^2 + (R_k(l) - R_k(n))^2} \\ &= \frac{R_j(l) - R_j(n)}{R_{nl}} (\delta_{lm} - \delta_{nm}), \end{aligned} \tag{A.14}$$

$$\begin{aligned} \frac{\partial}{\partial R_j(m)} \left\{ \frac{R_i(l) - R_j(n)}{R_{ln}} \right\} &= \left\{ \frac{\partial [R_i(l) - R_i(n)]}{\partial R_j(m)} R_{ln} - [R_i(l) - R_i(n)] \frac{\partial R_{ln}}{\partial R_j(m)} \right\} \frac{1}{R_{ln}^2} \\ &= \Bigg\{ [\delta_{lm}\delta_{ij} - \delta_{nm}\delta_{ij}] R_{ln} \\ &\quad - [R_i(l) - R_i(n)] \frac{R_j(l) - R_j(n)}{R_{nl}} (\delta_{lm} - \delta_{nm}) \Bigg\} \frac{1}{R_{ln}^2} \end{aligned} \tag{A.15}$$

we can write Eq.(A.11) as

$$\begin{aligned} \Phi_{ij}(l,m) &= \frac{\partial^2 E_{tot}}{\partial R_i(l) \partial R_j(m)} = -\frac{\partial F_i(l)}{\partial R_j(m)} \\ &= \sum_{n(\neq l)} F''_l(\rho_l) \left\{ \sum_{q(\neq l)} f'_q(R_{lq}) \frac{R_j(l) - R_j(q)}{R_{lq}} (\delta_{lm} - \delta_{qm}) \right\} f'_n(R_{ln}) \frac{R_i(l) - R_i(n)}{R_{ln}} \\ &+ \sum_{n(\neq l)} F'_l(\rho_l) f''_n(R_{ln}) \left\{ \frac{R_j(l) - R_j(n)}{R_{nl}} (\delta_{lm} - \delta_{nm}) \right\} \frac{R_i(l) - R_i(n)}{R_{ln}} \\ &+ \sum_{n(\neq l)} F''_n(\rho_n) \left\{ \sum_{q(\neq n)} f'_q(R_{nq}) \frac{R_j(n) - R_j(q)}{R_{nq}} (\delta_{nm} - \delta_{qm}) \right\} f'_l(R_{ln}) \frac{R_i(l) - R_i(n)}{R_{ln}} \\ &+ \sum_{n(\neq l)} F'_n(\rho_n) f''_l(R_{ln}) \left\{ \frac{R_j(l) - R_j(n)}{R_{nl}} (\delta_{lm} - \delta_{nm}) \right\} \frac{R_i(l) - R_i(n)}{R_{ln}} \\ &+ \sum_{n(\neq l)} \Phi''(R_{ln}) \left\{ \frac{R_j(l) - R_j(n)}{R_{nl}} (\delta_{lm} - \delta_{nm}) \right\} \frac{R_i(l) - R_i(n)}{R_{ln}} \\ &+ \sum_{n(\neq l)} [F'_l(\rho_l) f'_n(R_{ln}) + F'_n(\rho_n) f'_l(R_{ln}) + \Phi'(R_{ln})] \Bigg\{ [\delta_{lm}\delta_{ij} - \delta_{nm}\delta_{ij}] R_{ln} \\ &\quad - [R_i(l) - R_i(n)] \frac{R_j(l) - R_j(n)}{R_{nl}} (\delta_{lm} - \delta_{nm}) \Bigg\} \frac{1}{R_{ln}^2} \end{aligned} \tag{A.16}$$

Now we simplify the above equation by using the symmtrey of fcc structure.The first term of double summation can be rewritten as

$$\begin{aligned}
&\sum_{n(\neq l)} F_l''(\rho_l)\Big\{\sum_{q(\neq l)} f_q'(R_{lq})\frac{R_j(l)-R_j(q)}{R_{lq}}(\delta_{lm}-\delta_{qm})\Big\}f_n'(R_{ln})\frac{R_i(l)-R_i(n)}{R_{ln}}\\
=&\sum_{n(\neq l)} F_l''(\rho_l)\Big\{\sum_{q(\neq l)} f_q'(R_{lq})\frac{R_j(l)-R_j(q)}{R_{lq}}\delta_{lm}\Big\}f_n'(R_{ln})\frac{R_i(l)-R_i(n)}{R_{ln}}\\
&-\sum_{n(\neq l)} F_l''(\rho_l)\Big\{\sum_{q(\neq l)} f_q'(R_{lq})\frac{R_j(l)-R_j(q)}{R_{lq}}\delta_{qm}\Big\}f_n'(R_{ln})\frac{R_i(l)-R_i(n)}{R_{ln}}\\
=&\sum_{n(\neq l)} F_l''(\rho_l)f_n'(R_{ln})\frac{R_i(l)-R_i(n)}{R_{ln}}\delta_{lm}\Big\{\sum_{q(\neq l)} f_q'(R_{lq})\frac{R_j(l)-R_j(q)}{R_{lq}}\Big\}\\
&-\sum_{n(\neq l)} F_l''(\rho_l)\Big\{f_m'(R_{lm})\frac{R_j(l)-R_j(m)}{R_{lm}}\Big\}_{l\neq m} f_n'(R_{ln})\frac{R_i(l)-R_i(n)}{R_{ln}}. \qquad \text{(A.17)}
\end{aligned}$$

From the symmetry of fcc crystal, we have

$$\sum_{q(\neq l)} f_q'(R_{lq})\frac{R_j(l)-R_j(q)}{R_{lq}}\equiv 0, \qquad \text{(A.18)}$$

$$\sum_{n(\neq l)} f_q'(R_{ln})\frac{R_j(l)-R_j(n)}{R_{ln}}\equiv 0, \qquad \text{(A.19)}$$

therefore, we can get

$$\sum_{n(\neq l)} F_l''(\rho_l)\Big\{\sum_{q(\neq l)} f_q'(R_{lq})\frac{R_j(l)-R_j(q)}{R_{lq}}(\delta_{lm}-\delta_{qm})\Big\}f_n'(R_{ln})\frac{R_i(l)-R_i(n)}{R_{ln}}=0. \qquad \text{(A.20)}$$

Similarly, for the second term of double summation, we can write

$$\begin{aligned}
&\sum_{n(\neq l)} F_n''(\rho_n)\Big\{\sum_{q(\neq n)} f_q'(R_{nq})\frac{R_j(n)-R_j(q)}{R_{nq}}(\delta_{nm}-\delta_{qm})\Big\}f_l'(R_{ln})\frac{R_i(l)-R_i(n)}{R_{ln}}\\
=&\sum_{n(\neq l)} F_n''(\rho_n)f_l'(R_{ln})\frac{R_i(l)-R_i(n)}{R_{ln}}\delta_{nm}\Big\{\sum_{q(\neq n)} f_q'(R_{nq})\frac{R_j(n)-R_j(q)}{R_{nq}}\Big\}\\
&-\sum_{n(\neq l)} F_n''(\rho_n)\Big\{\sum_{q(\neq n)} f_q'(R_{nq})\frac{R_j(n)-R_j(q)}{R_{nq}}\delta_{qm}\Big\}f_l'(R_{ln})\frac{R_i(l)-R_i(n)}{R_{ln}}\\
=&\sum_{n(\neq l,m)} F_n''(\rho_n)f_l'(R_{ln})f_m'(R_{mn})\frac{R_j(m)-R_j(n)}{R_{mn}}\frac{R_i(l)-R_i(n)}{R_{ln}}. \qquad \text{(A.21)}
\end{aligned}$$

Accounting for Eqs.(A.20)and (A.21), we write Eq.(A.16) as

$$
\begin{aligned}
\mathbf{\Phi}_{ij}(l,m) &= \frac{\partial^2 E_{tot}}{\partial R_i(l)\partial R_j(m)} = -\frac{\partial F_i(l)}{\partial R_j(m)} \\
&= \sum_{n(\neq l)} F_l'(\rho_l) f_n''(R_{ln}) \frac{[R_j(l)-R_j(n)][R_i(l)-R_i(n)]}{R_{ln}^2}\delta_{lm} \\
&\quad -F_l'(\rho_l) f_m''(R_{lm}) \frac{[R_j(l)-R_j(m)][R_i(l)-R_i(m)]}{R_{lm}^2}\Big|_{l\neq m} \\
&\quad + \sum_{n(\neq l)} F_n'(\rho_n) f_l''(R_{ln}) \frac{[R_j(l)-R_j(n)][R_i(l)-R_i(n)]}{R_{ln}^2}\delta_{lm} \\
&\quad -F_m'(\rho_m) f_l''(R_{lm}) \frac{[R_j(l)-R_j(m)][R_i(l)-R_i(m)]}{R_{lm}^2}\Big|_{l\neq m} \\
&\quad + \sum_{n(\neq l)} \Phi''(R_{ln}) \frac{[R_j(l)-R_j(n)][R_i(l)-R_i(n)]}{R_{ln}^2}\delta_{lm} \\
&\quad -\Phi''(R_{lm}) \frac{[R_j(l)-R_j(m)][R_i(l)-R_i(m)]}{R_{lm}^2}\Big|_{l\neq m} \\
&\quad + \sum_{n(\neq l)} [F_l'(\rho_l) f_n'(R_{ln}) + F_n'(\rho_n) f_l'(R_{ln}) + \Phi'(R_{ln})] \Big\{ \frac{\delta_{ij}}{R_{ln}} \\
&\quad - \frac{[R_i(l)-R_i(n)][R_j(l)-R_j(n)]}{R_{ln}^3} \Big\}\delta_{lm} \\
&\quad -[F_l'(\rho_l) f_m'(R_{lm}) + F_m'(\rho_m) f_l'(R_{lm}) + \Phi'(R_{lm})] \Big\{ \frac{\delta_{ij}}{R_{lm}} \\
&\quad - \frac{[R_i(l)-R_i(m)][R_j(l)-R_j(m)]}{R_{lm}^3} \Big\}\Big|_{l\neq m} \\
&\quad + \sum_{n(\neq l,m)} F_n''(\rho_n) f_l'(R_{ln}) f_m'(R_{mn}) \frac{R_j(m)-R_j(n)}{R_{mn}} \frac{R_i(l)-R_i(n)}{R_{ln}}. \qquad \text{(A.22)}
\end{aligned}
$$

If we do summation over m to Eq.(A.22)and notice summation label is just a dumb label which has the property

$$
\begin{aligned}
&\sum_{n(\neq l)} F_l'(\rho_l) f_n''(R_{ln}) \frac{[R_j(l)-R_j(n)][R_i(l)-R_i(n)]}{R_{ln}^2} \\
&\equiv \sum_{m(\neq l)} F_l'(\rho_l) f_m''(R_{lm}) \frac{[R_j(l)-R_j(m)][R_i(l)-R_i(m)]}{R_{lm}^2}, \qquad \text{(A.23)}
\end{aligned}
$$

we can obtain

$$
\begin{aligned}
\sum_m \mathbf{\Phi}_{ij}(l,m) \;=\; & \sum_{n(\neq l)} F_l'(\rho_l) f_n''(R_{ln}) \frac{[R_j(l)-R_j(n)][R_i(l)-R_i(n)]}{R_{ln}^2} \\
& - \sum_{m(\neq l)} F_l'(\rho_l) f_m''(R_{lm}) \frac{[R_j(l)-R_j(m)][R_i(l)-R_i(m)]}{R_{lm}^2} \\
& + \sum_{n(\neq l)} F_n'(\rho_n) f_l''(R_{ln}) \frac{[R_j(l)-R_j(n)][R_i(l)-R_i(n)]}{R_{ln}^2} \\
& - \sum_{m(\neq l)} F_m'(\rho_m) f_l''(R_{lm}) \frac{[R_j(l)-R_j(m)][R_i(l)-R_i(m)]}{R_{lm}^2} \\
& + \sum_{n(\neq l)} \Phi''(R_{ln}) \frac{[R_j(l)-R_j(n)][R_i(l)-R_i(n)]}{R_{ln}^2} \\
& - \sum_{m(\neq l)} \Phi''(R_{lm}) \frac{[R_j(l)-R_j(m)][R_i(l)-R_i(m)]}{R_{lm}^2} \\
& + \sum_{n(\neq l)} [F_l'(\rho_l) f_n'(R_{ln}) + F_n'(\rho_n) f_l'(R_{ln}) + \Phi'(R_{ln})] \Bigg\{ \frac{\delta_{ij}}{R_{ln}} \\
& - \frac{[R_i(l)-R_i(n)][R_j(l)-R_j(n)]}{R_{ln}^3} \Bigg\} \\
& - \sum_{m(\neq l)} [F_l'(\rho_l) f_m'(R_{lm}) + F_m'(\rho_m) f_l'(R_{lm}) + \Phi'(R_{lm})] \Bigg\{ \frac{\delta_{ij}}{R_{lm}} \\
& - \frac{[R_i(l)-R_i(m)][R_j(l)-R_j(m)]}{R_{lm}^3} \Bigg\} \\
& + \sum_{n(\neq l,m)} F_n''(\rho_n) f_l'(R_{ln}) \frac{R_i(l)-R_i(n)}{R_{ln}} \\
& \times \Bigg\{ \sum_m f_m'(R_{mn}) \frac{R_j(m)-R_j(n)}{R_{mn}} \Bigg\}
\end{aligned}
\tag{A.24}
$$

or clearly we have

$$
\sum_m \mathbf{\Phi}_{ij}(l,m) \equiv 0 \tag{A.25}
$$

This is the direct result of Eq.(2.13).

If $l \neq m$, finally we can get

$$\begin{aligned}
\Phi_{ij}(l,m) &= \frac{\partial^2 E_{tot}}{\partial R_i(l)\partial R_j(m)} = -\frac{\partial F_i(l)}{\partial R_j(m)} \\
&= -F_l'(\rho_l) f_m''(R_{lm}) \frac{[R_j(l)-R_j(m)][R_i(l)-R_i(m)]}{R_{lm}^2} \\
&\quad -F_m'(\rho_m) f_l''(R_{lm}) \frac{[R_j(l)-R_j(m)][R_i(l)-R_i(m)]}{R_{lm}^2} \\
&\quad -\Phi''(R_{lm}) \frac{[R_j(l)-R_j(m)][R_i(l)-R_i(m)]}{R_{lm}^2} \\
&\quad -[F_l'(\rho_l) f_m'(R_{lm}) + F_m'(\rho_m) f_l'(R_{lm}) + \Phi'(R_{lm})] \Big\{ \frac{\delta_{ij}}{R_{lm}} \\
&\quad - \frac{[R_i(l)-R_i(m)][R_j(l)-R_j(m)]}{R_{lm}^3} \Big\} \\
&\quad + \sum_{n(\neq l,m)} F_n''(\rho_n) f_l'(R_{ln}) f_m'(R_{mn}) \frac{R_j(m)-R_j(n)}{R_{mn}} \frac{R_i(l)-R_i(n)}{R_{ln}}.
\end{aligned} \tag{A.26}$$

A.3 the proof of Eqs.(2.39-2.44)

From the definition

$$\begin{aligned}
F(\rho) = &- E_c \left[1 - \frac{\alpha}{\beta} \ln\left[\frac{\rho}{\rho_e}\right]\right] \left[\frac{\rho}{\rho_e}\right]^{\alpha/\beta} + \frac{1}{2}\phi_e \sum_{\Lambda} \exp[-(p_\Lambda - 1)\gamma] \\
&\times \left[1 + (p_\Lambda - 1)\delta - p_\Lambda \frac{\delta}{\beta} \ln\left[\frac{\rho}{\rho_e}\right]\right] \times \left[\frac{\rho}{\rho_e}\right]^{p_\Lambda \frac{\gamma}{\beta}},
\end{aligned} \tag{A.27}$$

we have

$$\begin{aligned}
F'(\rho) = \frac{\partial F(\rho)}{\partial \rho} &= -E_c \left\{ \frac{\partial}{\partial \rho} \left[1 - \frac{\alpha}{\beta} \ln\left[\frac{\rho}{\rho_e}\right]\right] \right\} \left[\frac{\rho}{\rho_e}\right]^{\alpha/\beta} - E_c \left[1 - \frac{\alpha}{\beta} \ln\left[\frac{\rho}{\rho_e}\right]\right] \frac{\partial}{\partial \rho} \left[\frac{\rho}{\rho_e}\right]^{\alpha/\beta} \\
&+ \frac{1}{2}\phi_e \sum_{\Lambda} \exp[-(p_\Lambda - 1)\gamma] \times \left\{ \frac{\partial}{\partial \rho} \left[1 + (p_\Lambda - 1)\delta - p_\Lambda \frac{\delta}{\beta} \ln\left[\frac{\rho}{\rho_e}\right]\right] \right\} \times \left[\frac{\rho}{\rho_e}\right]^{p_\Lambda \frac{\gamma}{\beta}} \\
&+ \frac{1}{2}\phi_e \sum_{\Lambda} \exp[-(p_\Lambda - 1)\gamma] \\
&\times \left[1 + (p_\Lambda - 1)\delta - p_\Lambda \frac{\delta}{\beta} \ln\left[\frac{\rho}{\rho_e}\right]\right] \times \frac{\partial}{\partial \rho} \left[\frac{\rho}{\rho_e}\right]^{p_\Lambda \frac{\gamma}{\beta}},
\end{aligned} \tag{A.28}$$

or

$$
\begin{aligned}
F'(\rho) &= -\frac{E_c}{\rho_e}\left\{-\frac{\alpha}{\beta}+\frac{\alpha}{\beta}\left[1-\frac{\alpha}{\beta}\ln\left[\frac{\rho}{\rho_e}\right]\right]\right\}\left[\frac{\rho}{\rho_e}\right]^{\alpha/\beta-1}+\frac{1}{2}\phi_e\sum_{\Lambda}\exp[-(p_\Lambda-1)\gamma] \\
&\quad\times\left\{-p_\Lambda\frac{\delta}{\beta}\frac{1}{\rho_e}\left[\frac{\rho}{\rho_e}\right]^{p_\Lambda\frac{\gamma}{\beta}-1}+\left[1+(p_\Lambda-1)\delta-p_\Lambda\frac{\delta}{\beta}\ln\left[\frac{\rho}{\rho_e}\right]\right]p_\Lambda\frac{\gamma}{\beta}\frac{1}{\rho_e}\left[\frac{\rho}{\rho_e}\right]^{p_\Lambda\frac{\gamma}{\beta}-1}\right\} \\
&= \frac{E_c}{\rho_e}\frac{\alpha^2}{\beta^2}\ln\left[\frac{\rho}{\rho_e}\right]\left[\frac{\rho}{\rho_e}\right]^{\alpha/\beta-1}+\frac{1}{2}\frac{\phi_e}{\rho_e}\sum_{\Lambda}\exp[-(p_\Lambda-1)\gamma] \\
&\quad\times\left\{-p_\Lambda\frac{\delta}{\beta}+p_\Lambda\frac{\gamma}{\beta}\left[1+(p_\Lambda-1)\delta-p_\Lambda\frac{\delta}{\beta}\ln\left[\frac{\rho}{\rho_e}\right]\right]\right\}\left[\frac{\rho}{\rho_e}\right]^{p_\Lambda\frac{\gamma}{\beta}-1}. \qquad \text{(A.29)}
\end{aligned}
$$

Then from Eq.(A.27), we can further obtain

$$
\begin{aligned}
F''(\rho) &= \frac{\partial F'(\rho)}{\partial\rho}=\frac{E_c}{\rho_e}\frac{\alpha^2}{\beta^2}\left\{\left[\frac{\rho}{\rho_e}\right]^{\frac{\alpha}{\beta}-1}\frac{\partial}{\partial\rho}\ln\left[\frac{\rho}{\rho_e}\right]+\ln\left[\frac{\rho}{\rho_e}\right]\frac{\partial}{\partial\rho}\left[\frac{\rho}{\rho_e}\right]^{\frac{\alpha}{\beta}-1}\right\} \\
&\quad+\frac{1}{2}\frac{\phi_e}{\rho_e}\sum_{\Lambda}\exp[-(p_\Lambda-1)\gamma] \\
&\quad\times\left\{-p_\Lambda\frac{\delta}{\beta}+p_\Lambda\frac{\gamma}{\beta}\left[1+(p_\Lambda-1)\delta-p_\Lambda\frac{\delta}{\beta}\ln\left[\frac{\rho}{\rho_e}\right]\right]\right\}\frac{\partial}{\partial\rho}\left[\frac{\rho}{\rho_e}\right]^{p_\Lambda\frac{\gamma}{\beta}-1} \\
&\quad+\frac{1}{2}\frac{\phi_e}{\rho}\sum_{\Lambda}\exp[-(p_\Lambda-1)\gamma]\times\left\{-p_\Lambda^2\frac{\delta\gamma}{\beta^2}\frac{\partial}{\partial\rho}\ln\left[\frac{\rho}{\rho_e}\right]\right]\right\}\left[\frac{\rho}{\rho_e}\right]^{p_\Lambda\frac{\gamma}{\beta}-1} \\
&= \frac{E_c}{\rho_e}\frac{\alpha^2}{\beta^2}\left\{\frac{1}{\rho_e}\left[\frac{\rho}{\rho_e}\right]^{\frac{\alpha}{\beta}-2}+\frac{1}{\rho_e}\left(\frac{\alpha}{\beta}-1\right)\ln\left[\frac{\rho}{\rho_e}\right]^{\frac{\alpha}{\beta}-2}\right\} \\
&\quad+\frac{1}{2}\frac{\phi_e}{\rho_e}\sum_{\Lambda}\exp[-(p_\Lambda-1)\gamma]\times\left\{-p_\Lambda\frac{\delta}{\beta}+p_\Lambda\frac{\gamma}{\beta}\left[1+(p_\Lambda-1)\delta-p_\Lambda\frac{\delta}{\beta}\ln\left[\frac{\rho}{\rho_e}\right]\right]\right\} \\
&\quad\times\frac{1}{\rho_e}\left(p_\Lambda\frac{\gamma}{\beta}-1\right)\left[\frac{\rho}{\rho_e}\right]^{p_\Lambda\frac{\gamma}{\beta}-2}+\frac{1}{2}\frac{\phi_e}{\rho_e}\sum_{\Lambda}\exp[-(p_\Lambda-1)\gamma]\times\left[-p_\Lambda^2\frac{\delta\gamma}{\beta^2}\right]\frac{1}{\rho_e}\left[\frac{\rho}{\rho_e}\right]^{p_\Lambda\frac{\gamma}{\beta}-2} \\
&= \frac{E_c}{\rho_e^2}\frac{\alpha^2}{\beta^2}\left[1+\left(\frac{\alpha}{\beta}-1\right)\ln\left[\frac{\rho}{\rho_e}\right]\right]\left[\frac{\rho}{\rho_e}\right]^{\frac{\alpha}{\beta}-2}+\frac{1}{2}\frac{\phi_e}{\rho_e^2}\sum_{\Lambda}\exp[-(p_\Lambda-1)\gamma] \\
&\quad\times\left\{-p_\Lambda^2\frac{\delta\gamma}{\beta^2}+\left(p_\Lambda\frac{\gamma}{\beta}-1\right)\left[-p_\Lambda\frac{\delta}{\beta}+p_\Lambda\frac{\gamma}{\beta}\left[1+(p_\Lambda-1)\delta-p_\Lambda\frac{\delta}{\beta}\ln\left[\frac{\rho}{\rho_e}\right]\right]\right]\right\}\left[\frac{\rho}{\rho_e}\right]^{p_\Lambda\frac{\gamma}{\beta}-2} \qquad \text{(A.30)}
\end{aligned}
$$

From the pair potential

$$\Phi(R)=-\phi_e[1+\delta(R/R_{1e}-1)]\exp[-\gamma(R/R_{1e}-1)], \qquad \text{(A.31)}$$

we have

$$\begin{aligned}\Phi'(R) &= \frac{\partial\Phi(R)}{\partial R} = -\phi_e\frac{\delta}{R_{1e}}\exp[-\gamma(\frac{R}{R_{1e}}-1)] \\ &\quad -\phi_e[1+\delta(\frac{R}{R_{1e}}-1)](-\frac{\gamma}{R_{1e}})\exp[-\gamma([\frac{R}{R_{1e}}-1)] \\ &= -\frac{\phi_e}{R_{1e}}\left\{\delta-\gamma\left[1+\delta(\frac{R}{R_{1e}}-1)\right]\right\}\exp[-\gamma(\frac{R}{R_{1e}}-1)] \qquad \text{(A.32)}\end{aligned}$$

and

$$\begin{aligned}\Phi''(R) &= \frac{\partial^2\Phi(R)}{\partial R^2} = \frac{\phi_e}{R_{1e}}\frac{\gamma\delta}{R_{1e}}\exp[-\gamma(\frac{R}{R_{1e}}-1)] \\ &\quad -\frac{\phi_e}{R_{1e}}\left\{\delta-\gamma\left[1+\delta(\frac{R}{R_{1e}}-1)\right]\right\}(-\frac{\gamma}{R_{1e}})\exp[-\gamma(\frac{R}{R_{1e}}-1)] \\ &= \frac{\phi_e\gamma}{R_{1e}^2}\left\{2\delta-\gamma\left[1+\delta(\frac{R}{R_{1e}}-1)\right]\right\}\exp[-\gamma(\frac{R}{R_{1e}}-1)] \qquad \text{(A.33)}\end{aligned}$$

Bibliography

[1] J.Mei, J.W.Davenport, and G.W.Fernando. Analytic embedded-atom potentials for fcc metals: Application to liquid and solid copper. *Phys.Rev.B*, 43:4653–4685, 1991.

[2] Murray S. Daw and M. I. Baskes. Embedded-atom method: Derivation and application to impurities, surfaces, and other defects in metals. *Phys. Rev. B*, 29:6443–6453, 1984.

[3] Murray S. Daw and M. I. Baskes. Semiempirical, quantum mechanical calculation of hydrogen embrittlement in metals. *Phys.Rev.Lett.*, 50:1285–1288, 1983.

[4] R. A. Johnson. Analytic nearest-neighbor model for fcc metals. *Phys. Rev. B*, 37:3924–3931, 1988.

[5] S. M. Foiles. Application of the embedded-atom method to liquid transition metals. *Phys.Rev. B*, 32:3409–3415, 1985.

[6] M.J.Puska, R.M.Nieminen, and M.Manninen. Atoms embedded in an electron gas: Immersion energies. *Phys.Rev.B*, 24:3037–3047, 1981.

[7] M. I. Baskes S. M. Foiles and M. S. Daw. Embedded-atom-method functions for the fcc metals cu, ag, au, ni, pd, pt, and their alloys. *Phys.Rev.B*, 33:7983–7991, 1986.

[8] S.M.Foiles and J.B.Adams. Thermodynamic properties of fcc transition metals as calculated with the embedded-atom method. *Phys.Rev.B*, 40:5909–5915, 1989.

[9] M.I.Baskes. Application of the embedded-atom method to covalent materials: A semiempirical potential for silicon. *Phys.Rev.Latt.*, 59:2666–2669, 1987.

[10] R. A. Johnson. Alloy models with the embedded-atom method. *Phys.Rev.B*, 39:12554–12559, 1989.

[11] J. Mei and J. W. Davenport. Molecular-dynamics study of self-diffusion in liquid transition metals. *Phys.Rev.B*, 42:9682–9684, 1990.

[12] D.J.Oh and R.A.Johnson. Simple embedded atom method model for fcc and hcp metals. *J. Mater. Res.*, 3:471–478, 1988.

[13] M.W.Finnis and J.E. Sinclair. A simple empirical n-body potential for transition metals. *Philos. Mag.*, A50:45–55, 1984.

[14] M.Manninen. Interatomic interactions in solids: An effective-medium approach. *Phys.Rev.B*, 34:8486–8495, 1986.

[15] J.K.Nϕrskove K. W. Jacobsen and M.J.Puska. Interatomic interactions in the effective-medium theory. *Phys.Rev.B*, 35:7423–7442, 1987.

[16] J.C. Slater. *Quantum Theory of Matter, 2nd ed.* McGraw-Hill, New York, 1990.

[17] C. D.Gelatt, H. Ehrenreich, and J.A.Weiss. Transition-metal hydrides: Electronic structure and the heats of formation. *Phys.Rev.B*, 17:1940–1957, 1978.

[18] A. C. Switendick. Electronic band structures of metal hydrides. *Solid State Commun.*, 8:1463f–1467, 1970.

[19] R. A. Johnson. Relationship between two-body interatomic potentials in a lattice model and elastic constants. *Phys.Rev.B*, 6:2094–2100, 1972.

[20] M. I. Baskes. Modified embedded-atom potentials for cubic materials and impurities. *Phys.Rev.B*, 46:2727–2742, 1992.

[21] Murray S. Daw and R. D. Hatcher. Application of the embedded atom method to phonons in transition metals. *Solid State Commun.*, 56:693–696, 1985.

[22] J.S.Nelson and and M.S.Daw E.C.Sowa. Calculation of phonons on the cu(100) surface by the embedded-atom method. *Phys.Rev.Lett.*, 61:1977–1980, 1988.

[23] R.A.Johnson. Phase stability of fcc alloys with the embedded-atom method. *Phys.Rev.B*, 41:9717–9720, 1990.

[24] S.M.Foiles. *Surf. Sci.*, 191:329–, 1987.

[25] M.S.Daw and S.M. Foiles. Order-disorder transition of au and pt (110) surfaces: The significance of relaxations and vibrations. *Phys.Rev.Lett.*, 59:2756–2759, 1987.

[26] M.S.Daw and S.M. Foiles. Theory of subsurface occupation, ordered structures, and order-disorder transitions for hydrogen on pd(111). *Phys.Rev.B*, 35:2128–2136, 1987.

[27] M. S.Daw T.E.Felter, S.M.Foiles and R.H. Stulen. Order-disorder transitions and subsurface occupation for hydrogen on pd(111). *Surf. Sci*, 171:L379–L386, 1986.

[28] M.S Daw, M.I.Baskes, C.L.Bisson, and W.G.Wolfer. *Modeling Environmental Effects on Crack Growth Processes.* The Metallurgical Society, Warrendale,PA, 1986.

[29] S.M.Foiles. *Surf. Sci.*, 191:L779–L791, 1987.

[30] Murray S. Daw and Stephen M. Foiles. Calculations of the energetics and structure of pt(110) using the embedded atom method. *J.Vac.Sci.Technol. A*, 4:1412–1413, 1986.

[31] J.H. Rose, J.R.Smith, F.Guinea, and J.Ferrante. Universal features of the equation of state of metals. *Phys.Rev.B*, 29:2963–2969, 1984.

[32] Max Born and Keun Huang. *Dynamical Theory of Crystal Lattices.* Oxford University Press, Oxford, 1954.

[33] A.A.Maradudin, E.W.Montroll, G.H. Weiss, and I.P.Ipatova. Theory of lattice dynamics in the harmonic approximation. In Herry Ehrenreich, Frederick Seitz, and David Turnbull, editors, *Solid State Physics*, volume supplement 3, New York and London, 1971. ACADEMIC PRESS.

[34] W. A. Kamitakahara and B. N. Brockhouse. Crystal dynamics of silver. *Phys. Lett.*, 29A:639–640, 1969.

[35] E.C.Svensson, B.N.Brockhouse, and J.M.Rowe. Crystal dynamics of copper. *Phys.Rev.*, 155:619–632, 1967.

[36] A.P.Miiller and B.N.Brockhouse. Crystal dynamics and electronic specific heats of palladium and copper. *Can. J. Phys.*, 49:704–723, 1971.

[37] D.H.Dutton and B.N.Brocihouse. Crystal dynamics of platinum by inelastic neutron scattering. *Can.J.Phys.*, 50:2915–2923, 1972.

[38] R.J.Birgeneau, J.Cordes, G.Dolling, and A.D.B.woods. Normal modes of vibration in nickel. *Phys.Rev.*, 136:A1359–A1365, 1964.

[39] J.W.Lynn, H.G.Smith, and R.M.Nicklow. Lattice dynamics of gold. *Phys.Rev.B*, 8:3493–3499, 1973.

[40] J. K. Baria. Themperature dependent lattice mechanical properties of some fcc transition metals. *Chin. J. Phys.*, 42:287–306, 2004.

[41] M. Singh and J. Pure. Relationship between two-body interatomic potentials in a lattice model and elastic constants. *App. Phys.*, 22:741–2100, 1984.

[42] C. Domb and Slater. Relationship between two-body interatomic potentials in a lattice model and elastic constants. *Phil. Mag.*, 43:1083–2100, 1952.

[43] S.Narasimhan and S.D.Gironcoli. *ab initio* calculation of the thermal properties of cu: Performance of the *lda* and *gga*. *Phys.Rev.B*, 65:064302–1–064302–7, 2002.

[44] Rosemary A. MacDonald and william M. MacDonald. Thermodynamic properties of fcc metals at high temperatures. *Phys.Rev.B*, 15:1715–1724, 1981.

[45] Y.S.Touloukian, R. K. Kirby, R.E.Taylor, and P.D.Desai. Thermophysical properties of matter, the tprc data series. In Y.S.Touloukian and C.Y.Ho, editors, *Thermal Expansion, Metallic Elements and alloys*, volume 12, New York, 1977. Plenum DAta Company.

[46] Jianjun Xie, Stefano de Gironocoli, Stefano Baroni, and Matthias Scheffler. Frist-principles calculation of the thermal properties of silver. *Phys.Rev.B*, 59:965–969, 1999-II.

[47] Duane C. Wallace. *Thermodynamics of Crystals.* John Wiley and Sons, Inc., Canada, Toronto, 1972.

[48] Charles Kittel. *Introduction to Solid State Physics.* John Wiley and Sons, Inc., New York, Chichester, 1996.

[49] Jianjun Xie and S.P. Chen. Thermodynamic properties and lattice dynamics of silver at high pressure: A first-principles study. *Philosophical Magazine B*, 79(6):911–919, 1999.

[50] Y.S.Touloukian and E. H.Buyco. Thermophysical properties of matter, the tprc data series. In Y.S.Touloukian and C.Y.Ho, editors, *Specific Heat, Metallic Elements and alloys*, volume 4, New York, 1970. Plenum DAta Company.

[51] C.V.Pandya, P.R.Vyas, T.C.Pandya, and V. B.Gohel. Volume variation of gruneisen parameters of fcc transition metals. *Bull.Mater.Sci.*, 25:63–67, 2002.

[52] Gerald Burns. *Solid State Physics.* Academic Pres, Inc.(London) Ltd., Orlando, Florida, 1985.

[53] D.L. Martin. Specific heat of copper, silver, and gold below 30^0k. *Phys.Rev.*, 141:576–582, 1966.

[54] W.D.Compton, K.A.Gschneidner, M.T.Hutchings, Herbert Rabin, and Mario P.Tosi. Solid states physics. In R.Seitz and D.Turnbull, editors, *Advances in Research and Applications*, volume 16, New York and London, 1964. Academic Press.

[55] D.L.Martin. Relationship between two-body interatomic potentials in a lattice model and elastic constants. *Can. J. Phys.*, 38:2094–2100, 1960.

[56] J.R.Neighbours and G.A.Llers. Elastic constants of silver and gold. *Phys.Rev.*, 111:707–712, 1958.

[57] W. C. Overton, Jr., and John Gaffney. Temperature variation of the elastic constants of cubic elements. i. copper. *Phys. Rev.*, 98:969–977, 1955.

[58] T.Çağin, G.Derli, M.Uludoğan, and M.Tomak. Thermal and mechanical properties of some fcc transition metals: *Phys.Rev. B*, 59:3486–3473, 1999-I.

[59] K.A.Gschneidner. *Solid state phys. advances in research and applications (eds).* Academic Press, New York, 1964.

[60] W.B.Daniels and C.S.Smith. Pressure derivatives of the elastic constants of copper, silver, and gold to 10 000 bars. *Phys. Rev.*, 111:713–721, 1958.

[61] John M. Wills and Walter A. Harrison. Interionic interactions in transition metals. *Phys. Rev. B*, 28:4363–4373, 1983.

[62] G.D.Barrera and A. Batana. *Phys. Status Solidi (b)*, 179:59–70, 1993.

[63] G.D.Barrera and A. Batana. Quasiharmonic lattice dynamics of noble metals. *Phys. Rev. B*, 47:8588–8593, 1993.